PHILOSOPHICAL TRANSACTIONS OF THE ROYAL SOCIETY A MATHEMATICAL, PHYSICAL & ENGINEERING SCIENCES

The Dissolution of Calcite in Aqueous Solution at pH $\textless$ 4: Kinetics and Mechanism

R. G. Compton and P. R. Unwin

Phil. Trans. R. Soc. Lond. A 1990 **330**, 1-45
doi: 10.1098/rsta.1990.0001

Phil. Trans. R. Soc. Lond. A **330**, 1–45 (1990)

Printed in Great Britain

THE DISSOLUTION OF CALCITE IN AQUEOUS SOLUTION AT pH < 4: KINETICS AND MECHANISM

BY R. G. COMPTON AND P. R. UNWIN

Physical Chemistry Laboratory, University of Oxford, South Parks Road, Oxford OX1 3QZ, U.K.

(*Communicated by J. S. Rowlinson, F.R.S. – Received* 5 *August* 1988 – *Revised* 7 *February* 1989)

[Plates 1–3]

CONTENTS

The requirements of any experimental investigation of a reaction, such as dissolution or precipitation, at the solid–liquid interface are delineated, and it is shown that no previously adopted experimental method successfully meets all of these criteria. A new strategy for studying such reactions is therefore proposed, and described specifically for the dissolution kinetics of calcium carbonate in acidic aqueous solution. This technique involves locating a calcite crystal in part of one wall of a rectangular duct, through which reactant flows under laminar conditions, and positioning either an amperometric or potentiometric detector electrode immediately adjacent to and downstream of the crystal. The rate of the reaction at the crystal

 [Published 6 February 1990

surface is then followed by measuring the concentration of the reactant or products reaching the electrode as a function of solution flow rate. In this way both transport (to the crystal and detection system) and the surface topography of the crystal are defined and controllable, and, most importantly, the concentrations interrogated by the detector electrode are those pertaining at the crystal surface and not the bulk values, which are those probed with other (previous) methods. A mechanistic model for the dissolution reaction at pH < 4,

$$H^+ + CaCO_3 \rightarrow Ca^{2+} + HCO_3^-,$$

is developed, and it is recognized that half-, first- and second-order reactions in surface H^+ constitute possible candidate heterogeneous processes. The model also takes the following homogeneous (solution) reactions into account:

$$HCO_3^- + H^+ \rightleftharpoons H_2CO_3 \xrightarrow{k_{H_2CO_3}} CO_2 + H_2O,$$
$$K_{H_2CO_3} = a_{H^+} a_{HCO_3^-} / a_{H_2CO_3}.$$

The backward implicit finite difference method is used to provide theory for the proposed flow cell experiment. Specifically this relates the rate of an *n*th order process at the crystal surface to the transport-limited current at an amperometric detector electrode, as a function of solution flow rate and cell–crystal–electrode geometry. The computational method selected allows both the full parabolic velocity profile and any value of *n* to be considered. The validity of the numerical approach is checked by invoking the Lévêque approximation (linearizing the parabolic velocity profile) and solving the problem analytically for $n = 0$ and 1. The numerical method is extended so that both parallel heterogeneous and homogeneous reactions are covered, specifically so that theory describing the mechanistic model can be derived as related to the flow cell experiment. The design and construction of the necessary experimental apparatus is described, along with experiments devised to prove the validity of the experimental approach. The results of flow cell dissolution experiments carried out with 0.25–1.0 mM HCl solutions are presented, and it is shown for the first time that the reaction between H^+ and calcite is not transport-controlled. Assuming $k_{H_2CO_3} = 20\ s^{-1}$ and $K_{H_2CO_3} = 3.06 \times 10^{-4}$ M, a best fit to the data is obtained for a first-order heterogeneous process with a rate constant of (0.043 ± 0.015) cm s^{-1}.

1. Introduction

The process of dissolution of calcium carbonate in aqueous solution has received continuous attention by chemists, geologists, soil scientists and others for over a century (see, for example, Boguski 1876; Boguski & Kajander 1877; Spring 1887, 1888; Brunner 1904; King & Liu 1933; Moelwyn-Hughes 1933; Gortikov & Panteleva 1937; Tominaga *et al.* 1939; Erga & Terjesen 1956; Kaye 1957; Weyl 1958; Terjesen *et al.* 1961; Sippel & Glover 1964; Nestaas & Terjesen 1969; Boomer *et al.* 1972; Wentzler & Aplan 1972; Berner & Morse 1974; Morse 1974; Lund *et al.* 1975; Barton & Vatanathan 1976; Plummer & Wigley 1976; Sjöberg 1976; Plummer *et al.* 1978; Sjöberg 1978; Morse & Berner 1979; Plummer *et al.* 1979; Dreybrodt 1981; Sverdrup & Bjerle 1982; Morse 1983; Reddy 1983; Sjöberg 1983; Sjöberg & Rickard 1983; Rickard & Sjöberg 1983; Compton & Daly 1984; Sjöberg & Rickard 1984; Baumann *et al.* 1985; Buhmann & Dreybrodt 1985*a*, *b*; Daly 1985; Sjöberg & Rickard 1985; von Tress *et al.* 1985; Compton *et al.* 1986; Compton & Daly 1987; Ferret *et al.* 1987). The motivation for these studies, as well as interest in the fundamental processes governing dissolution, include understanding both natural and hard-water systems (Stumm & Morgan 1981), particularly

with regard to karstification (Dreybrodt 1981; Buhmann & Dreybrodt 1985*a*, *b*) (i.e. the formation of underground drainage systems in limestone regions) and the distribution of carbonate species in oceans (Petersen 1966; Berner & Morse 1974; Morse 1974; Morse & Berner 1979; Morse 1983). The study of the reaction is currently environmentally topical in association with neutralization strategies for acid lakes (Fraser & Britt 1982; Hultberg & Anderson 1982; Sverdrup & Bjerle 1982; Sverdrup 1983, 1984; Sverdrup & Bjerle 1984; Warfringe *et al.* 1984; Wright 1985; Lessmark & Thörnelöf 1986; Sverdrup 1986; Davison & House 1988).

In the following, we briefly survey and summarize the work on calcite dissolution of the past 100 years, and identify the current state of knowledge (and ignorance). An entirely new strategy for investigating the mechanism of the process is then suggested and, in the remainder of the paper, experiments and theory are presented that lead, for the first time, to the unambiguous identification of the heterogeneous kinetics and mechanism of calcite dissolution at pH < 4.

Initially, it is instructive to consider, in general terms, the requirements of any experimental investigation of calcite dissolution, or, indeed, of any reaction at a solid–liquid interface, necessary to provide a veracious description of the heterogeneous process and its kinetics. The following criteria are desirable.

1. Well-defined, calculable and controllable transport of (*a*) the reactant to the interface (King & Liu 1933; Gortikov & Panteleva 1937; Tominaga *et al.* 1939; Kaye 1957; Litt & Serad 1964; Karshin & Grigoryan 1970; McDonald & Wright 1970; Barton & Wilde 1971*a*, *b*; Boomer *et al.* 1972; Linge & Nancollas 1973; Lund *et al.* 1973; Barton & McConnel 1974, 1975; Lund *et al.* 1975; Barton & McConnel 1979*a*, *b*; Spiro & Jago 1982; Rickard & Sjöberg 1983; Sjöberg 1983; Sjöberg & Rickard 1983; Cheng *et al.* 1984; Compton & Daly 1984; Meares 1984; Sjöberg & Rickard 1984; Spiro 1984; Daly 1985; Sjöberg & Rickard 1985; Compton *et al.* 1986; Compton & Daly 1987) and (*b*) the reaction products to the detection system.

2. Control of the surface topography of the solid (Spring 1887, 1888; Karshin & Grigoryan 1970; Compton & Daly 1984; Daly 1985; Compton *et al.* 1986; Compton & Daly 1987).

3. Chemostatic control of the reaction conditions (Wentzler & Aplan 1972; Berner & Morse 1974; Morse 1974; Sjöberg 1978; Tomson & Nancollas 1978; Kier 1980; Sverdrup & Bjerle 1982; Rickard & Sjöberg 1983; Sjöberg 1983; Sjöberg & Rickard 1983, 1984, 1985).

As an extension to (1), if fast surface reactions are to be investigated then high rates of transport of the reactant to the interface are necessary (Unwin & Compton 1989) otherwise the experiment will simply measure the rate of transport in the liquid phase.

A summary of some of the experimental techniques used to investigate calcite dissolution kinetics is presented in table 1. Although the early workers clearly recognized the need for controlled hydrodynamics (King & Liu 1933; Gortikov & Panteleva 1937; Tominaga *et al.* 1939; Kaye 1957; Weyl 1958), their work was hampered by both the lack of available theoretical treatments of transport in the particular experimental geometries utilized, and of suitable methods of following the progress of the reaction. Subsequently, techniques using suspensions of powdered material (Erga & Terjesen 1956; Terjesen *et al.* 1961; Nestaas & Terjesen 1969; Wentzler & Aplan 1972; Berner & Morse 1974; Morse 1974; Barton & Vatanathan 1976; Plummer & Wigley 1976; Sjöberg 1976; Plummer *et al.* 1978; Sjöberg 1978; Plummer *et al.* 1979; Sverdrup & Bjerle 1982; Reddy 1983; von Tress *et al.* 1985; Ferret

PHILOSOPHICAL TRANSACTIONS OF THE ROYAL SOCIETY A MATHEMATICAL, PHYSICAL & ENGINEERING SCIENCES

TABLE 1. A SUMMARY OF EXPERIMENTAL METHODS USED IN THE STUDY OF CALCITE DISSOLUTION KINETICS IN AQUEOUS SOLUTION

method	mass transport	surface topography	monitoring of reaction	chemostatic control
1. rotating disc – single crystal (Gortikov & Panteleva 1937; Tominaga *et al.* 1939; Boomer *et al.* 1972; Lund *et al.* 1975; Rickard & Sjöberg 1983; Sjöberg 1983; Sjöberg & Rickard 1983; Compton & Daly 1984; Sjöberg & Rickard 1984; Daly 1985; Sjöberg & Rickard 1985; Compton *et al.* 1986; Compton & Daly 1987)	defined and calculable (von Karman 1921; Cochran 1934; Levich 1942)	defined: polished/cleaved crystals (Gortikov & Panteleva 1937; Tominaga *et al.* 1939; Boomer *et al.* 1972; Lund *et al.* 1975; Rickard & Sjöberg 1983; Sjöberg 1983;Sjöberg & Rickard 1983; Compton & Daly 1984; Sjöberg & Rickard 1984; Daly 1985; Sjöberg & Rickard 1985; Compton *et al.* 1986; Compton & Daly 1987)	bulk solution: (a) pH electrode $[-\mathrm{d}[\mathrm{H}^+]^\infty/\mathrm{d}t]$ (Rickard & Sjöberg 1983; Sjöberg 1983; Sjöberg & Rickard 1983, 1984, 1985) (b) Ca^{2+} ion-selective electrode $[\mathrm{d}[\mathrm{Ca}^{2+}]^\infty/\mathrm{d}t]$ (Compton & Daly 1984; Daly 1985; Compton *et al.* 1986; Compton & Daly 1987) (c) evolution of CO_2 $[\mathrm{d}[\mathrm{CO}_2]/\mathrm{d}t]$ (Tominaga *et al.* 1939) *ex situ*: sampling – spectrophotometric Ca^{2+} analysis (Boomer *et al.* 1972; Lund *et al.* 1975)	(a) pH-stat method (Rickard & Sjöberg 1983; Sjöberg 1983; Sjöberg & Rickard 1983, 1984, 1985) (b) measurement of initial rates (Gortikov & Panteleva 1937; Tominaga *et al.* 1939; Boomer *et al.* 1972; Lund *et al.* 1975; Rickard & Sjöberg 1983; Sjöberg 1983;Sjöberg & Rickard 1983; Compton & Daly 1984; Sjöberg & Rickard 1984; Daly 1985; Sjöberg & Rickard 1985; Compton *et al.* 1986; Compton & Daly 1987)
2. rotating cylinder of marble (King & Liu 1933)	defined and calculable (Eisenberg *et al.* 1954*a*, *b*; Gabe 1974; Gabe & Walsh 1983)	polished cylinder (King & Liu 1933)	*ex situ*: mass of cylinder before and after reaction (King & Liu 1933)	measurement of initial rates (King & Liu 1933)
3. wall-jet-limestone block (Kaye 1957)	defined and calculable (Glauert 1956; Yamada & Matsuda 1973)	polished surface (Kaye 1957)	*ex situ*: measurement of resulting pit depth (Kaye 1957)	flow system, constant $[\mathrm{H}^+]^\infty$ (Kaye 1957)
4. free-jet-single crystal (Weyl 1958)	defined (Schlichting 1933; Bickley 1937)	defined: polished/cleaved crystal (Weyl 1958)	*ex situ*: measurement of resulting pit depth (Weyl 1958)	flow system – constant $[\mathrm{H}^+]^\infty$ (Weyl 1958)
5. stirred suspension of powdered material (Erga & Terjesen 1956; Terjesen *et al.* 1961; Nestaas & Terjesen 1969; Wentzler & Aplan 1972; Berner & Morse 1974; Morse 1974; Barton & Vatanathan 1976; Plummer & Wigley 1976; Sjöberg 1976; Plummer *et al.* 1978; Sjöberg 1978; Plummer *et al.* 1979; Sverdrup & Bjerle 1982; Reddy 1983; von Tress *et al.* 1985; Ferret *et al.* 1987)	poorly defined – empirical treatment necessary (Brian *et al.* 1969; Berner 1971; Berner & Morse 1974; Morse 1974; Plummer & Wigley 1976; Plummer *et al.* 1978; Sjöberg 1978; Morse 1983)	difficult to control	bulk solution: pH electrode $[-\mathrm{d}[\mathrm{H}^+]^\infty/\mathrm{d}t]$ (Erga & Terjesen 1956; Terjesen *et al.* 1961; Wentzler & Aplan 1972; Berner & Morse 1974; Morse 1974; Barton & Vatanathan 1976; Plummer & Wigley 1976; Sjöberg 1976; Plummer *et al.* 1978; Sjöberg 1978; Plummer *et al.* 1979; Sverdrup & Bjerle 1982; Reddy 1983; von Tress *et al.* 1985; Ferret *et al.* 1987)	via pH-stat method (Wentzler & Aplan 1972; Berner & Morse 1974; Morse 1976; Sjöberg 1978; Tomson & Nancollas 1979; Kier 1980; Sverdrup & Bjerle 1982)
6. single crystal-stirred solution (Sjöberg 1978)				

et al. 1987), popularized from the 1950s onwards, made available large surface areas; thereby allowing fairly slow reaction rates to be studied (fluxes as small as 6×10^{-13} mol (Ca^{2+}) cm^{-2} s^{-1} have been measured (Morse 1974)). Unfortunately, this convenience is traded against a loss in the definition of mass transport in such systems, making approximate treatments of this process necessary (Brian *et al.* 1969; Berner 1971; Berner & Morse 1974; Morse 1974; Plummer & Wigley 1976; Plummer *et al.* 1978; Sjöberg 1978; Morse 1983). In particular, particles generally have to be treated as fully suspended spheres (Berner 1971; Berner & Morse 1974; Morse 1974; Plummer & Wigley 1976; Plummer *et al.* 1978; Sjöberg 1978; Morse 1983). Transport to small particles (less than 10 μm in diameter) is then assumed to occur via a stationary diffusion layer. Calcite particles, however, are invariably non-spherical (Sjöberg & Rickard 1983). Moreover, transport in suspensions consisting of larger particles comprises both convection and diffusion, and average mass-transfer rates have to be estimated from literature correlations (Brian *et al.* 1969; Plummer *et al.* 1976).

The degree of transport control in a heterogeneous reaction involving particulates is generally deduced from the effect of stirring rate on reaction rate, a lack of stirring dependence being taken to imply a lack of transport control (Sjöberg & Rickard 1983). However, it has been shown (Sjöberg & Rickard 1983) that, in systems with poorly defined hydrodynamics, a lack of stirring dependence may not directly reflect the role of mass transport. This makes both the interpretation of rate data and comparison between independent studies difficult. A further disadvantage is that the rate of reaction measured in such systems is based on measuring chemical changes in bulk solution, distant from the reaction site. This, as recently pointed out (Sjöberg & Rickard 1983), can 'only provide indirect information about processes occurring at or near the solid–liquid interface'.

To overcome some of the difficulties associated with powder experiments, workers have more recently turned to the rotating disc method (Gortikov & Panteleva 1937; Tominaga *et al.* 1939; Boomer *et al.* 1972; Lund *et al.* 1975; Rickard & Sjöberg 1983; Sjöberg & Rickard 1983; Compton & Daly 1984; Sjöberg & Rickard 1984; Daly 1985; Sjöberg & Rickard 1985; Compton *et al.* 1986; Compton & Daly 1987). This technique, which has found considerable application in the study of electrode reaction mechanisms (see, for example, Filinovskii & Pleskov 1984), allows the rate of mass transport to the surface of the crystal to be controlled through variation of the rotation speed, whereas the well-defined hydrodynamics (von Karman 1921; Cochran 1934) permit the calculation of the mass transport rates (Levich 1942). An additional merit of rotating disc methodology is that the use of single crystals permits the (reproducible) treatment of surfaces (Compton & Daly 1984; Daly 1985; Compton *et al.* 1986; Compton & Daly 1987). However, though transport in the vicinity of the disc is defined, transport to the detector (located in bulk solution) is not. Hence, this method of measuring reaction rates via variations in bulk concentrations naturally suffers from the same limitations described with regard to experiments on powders. Another disadvantage of the rotating disc method is the implicit batch nature of the system; products accumulate in the reaction medium, thereby dictating the kinetic measurements are restricted to short times so that significant changes in the solution composition are avoided. In comparison with powder methods, the slowest reaction rate that may be measured by the rotating disc technique is estimated to be about 2×10^{-10} mol cm^{-2} s^{-1} for a typical rotating disc of area 0.7 cm^2 (Sjöberg & Rickard 1983).

To summarize, no existing experimental method satisfactorily meets all of the criteria

delineated above. Given the importance of understanding the mechanism of calcite dissolution, the aim of this paper is therefore to present a new strategy for the study of calcite dissolution kinetics. It should be emphasized that the method, although presented here with reference to the dissolution of calcite, is applicable to the study of reactions at the solid–liquid interface in general.

2. The general approach

The overall reaction defining the dissolution of calcite in aqueous solution is described by the following equations:

$$CaCO_3 + H^+ \rightleftharpoons Ca^{2+} + HCO_3^-, \quad [1]$$

$$CaCO_3 + H_2CO_3 \rightleftharpoons Ca^{2+} + 2HCO_3^-, \quad [2]$$

$$CaCO_3 + H_2O \rightleftharpoons Ca^{2+} + HCO_3^- + OH^-, \quad [3]$$

and according to Plummer *et al.* (1978), the overall rate of dissolution, R, determined by the net difference in the forward and backward rates of each of the processes defined above, is given by an expression of the form

$$R = k_1' a_{H^+} + k_2' a_{H_2CO_3^*} + k_3' a_{H_2O} - k_4' a_{Ca^{2+}} a_{HCO_3^-}, \quad (1)$$

where a_i represents the activity of the species i in the bulk of the solution, and $H_2CO_3^*$ signifies the total concentration of dissolved CO_2 (in the form of H_2CO_3 and CO_2).

Using the rotating disc method, Compton & Daly (1984) showed that under pure dissolution conditions in the pH range 3.0–6.2, and because in the absence of dissolved CO_2, reaction [2] was negligible, Plummer's equation reduced to

$$R = k_1' a_{H^+} + k_3' a_{H_2O}. \quad (2)$$

Although equations (1) and (2) identify the reacting species in the dissolution process, the fact that it is measured by changes in the concentration of (usually) H^+ or Ca^{2+} in bulk solution, and that the concentrations in the equation are those in bulk solution, means that the mechanistic information they convey is strictly limited. In particular, we note that this information can only be determined with a knowledge of the influence on the reaction rate of the concentrations of Ca^{2+}, H^+, etc., at the surface of the dissolving crystal. We are thus led to the following experimental strategy.

A calcite crystal forms part of one wall of a channel (rectangular duct) through which reactant flows under laminar conditions. Immediately downstream of, and adjacent to, the crystal is located either an amperometric or potentiometric detector electrode, as shown in figure 1. This electrode is used to measure the concentration of reactant, or products, reaching the electrode surface which, in turn, is governed by the kinetics of the dissolution reaction. For relatively high concentrations of protons (greater than 10^{-4} M), an amperometric electrode – held at a potential such that the protons are electrolysed at a transport-controlled rate – represents the most sensitive means of following the reaction, whilst at lower concentrations of protons this is best replaced by a (potentiometric) pH or Ca^{2+}-selective microelectrode. With this protocol the following are true.

1. Transport of the various species, to both the crystal and detector electrode is defined, calculable and controllable (Levich 1962).

2. The surface may be prepared (reproducibly) in a variety of ways, as shown in figure 1.

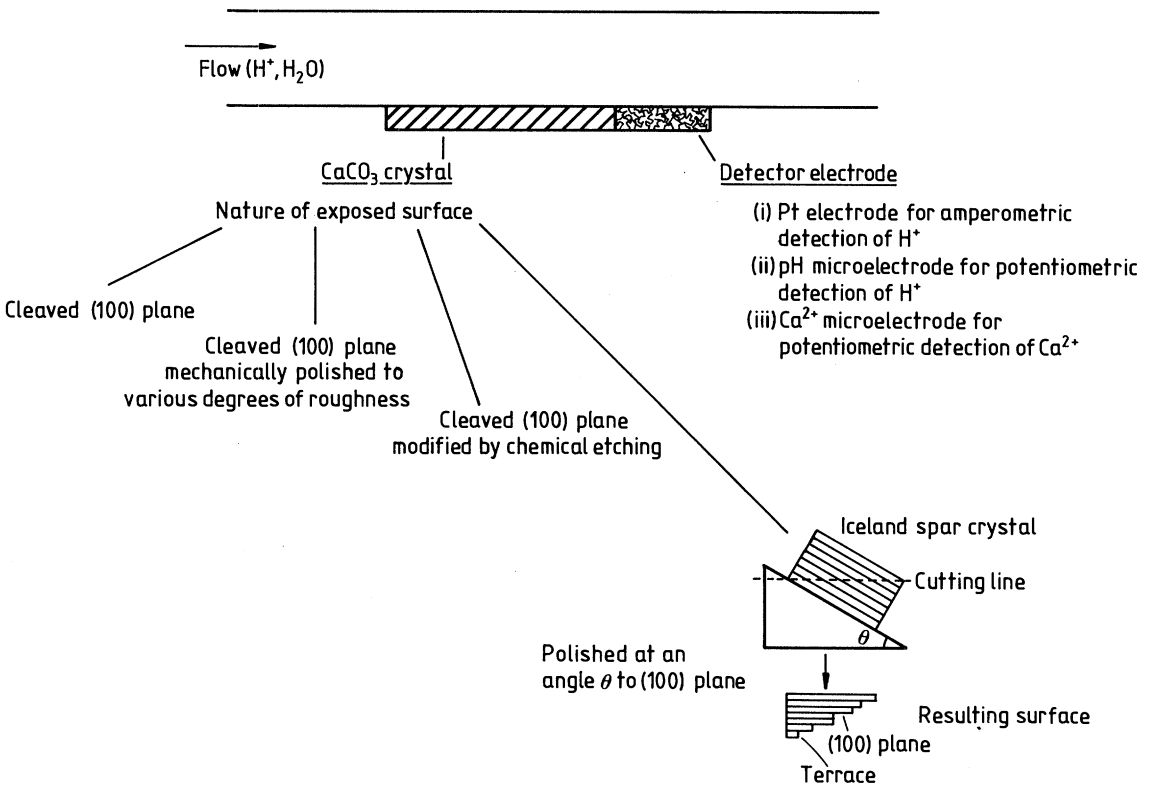

FIGURE 1. Flow cell strategy for the investigation of dissolution kinetics.

3. The detector electrode measures the flux of species i to the electrode, which is describable in terms of the flux at the crystal surface. This is to be compared with the existing methods, described above, which measure the depletion–production of i in the bulk solution.

4. Precise chemostatic control of the reaction environment may be exercised (reactants flow into the channel upstream, and products flow to waste downstream).

5. Most importantly, because the detector electrode is located immediately downstream of the dissolving surface, the concentrations interrogated are related to those pertaining at the crystal surface, and not to bulk values.

Further bonuses of the channel electrode method arise from the fact that the crystal–electrode surface is non-uniformly accessible to the reactant (e.g. for a transport-controlled reaction at the wall, the flux of material to the interface varies as the cube-root of distance down the channel). This has two important consequences.

1. Similar reaction mechanisms are more readily distinguished than with steady-state measurements at conventional hydrodynamic electrodes such as the rotating disc (Compton & Unwin 1986; Unwin & Compton 1989).

2. The average rate of mass transport depends on both the solution velocity and the length of the substrate. Higher rates of transport are thus attainable, and consequently fast heterogeneous processes may be studied (Unwin & Compton 1989).

This paper is concerned with the use of the channel flow cell methodology to study the mechanism of calcite dissolution under acidic conditions, with pH < 4. The nature of the process at higher pH will be reported in a separate publication (Compton & Pritchard 1990).

The results of previous work (alluded to above) at ambient temperatures have identified reaction [1] as the dominant reaction and have shown that reactions [2] and [3] contribute negligibly to the overall rate in the pH range in question. Plummer's equation thus reduces to

$$R = k_1'([H^+]^\infty)^n, \tag{3}$$

where $[H^+]^\infty$ is the bulk concentration of protons (the presence of inert electrolyte allowing us to replace activity by concentration), $n = 1$, and the rate constant k_1' is found to describe mass transport to the surface of the crystal. Other workers have agreed unanimously with Plummer that the process is transport-controlled, and have generally agreed on a value of unity for n (King & Liu 1933; Gortikov & Panteleva 1937; Tominaga *et al.* 1939; Kaye 1957; Weyl 1958; Berner & Morse 1974; Barton & Vatanathan 1976; Plummer *et al.* 1978; Sjöberg 1978; Plummer *et al.* 1979; Sverdrup & Bjerle 1982; Morse 1983; Compton & Daly 1984; Daly 1985; Compton *et al.* 1986; Compton & Daly 1987). Sjöberg has, however, suggested that $n = 0.9$ (Rickard & Sjöberg 1983; Sjöberg 1983; Sjöberg & Rickard 1983, 1984, 1985) because of the 'formation of aqueous CO_2 and the consequent disturbance of purely Fickian H^+ gradient through the diffusion layer' (Sjöberg & Rickard 1983). It is thus evident that all previous work in this area has simply reflected the measurement of mass transport rates in whatever vessel the calcite dissolution has been studied. Our aim is to use the channel flow cell to interrogate surface concentrations at the dissolving crystal surface, establish a heterogeneous rate law for the reaction, and to make mechanistic deductions as to the nature of the chemical dissolution process.

3. Theory

This section is in two parts. In § (*a*), we set out the general chemical kinetic equations relating to calcite dissolution at pH < 4, whereas in § (*b*) we solve the corresponding mass-transport equations incorporating the relevant chemical behaviour pertinent to the channel flow cell described above.

(*a*) *Mechanistic model*

Adopting the accepted scheme for dissolution (see, for example, Soustelle *et al.* 1985, and references therein) as comprising the sequential steps of (*a*) transport of the reactant from bulk solution to the solid–liquid interface, (*b*) adsorption of the reactant onto the surface, (*c*) diffusion of the reactant on the surface to a reactive (kink) site, (*d*) reaction, (*e*) diffusion of products away from the site, (*f*) product desorption, and (*g*) transport of products to bulk solution, we may write the mechanism for the reaction between calcite and H^+ specifically as:

$$H^+_{(\infty)} \overset{k_T}{\rightarrow} H^+_{(o)} \tag{4}$$

$$H^+_{(o)} \rightleftharpoons H^+_{(s)} \tag{5}$$

$$H^+_{(s)} \rightleftharpoons H^+_{(r)} \tag{6}$$

$$H^+_{(r)} + [CaCO_3] \rightleftharpoons HCO^-_{3(r)} + Ca^{2+}_{(r)} \tag{7a}$$

$$H^+_{(r)} + CaHCO^+_{3(r)} \rightleftharpoons HCO^-_{3(r)} + H^+_{(r)} + Ca^{2+}_{(r)} \tag{7b}$$

$$\left.\begin{aligned} HCO^-_{3(r)} &\rightleftharpoons HCO^-_{3(s)} \\ Ca^{2+}_{(r)} &\rightleftharpoons Ca^{2+}_{(s)} \end{aligned}\right\} \tag{8}$$

$$\left.\begin{aligned} HCO^-_{3(s)} &\rightleftharpoons HCO^-_{3(o)} \\ Ca^{2+}_{(s)} &\rightleftharpoons Ca^{2+}_{(o)} \end{aligned}\right\} \quad [9]$$

$$\left.\begin{aligned} HCO^-_{3(o)} &\xrightarrow{k_T} HCO^-_{3(\infty)} \\ Ca^{2+}_{(o)} &\xrightarrow{k_T} Ca^{2+}_{(\infty)} \end{aligned}\right\} \quad [10]$$

where the subscripts ∞, o, s and r are used to distinguish between 'sites' in bulk solution, at the edge of the outer Helmholtz plane, on the crystal surface (sites of adsorption) and at 'reaction' sites on the crystal respectively.

The reaction of H^+ at reaction (e.g. kink) sites on the crystal surface is represented by step [7*a*]. The inclusion of step [7*b*] recognizes that the reaction may involve a pre-equilibrium protonation of a carbonate site to give a $Ca—HCO_3^+$ surface complex, which subsequently reacts with an additional proton.

By considering each of the steps outlined above as being possibly rate-limiting, we deduce the rate laws shown in table 2 for the reaction between H^+ and calcite. Here $K_a = k_a/k_{-a}$. The flux of H^+ at the crystal surface, J_{H^+}, has been written in terms of $H^+_{(o)}$ (apart from when step [1] is the rate-limiting step). The message from table 2 is that half-, first- and second-order reactions in 'surface' H^+ need to be considered as candidate mechanisms. 'Surface' describes H^+ at o, s or r. In addition, it may be necessary to include the effects of the parallel reaction between calcite and water, described by reaction [3] in the heterogeneous process (see below).

TABLE 2. RATE LAWS FOR THE REACTION BETWEEN H^+ AND CALCITE AS DEFINED BY REACTIONS [4]–[10]

rate limiting step	J_{H^+}
[4]	$k_T [H^+_{(\infty)}]$
[5]	$k_5 [H^+_{(o)}]$
[6]	$k_6 K_5 [H^+_{(o)}]$
[7*a*]	$k_{7a} K_6 K_5 [H^+_{(o)}]$
[7*b*]	$k_{7b} K_{7a} K_6^2 K_5^2 [H^+_{(o)}]^2$
[8]	$k_8 K_{7b} K_{7a} K_6 K_5 [H^+_{(o)}]$
	$k_8 (K_{7a} K_6 K_5 [H^+_{(o)}])^{\frac{1}{2}a}$
[9]	$k_9 K_8 K_{7b} K_{7a} K_6 K_5 [H^+_{(o)}]$
	$k_9 K_8 (K_{7a} K_6 K_5 [H^+_{(o)}])^{\frac{1}{2}a}$
[10]	$k_T K_9 K_8 K_{7b} K_{7a} K_6 K_5 [H^+_{(o)}]$
	$k_T K_9 K_8 (K_{7a} K_6 K_5 [H^+_{(o)}])^{\frac{1}{2}a}$

[a] Disregarding step [7*b*], and assuming $[Ca^{2+}_{(k)}] = [HCO^-_{3(k)}]$, where k = r or s.

The scheme outlined above is further complicated by homogeneous processes in solution involving H^+, HCO_3^- and Ca^{2+}. In particular, H^+ and HCO_3^- will equilibrate to give carbonic acid

$$H^+(aq) + HCO_3^-(aq) \underset{k_{-11}}{\overset{k_{11}}{\rightleftharpoons}} H_2CO_3(aq), \quad [11]$$

which itself undergoes dehydration:

$$H_2CO_3(aq) \xrightarrow{k_{H_2CO_3}} CO_2(aq) + H_2O. \quad [12]$$

These reactions have in themselves been the subject of a number of studies, as illustrated by the data in table 3. The value for the 'true' dissociation constant of carbonic acid at infinite dilution,

$$K_{H_2CO_3} = a_{H^+} a_{HCO_3^-} / a_{H_2CO_3}, \quad (4)$$

is 1.72×10^{-4} M at 25 °C (Wissbrun *et al.* 1954), with values for k_{11} and k_{-11} of 4.7×10^{10} M^{-1} s^{-1} and 8.0×10^{6} s^{-1} respectively (Eigen & Hammes 1963). Unfortunately, there is no data on the effect of ionic strength on $K_{H_2CO_3}$ for the concentrations employed in this study (*ca.* 1 M KCl). We have therefore estimated this from

$$K_{H_2CO_3} \approx \frac{[H^+]\,[HCO_3^-]}{[H_2CO_3]} \times \gamma_{H^+} \gamma_{HCO_3^-}, \quad (5)$$

where γ_i is the activity coefficient of the species i in the particular ionic medium. The value of $\gamma_{HCO_3^-}$ in KCl is taken from Walker *et al.* (1927), whereas γ_{H^+} in KCl is given by Harned & Owen (1943). We have assumed that $a_{H_2CO_3} \approx [H_2CO_3]$ is a reasonable approximation.

TABLE 3. SUMMARY OF EXPERIMENTAL VALUES OF $k_{H_2CO_3}$ CORRECTED TO 25 °C

author	method	$k_{H_2CO_3}/s^{-1}$
van Eldik & Palmer (1982)	pressure jump, spectrophotometric	18
Knoche (1980)	pressure jump, conductometric	28
Patel *et al.* (1973)	pressure jump, conductometric	29
	stopped flow, spectrophotometric	22 (0.005 M NaCl)
		19 (0.5 M NaCl)
	concentration jump, spectrophotometric	22
Ho & Sturtevant (1963)	stopped flow, spectrophotometric	18
Rossi-Bernadi & Berger (1968)	continuous flow, potentiometric	26
Gibbons & Edsall (1963)	stopped flow, spectrophotometric	14
Magid & Turbeck (1968)	pH-stat	18
Scheuer *et al.* (1958)	stopped flow, spectrophotometric	22
Eigen *et al.* (1961)	temperature jump	15
Pearson *et al.* (1956)	continuous flow, conductometric	28
Berger & Stoddart (1965)	stopped flow, spectrophotometric	24
	stopped flow, thermometric	22
Sirs (1958)	stopped flow, potentiometric	24
Roughton (1941)	continuous flow, thermometric	28
Gibson & Roughton (1955)	stopped flow, spectrophotometric	22
Brinkman *et al.* (1933)	continuous flow, photoelectric	23
	manometric CO_2 determination	20

A surprisingly wide range of values for $k_{H_2CO_3}$ have been determined experimentally, as shown in table 3 (which provides a summary of the results of studies in this area). It has been suggested that in some cases the apparent discrepancies may simply reflect an inappropriate estimate of $K_{H_2CO_3}$ used in the calculation of $k_{H_2CO_3}$ (Knoche 1980). The most recent paper on carbonic acid dehydration (van Eldik & Palmer 1982) proposes that the value of 19 s^{-1} for $k_{H_2CO_3}$ determined by Patel *et al.* (1973) should be taken as the most reliable. The rather low value of Gibbons & Edsall has been explained by the fact that phosphate (used as a buffer in their solutions) was considered to have a catalytic effect on the rate of dehydration, and the rate constant was therefore corrected. Magid & Turbeck (1968), however, showed this to be a false assumption.

PHILOSOPHICAL TRANSACTIONS OF THE ROYAL SOCIETY A MATHEMATICAL, PHYSICAL & ENGINEERING SCIENCES

It is also necessary to consider the formation of the $CaHCO_3^+$ ion pair in solution,

$$CaHCO_3^+ \rightleftharpoons Ca^{2+} + HCO_3^-, \qquad [13]$$

with
$$K_{CaHCO_3^+}(25\ ^\circ C) = a_{Ca^{2+}} a_{HCO_3^-}/a_{CaHCO_3^+} = 0.1\ \text{M}, \qquad (6)$$

as determined by Jacobson & Langmuir (1974). Provided that the solution does not contain additional Ca^{2+} (as a background ion), then the process described by [13] may be neglected (see, for example, Sjöberg & Rickard 1983). As a final point we note that neither K^+ nor Cl^-, constituting the background electrolyte in this study, form any major complexes with H^+, HCO_3^- or Ca^{2+} (Sillen & Martell 1964).

Given reactions [11] and [12], we may write the following rate equations for H^+, HCO_3^- and H_2CO_3 in solution;

$$d[H^+]/dt = k_{-11}[H_2CO_3] - k_{11}[H^+]\,[HCO_3^-], \qquad (7)$$

$$d[HCO_3^-]/dt = k_{-11}[H_2CO_3] - k_{11}[H^+]\,[HCO_3^-], \qquad (8)$$

$$d[H_2CO_3]/dt = k_{11}[H^+]\,[HCO_3^-] - (k_{H_2CO_3} + k_{-11})\,[H_2CO_3], \qquad (9)$$

from which we deduce

$$\frac{d[HCO_3^-]}{dt} = \frac{d[H^+]}{dt} = \frac{-k_{H_2CO_3}[H^+]\,[HCO_3^-]}{K_{H_2CO_3} + [H^+] + [HCO_3^-]}, \qquad (10)$$

by assuming reaction [11] to be at equilibrium.

Having identified the heterogeneous and homogeneous processes requiring consideration in general terms, the next section will deal with the formulation and solution of the corresponding mass-transport equations describing H^+ and HCO_3^- within the channel flow cell shown schematically in figure 1.

(*b*) *Mass transport in the channel flow cell*

The backwards implicit finite difference (BIFD) method (see, for example, Smith 1985) readily allows the theoretical description of the steady-state convective–diffusion–kinetic behaviour of species flowing under laminar conditions in a channel cell when the walls of the latter are subject to a variety of possible boundary conditions. The BIFD method was originally introduced by Anderson and co-workers for treating the case of simple electron-transfer at channel electrodes operated under transport-limited conditions (Anderson & Moldovenu 1984; Moldoveanu *et al.* 1984; Fosdick & Anderson 1986, 1988; Fosdick *et al.* 1986). The method was generalized by Compton and co-workers to cover electrode reactions involving coupled homogeneous kinetics, for which the transport-limited current, current–voltage and electron spin resonance (ESR) signal-flow rate behaviours were computed (Compton *et al.* 1988*a*, *b*, *c*). Here, we use the BIFD method to solve the general problem of the extent to which a channel electrode (held at a potential such that a reactant R (stable in solution) undergoes electrolysis at a transport-limited rate) is shielded from R as a consequence of its reaction at a portion of the wall of the channel flow cell located immediately upstream of the electrode. The method is developed to cover the case where R (= H^+) is involved in the homogeneous equilibrium relevant to the $CaCO_3$ dissolution problem.

Case (i): R *kinetically stable in solution*

Consideration of this case is useful towards the general $CaCO_3$ problem on two counts. Firstly, by comparison with the behaviour when R is unstable, it allows the delineation of the conditions under which homogeneous kinetics are negligible. This is particularly relevant to the dissolution of calcite, because, as discussed above, there is some uncertainty in the rate of dehydration of carbonic acid. Thus one needs to assess the conditions under which the effects of the homogeneous processes are negligible, and examine whether they are attainable experimentally. Secondly, the mathematical problem is soluble analytically for certain channel electrode or crystal geometries when the reaction of R at the crystal substrate is first (Unwin *et al.* 1989) or zero order (Appendix A) in R, and thus provides a means of testing the validity of the numerical strategy.

The coordinate system adopted to describe the channel cell–crystal–electrode geometry is defined in figure 2. With this notation, the steady-state convective–diffusion equation pertinent to the transport of R within the flow cell is given by

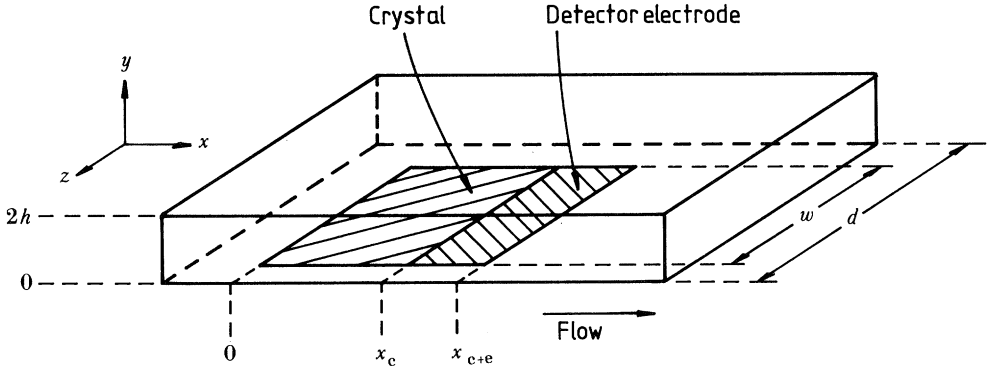

FIGURE 2. Coordinate system and notation defining the flow cell and crystal–electrode geometry.

$$\frac{d[R]}{dt} = 0 = D_R \nabla^2[R] - \left(v_x \frac{\partial[R]}{\partial x} + v_y \frac{\partial[R]}{\partial y} + v_z \frac{\partial[R]}{\partial z} \right), \tag{11}$$

where D_R is the diffusion coefficient of R and v_x, v_y and v_z are the solution velocities in the respective cartesian directions. After a lead-in length, written in terms of the Reynolds number, *Re* (Levich 1962):

$$l_e \approx 0.1 \times h \times Re, \tag{12}$$

where h is defined in figure 2 and *Re* is given by (Bird *et al.* 1960):

$$Re = v_0 h/\nu, \tag{13}$$

where v_0 is the velocity in the centre of the channel and ν is the kinematic viscosity, fully developed Poiseuille flow is established, such that

$$v_x = v_0[1 - ((y-h)^2/h^2)], \quad v_y = v_z = 0. \tag{14}$$

Provided that $h \ll d$ and $w < d$, equation (14) will apply across that part of the width of the channel in which the crystal and electrode are situated (see figure 2). Under conditions for which diffusion in the direction of convective flow and diffusional side-edge effects can be

neglected (Flanagan & Marcoux 1974; Aoki *et al.* 1987), the following approximation is reasonable (Levich 1962):

$$D_{\mathrm{R}}\nabla^2[\mathrm{R}] \approx D_{\mathrm{R}}\partial^2[\mathrm{R}]/\partial y^2, \tag{15}$$

and thus (11) reduces to

$$\frac{\partial[\mathrm{R}]}{\partial t} = 0 = D_{\mathrm{R}}\frac{\partial^2[\mathrm{R}]}{\partial y^2} - v_0\left[1-\frac{(y-h)^2}{h^2}\right]\frac{\partial[\mathrm{R}]}{\partial x}. \tag{16}$$

The boundary conditions relevant to the problem under consideration are:

$$x = 0(\text{all } y), \quad [\mathrm{R}] = [\mathrm{R}]^{\infty}, \tag{17}$$

$$0 < x \leqslant x_{\mathrm{c}}(y = 0), \quad D_{\mathrm{R}}\partial[\mathrm{R}]/\partial y = k_n[\mathrm{R}]^n, \tag{18}$$

$$0 < x \leqslant x_{\mathrm{c+e}}(y \to 2h), \quad \partial[\mathrm{R}]/\partial y = 0, \tag{19}$$

$$x_{\mathrm{c}} < x \leqslant x_{\mathrm{c+e}}(y = 0), \quad [\mathrm{R}] = 0. \tag{20}$$

Equation (18) describes the consumption of R at the crystal surface via an nth-order heterogeneous process in R, whereas (20) corresponds to the transport-controlled reaction of R at the electrode surface. For the special cases of $n = 0$ and $n = 1$, and under conditions in which the parabolic velocity profile may be linearized (i.e. when $[x_{\mathrm{c+e}}D/h^2v_0] \ll 1$) such that

$$v_x \approx 2v_0[1-(y-h)/h], \tag{21}$$

equation (16) may be solved analytically, with boundary conditions (17)–(20) to give the transport-limited current at the detector electrode as a function of k_n, the solution flow rate V_{f} ($= \frac{4}{3}v_0 hd$), and cell–crystal–electrode geometry. We have presented theory for the $n = 1$ case elsewhere (Unwin *et al.* 1989), and the result is quoted in Appendix A for comparison with the numerical results to be developed below. Appendix A also contains an analytical solution for the $n = 0$ case, so that the validity of the numerical method may be tested.

The solution of (16) with (17)–(20) using the BIFD method provides results of a much more general nature than may be obtained by using analytical methods of solution, allowing both the full parabolic velocity profile to be retained, and the consideration of any value of n. The method is described in Appendix B.

The validity of the BIFD calculation is demonstrated by comparing the results of the BIFD method for $n = 0$ and 1 to the corresponding analytical solution to these problems, as embodied by (A 36), (A 37), (A 40) and (A 41), under conditions for which the Lévêque approximation (21) is reliable, i.e. such that $x_{\mathrm{c+e}}D/h^2v_0 \ll 1$ (see above). By using values of $h = 0.02$ cm, $D = 10^{-5}$ cm^2 s^{-1}, $x_{\mathrm{c+e}} = 0.02$ cm, $d = 0.6$ cm, and $V_{\mathrm{f}} = 1.0$ cm^3 s^{-1} in the BIFD calculation, it can be seen that this constraint is satisfied.

The extent to which the electrode is shielded from the reactant, as a consequence of the reaction of the latter on the crystal, is best represented in terms of the shielding factor, S_{f}, defined by (A 28). $S_{\mathrm{f}}-\tilde{k}_0$ and $S_{\mathrm{f}}-\tilde{k}_1$ relations calculated numerically and analytically are compared in figures 3 and 4 for χ_{c} (defined by (A9)) = 0.5, 0.8 and 0.9. Excellent agreement between the numerical and analytical treatment of the problem for $n = 0$ and $n = 1$ is apparent, and this may be taken to vindicate the validity of the numerical approach. On a general note, it is clear from figures 3 and 4 that maximum sensitivity in the determination of $\tilde{k}_n$ from S_{f} will result from maximizing the value of χ_{c} (used experimentally).

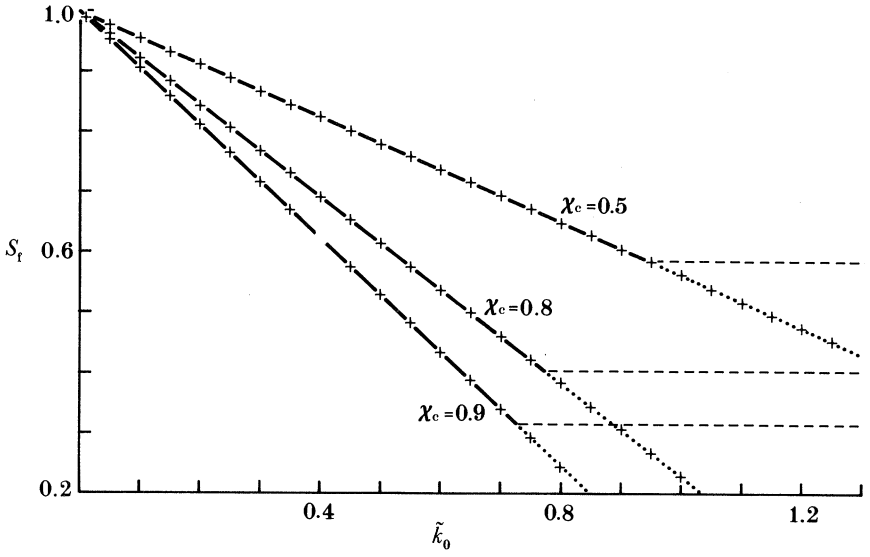

FIGURE 3. 'Working curves' relating the shielding factor, S_f, to $\tilde{k}_0$ for crystal–electrode geometries defined by χ_c = 0.5, 0.8 and 0.9: ——, analytical calculation; +, numerical BIFD calculation (for which the parameters are defined in the text).

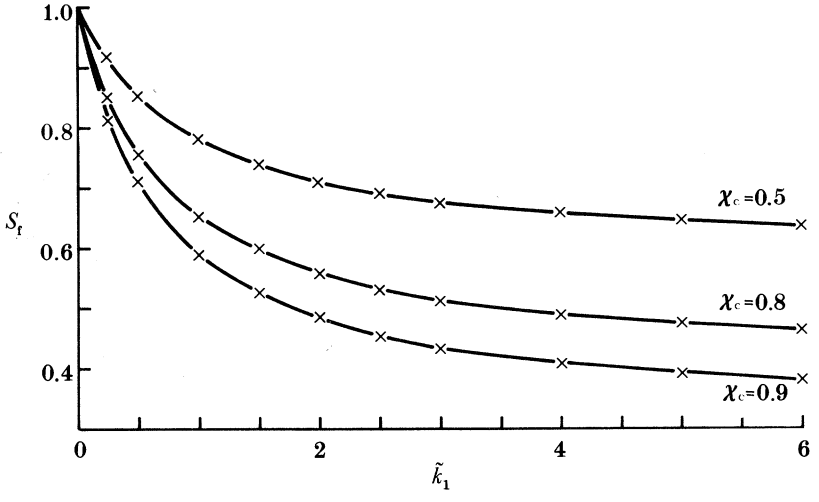

FIGURE 4. 'Working curves' relating S_f to $\tilde{k}_1$ for χ_c = 0.5, 0.8 and 0.9: ——, analytical calculation; ×, numerical BIFD calculations (parameters are defined in the text).

Besides being able to handle the full parabolic velocity profile describing the flowing solution in the channel, the BIFD method also facilitates the description of heterogeneous processes without any restriction on n. Thus we are able to produce $S_f - \tilde{k}_n$ working curves for $n = \frac{1}{2}$ and 2, as dictated by the reaction scheme proposed in the previous section. $\tilde{k}_n$ is defined by

$$\tilde{k}_n = [2h^2\,\mathrm{d}x_{c+e}/3V_f D_R^2]^{\frac{1}{3}} k_n([R]^\infty)^{n-1}.$$

The working curves shown in figures 5 and 6 were generated using the following parameters: $h = 0.01$ cm, $D = 7.6 \times 10^{-5}$ cm^2 s^{-1}, $[R]^\infty = 10^{-6}$ mol dm^{-3}, $x_{c+e} = 0.1$ cm, $d = 0.6$ cm,

$V_f = 0.1$, 1.0 and 10 cm^3 s^{-1}, which ensured that the Lévêque approximation would be valid, and thus allowed the presentation of the theoretical data in terms of a normalized rate constant, $\tilde{k}_n$. It is clear by comparing the forms of the working curves in figures 3–6 that discriminating between each of the processes should be easy using the proposed technique.

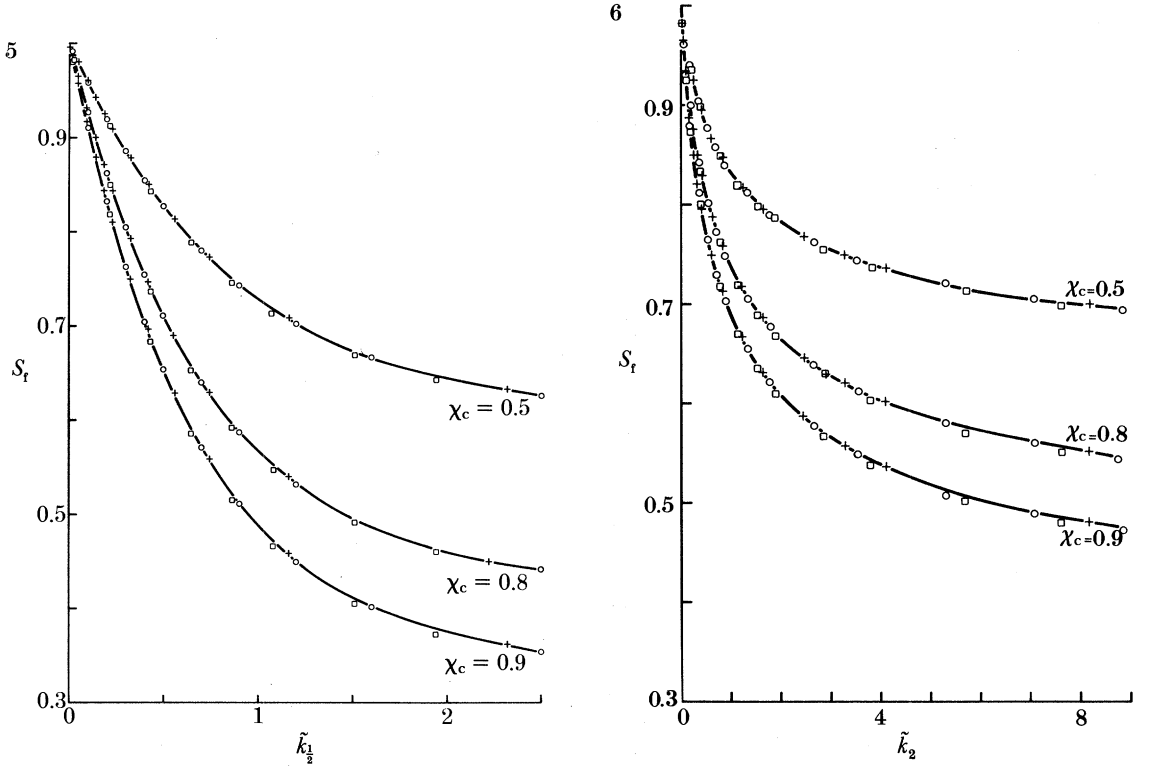

FIGURE 5. 'Working curves' of S_f against $\tilde{k}_{\frac{1}{2}}$ for $\chi_c = 0.5$, 0.8 and 0.9: ——, analytical calculation; numerical calculation using $x_c = 0.05$, 0.08 or 0.09 cm, $x_{c+e} = 0.1$ cm; $h = 0.01$ cm, $[R]^\infty = 10^{-6}$ mol cm^{-3}, $D = 7.6 \times 10^{-5}$ cm^2 s^{-1} and $V_f = 0.1$ (□); 1.0 (○) or 10.0 (+) cm^3 s^{-1}.

FIGURE 6. 'Working curves' of S_f against $\tilde{k}_2$ for $\chi_c = 0.5$, 0.8 and 0.9: ——, analytical calculation; numerical calculation using $x_c = 0.05$, 0.08 or 0.09 cm, $x_{c+e} = 0.1$ cm, $h = 0.01$ cm, $[R]^\infty = 10^{-6}$ mol cm^{-3}, $D = 7.6 \times 10^{-5}$ cm^2 s^{-1} and $V_f = 0.1$ (□), 1.0 (○) or 10.0 (+) cm^3 s^{-1}.

The ranges of rate constants that may be measured using the technique are delineated in table 4. The experimental parameters have been tuned within the region of those commonly available, to show the maximum and minimum rate constants that may be determined. We assume that S_f values must lie between 0.9 and 0.4, for the specific case of $\chi_c = 0.9$, if k_n is to be determined with reasonable accuracy (Unwin *et al.* 1989). It is clear that the technique permits the study of a wide range of reaction rates, and that both slow (approaching those levels that have previously only been studied with methods using powdered materials) and fast reactions may be investigated.

The BIFD method outlined above is readily modified to account for the case when the reaction at the crystal involves parallel heterogeneous processes (see Appendix B, table 9). With regard to the dissolution of calcite, particular significance is placed upon identifying the relative importance of the reaction with water as compared to that with H^+, as discussed in §2. We

TABLE 4. TYPICAL RANGE OF HETEROGENEOUS RATE CONSTANTS THAT MAY BE MEASURED USING THE FLOW CELL TECHNIQUE WITH AMPEROMETRIC DETECTION

(The data relate to $\chi_c = 0.9$, $d = 0.6$ cm and $D = 10^{-5}$ cm^2 s^{-1}, whereas the other parameters have been tuned to show the maximum and minimum rate constants (respectively at small (0.4) and large (0.9) S_f) that may be measured.)

S_f	$\tilde{k}_0$	$\tilde{k}_{\frac{1}{2}}$	$\tilde{k}_1$	$\tilde{k}_2$	h/cm	V_f/(cm^3 s^{-1})	$[R]^\infty$/(mol cm^{-3})	x_{c+e}/cm	k_0/(mol cm^{-2} s^{-1})	$k_{\frac{1}{2}}$/(mol$^{\frac{1}{2}}$ cm^{-2} s^{-1})	k_1/(cm s^{-1})	k_2/(mol^{-1} cm^4 s^{-1})
0.9	0.11	0.11	0.13	0.15	0.02	10^{-3}	10^{-7}	0.4	4.7×10^{-11}	1.5×10^{-7}	5.5×10^{-4}	6.4×10^{3}
0.9	0.11	0.11	0.13	0.15	0.02	10^{-3}	10^{-5}	0.4	4.7×10^{-9}	1.5×10^{-6}	5.5×10^{-4}	6.4×10^{1}
0.9	0.11	0.11	0.13	0.15	0.05	10^{-3}	10^{-7}	0.4	6.9×10^{-12}	2.2×10^{-8}	8.2×10^{-5}	9.4×10^{2}
0.9	0.11	0.11	0.13	0.15	0.05	10^{-3}	10^{-5}	0.4	6.9×10^{-10}	2.2×10^{-7}	8.2×10^{-5}	9.4
0.4	0.64	1.6	4.7	30	0.02	0.5	10^{-7}	0.1	9.4×10^{-10}	7.4×10^{-6}	6.9×10^{-2}	4.4×10^{6}
0.4	0.64	1.6	4.7	30	0.02	0.5	10^{-5}	0.1	9.4×10^{-8}	7.4×10^{-5}	6.9×10^{-2}	4.4×10^{4}
0.4	0.64	1.6	4.7	30	0.01	0.5	10^{-7}	0.1	1.5×10^{-9}	1.2×10^{-5}	1.1×10^{-1}	6.9×10^{6}
0.4	0.64	1.6	4.7	30	0.01	0.5	10^{-5}	0.1	1.5×10^{-7}	1.2×10^{-4}	1.1×10^{-1}	6.9×10^{4}

therefore need to consider parallel zero- and nth-order behaviour. In this context, equation (18) describing the flux of R at the crystal boundary becomes

$$0 < x \leqslant x_c(y=0), \quad D_R\,\partial[R]/\partial y = k_0 + k_n[R]^n \quad (n \neq 0). \tag{22}$$

The other boundary conditions are unchanged.

The addition of a second variable dictates that theoretical shielding factor behaviour is best represented in terms of S_f–$\tilde{k}_0$–$\tilde{k}_n$ plots. Figure 7*a* shows an example of a three-dimensional plot for $\chi_c = 0.9$ and $n = \frac{1}{2}$. Plots of $S_f/S_f(\tilde{k}_{\frac{1}{2}})$ and $S_f/S_f(\tilde{k}_0)$ against $\tilde{k}_0$ and $\tilde{k}_{\frac{1}{2}}$ (shown in figure 7*b*, *c*) highlight the kinetic zones in which the S_f-kinetic behaviour is characteristic of the half- or zeroth-order process, a value of $S_f/S_f(\tilde{k}_0) \to 1$ indicating that the zeroth-order process dominates, whereas $S_f/S_f(\tilde{k}_{\frac{1}{2}}) \to 1$ suggests that the behaviour tends to be half order.

We next consider the application of the method to describe the scheme involving the additional homogeneous reactions defined by reactions [11] and [12].

Case (ii): R = H^+; H^+-HCO_3^- *equilibration and* H_2CO_3 *dehydration in solution*

We need to rewrite (16) for both H^+ and HCO_3^-:

$$0 = D_{H^+}\frac{\partial^2[H^+]}{\partial y^2} - v_0\left[1-\frac{(y-h)^2}{h^2}\right]\frac{\partial[H^+]}{\partial x} - \frac{k_{H_2CO_3}[H^+]\,[HCO_3^-]}{K_{H_2CO_3}+[H^+]+[HCO_3^-]}, \tag{23}$$

$$0 = D_{HCO_3^-}\frac{\partial^2[HCO_3^-]}{\partial y^2} - v_0\left[1-\frac{(y-h)^2}{h^2}\right]\frac{\partial[HCO_3^-]}{\partial x} - \frac{k_{H_2CO_3}[H^+]\,[HCO_3^-]}{K_{H_2CO_3}+[H^+]+[HCO_3^-]}, \tag{24}$$

with the appropriate boundary conditions:

$$x = 0 \text{ (all } y), \quad [H^+] = [H^+]^\infty, [HCO_3^-] = 0, \tag{25}$$

$$0 < x \leqslant x_c(y=0), \quad D_{H^+}\partial[H^+]/\partial y = k_n[H^+]^n = -D_{HCO_3^-}\partial[HCO_3^-]/\partial y, \tag{26}$$

$$x_c < x \leqslant x_{c+e}(y=0), \quad [H^+] = 0, \partial[HCO_3^-]/\partial y = 0, \tag{27}$$

$$0 < x \leqslant x_{c+e}(y=2h), \quad \partial[H^+]/\partial y = \partial[HCO_3^-]/\partial y = 0. \tag{28}$$

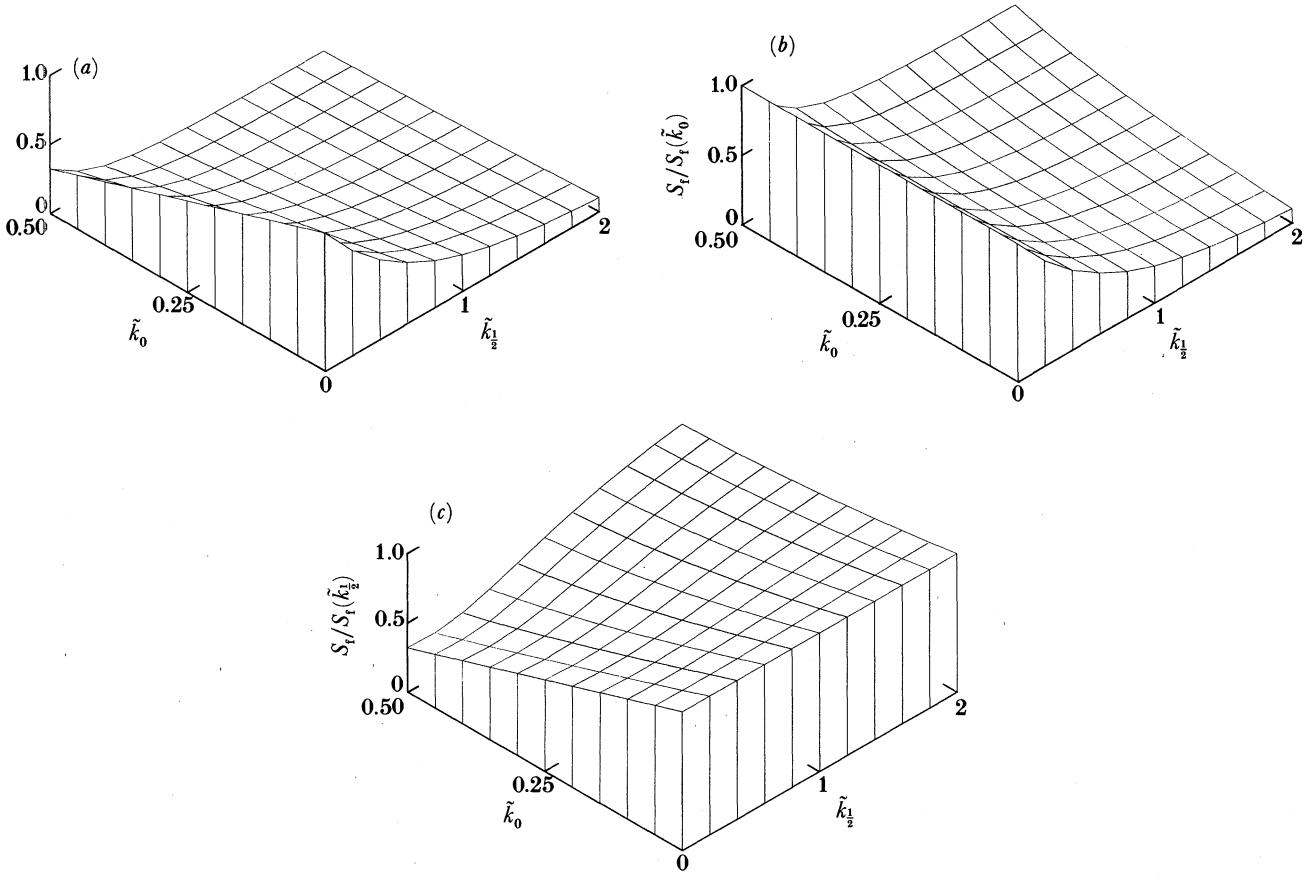

FIGURE 7. (*a*) Three-dimensional 'working plot' of S_f against $\tilde{k}_0$ and $\tilde{k}_{\frac{1}{2}}$ for $\chi_c = 0.9$. (*b*) $S_f/S_f(\tilde{k}_0)$ against $\tilde{k}_0$ and $\tilde{k}_{\frac{1}{2}}$: highlighting the zeroth-order characteristics of the S_f–$\tilde{k}_0$–$\tilde{k}_{\frac{1}{2}}$ behaviour for $\chi_c = 0.9$. (*c*) $S_f/S_f(\tilde{k}_{\frac{1}{2}})$ against $\tilde{k}_0$ and $\tilde{k}_{\frac{1}{2}}$: highlighting the half-order characteristics of the S_f–$\tilde{k}_0$–$\tilde{k}_{\frac{1}{2}}$ behaviour for $\chi_c = 0.9$.

Equation (26) implies that we will (initially) consider the heterogeneous process to be pure *n*th order. The details of the BIFD calculation for this case are given in Appendix B (table 10).

Under conditions for which the Lévêque approximation is valid, the theoretical results are conveniently presented as contour diagrams; lines of equal S_f as a function of $\tilde{k}_n$, and a normalized rate constant describing the dehydration of H_2CO_3,

$$\tilde{k}_{H_2CO_3} = k_{H_2CO_3}(4h^4 x_{c+e}^2 d^2/9D_{H^+} V_f^2)^{\frac{1}{3}}. \tag{29}$$

The latter has been defined in terms of D_{H^+}, but note that the theoretical results that follow relate to unequal diffusion coefficients for H^+ and HCO_3^- (7.6×10^{-5} and 1.0×10^{-5} $cm^2\ s^{-1}$ respectively). Figure 8*a*, *b* shows contour diagrams for $n = 1$, with $[H^+]^\infty$ of 10^{-3} and 10^{-4} M. The data relate to a crystal–electrode geometry, defined by $\chi_c = 0.9$, whereas $K_{H_2CO_3} = 3.06 \times 10^{-4}$ M (as predicted for the conditions of this study).

For the range of $\tilde{k}_{H_2CO_3}$ considered in figure 8 (10^{-2}–10^2), it is apparent that for $\tilde{k}_1 < 0.4$, an increase in $\tilde{k}_{H_2CO_3}$ (at constant $\tilde{k}_1$) produces a decrease in S_f. In essence, promoting the homogeneous reaction leads to a consumption of protons (in solution) in addition to those destroyed in the heterogeneous process. Hence, the flux of H^+ to the electrode (i.e. S_f) decreases. For larger values of $\tilde{k}_1$, however, S_f goes through a minimum as $\tilde{k}_{H_2CO_3}$ increases (at constant

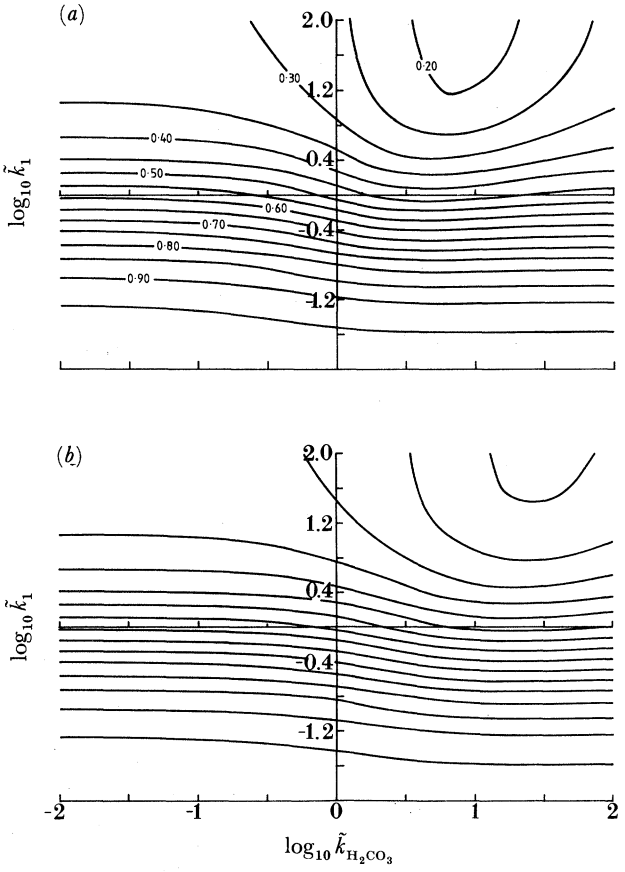

FIGURE 8. Contour plots of S_f against $\tilde{k}_1$ and $\tilde{k}_{H_2CO_3}$ (defined in terms of D_{H^+}) for $D_{H^+}/D_{HCO_3^-} = 7.6$ and $K_{H_2CO_3} = 3.06 \times 10^{-4}$ M. The data relate to $\chi_c = 0.9$ and $[H^+]^\infty = 10^{-6}$ mol cm^{-3} (*a*) and 10^{-7} mol cm^{-3} (*b*).

$\tilde{k}_1$). This is because the zone over which the homogeneous reactions occur is compressed closer to the surface of the crystal as $\tilde{k}_{H_2CO_3}$ is increased. Although the effect of this is to reduce the flux of H^+ at the crystal surface, the concentration of H^+ further from the surface is (increasingly) unperturbed from the value expected in the absence of homogeneous kinetics. Thus, because the concentration profile 'probed' by the detector electrode extends some distance away from the crystal in the direction normal to it (governed by x_c, x_{c+e}, D, V_f), the effect of the homogeneous processes tends to become 'masked' from the detector electrode. Figure 9*a*, *b*, *c* illustrates this point, displaying plots of

$$[[H^+]_{\tilde{k}_{H_2CO_3}=0} - [H^+]_{\tilde{k}_{H_2CO_3}=a}]/[H^+]_{\tilde{k}_{H_2CO_3}=0},$$

in the vicinity of a crystal, 0.09 cm long, for the specific case of a transport-controlled heterogeneous process. The data correspond to $[H^+]^\infty = 10^{-6}$ mol cm^{-3}; the other parameters being $V_f = 1.0$ cm^3 s^{-1}, $h = 0.02$ cm, $d = 0.6$ cm. Values of $\log_{10} a$ examined were -2.0, 1.0 and 2.5 (n and $K_{H_2CO_3}$ were as defined previously). Of course when the homogeneous process is negligible ($\log_{10} a = -2$), the distribution of H^+ barely differs from that in the absence of homogeneous kinetic complications. Increasing the influence of the homogeneous reaction perturbs the H^+-distribution, as compared with $[H^+]_{\tilde{k}_{H_2CO_3}=0}$, over a significant distance from the crystal surface, but this perturbation is confined closer to the surface for larger $\tilde{k}_{H_2CO_3}$ ($\log_{10} a = 2.5$; figure 9*c*).

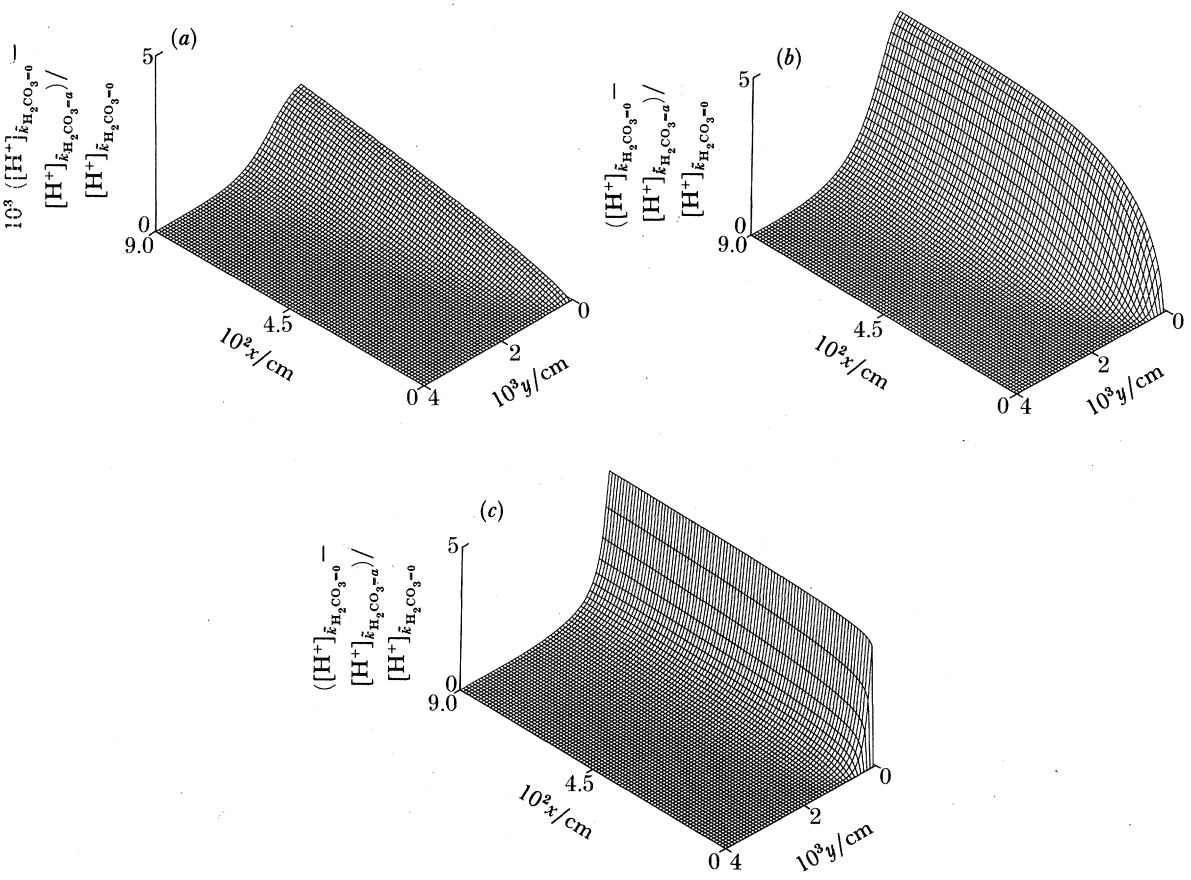

FIGURE 9. $([H^+]_{\tilde{k}_{H_2CO_3}=0} - [H^+]_{\tilde{k}_{H_2CO_3}=a})/[H^+]_{\tilde{k}_{H_2CO_3}=0}$ across $\frac{1}{10}$th of a channel of $h = 0.02$ cm, for the transport-controlled reaction of H^+ (bulk concentration 10^{-6} mol cm^{-3}) at a crystal of length 0.09 cm. The data was generated using $K_{H_2CO_3} = 3.06 \times 10^{-4}$ M, $V_f = 1.0$ cm^3 s^{-1} and relates to $\log_{10} a = -2$ (*a*), 1 (*b*) and 2.5 (*c*).

It follows from the above that the function $S_f(\tilde{k}_{H_2CO_3})/S_f(\tilde{k}_{H_2CO_3} = 0)$ against $\tilde{k}_{H_2CO_3}$ displays a minimum, whilst tending to unity as $\tilde{k}_{H_2CO_3}$ tends to zero or infinity. This behaviour is illustrated in figure 10 (generated by using $x_{c+e} = 0.1$ cm (i.e. $\chi_c = 0.9$) and the parameters used to produce figure 9*a*, *b*, *c*). At the same time, the flux of H^+ (normalized with respect to the flux predicted in the absence of homogeneous complications) at the crystal surface,

$$\frac{J_{H^+}}{J_{H^+}(\tilde{k}_{H_2CO_3} = 0)} = \int_0^{x_c} \frac{\partial[H^+]}{\partial y}\bigg|_{y=0} dx \Big/ \int_0^{x_c} \frac{\partial[H^+]}{\partial y}\bigg|_{y=0} dx, \tag{30}$$

varies from 1 to 0.5 as $\tilde{k}_{H_2CO_3}$ is increased. That is to say the behaviour switches from all protons being consumed on the surface to one proton consumed on the surface (for every two consumed overall).

That the behaviour described by figure 10 is seen to be most pronounced when the surface process is fast (see figure 8*a*, *b*) is, of course, because of the rate of the homogeneous process being both $[H^+]$- and $[HCO_3^-]$-dependent (equations (23) and (24)). The form of the homogeneous kinetic terms in these equations also explains why $dS_f/d\tilde{k}_{H_2CO_3} = 0$ tends to smaller $\tilde{k}_{H_2CO_3}$ for larger $[H^+]^\infty$, again evidenced by figure 8*a*, *b*. From the above discussion it also follows that $dS_f/d\tilde{k}_{H_2CO_3} = 0$ shifts to higher $\tilde{k}_{H_2CO_3}$, with the minimum broadening, as χ_c increases. This is a direct consequence of the detector electrode 'probing' the concentration

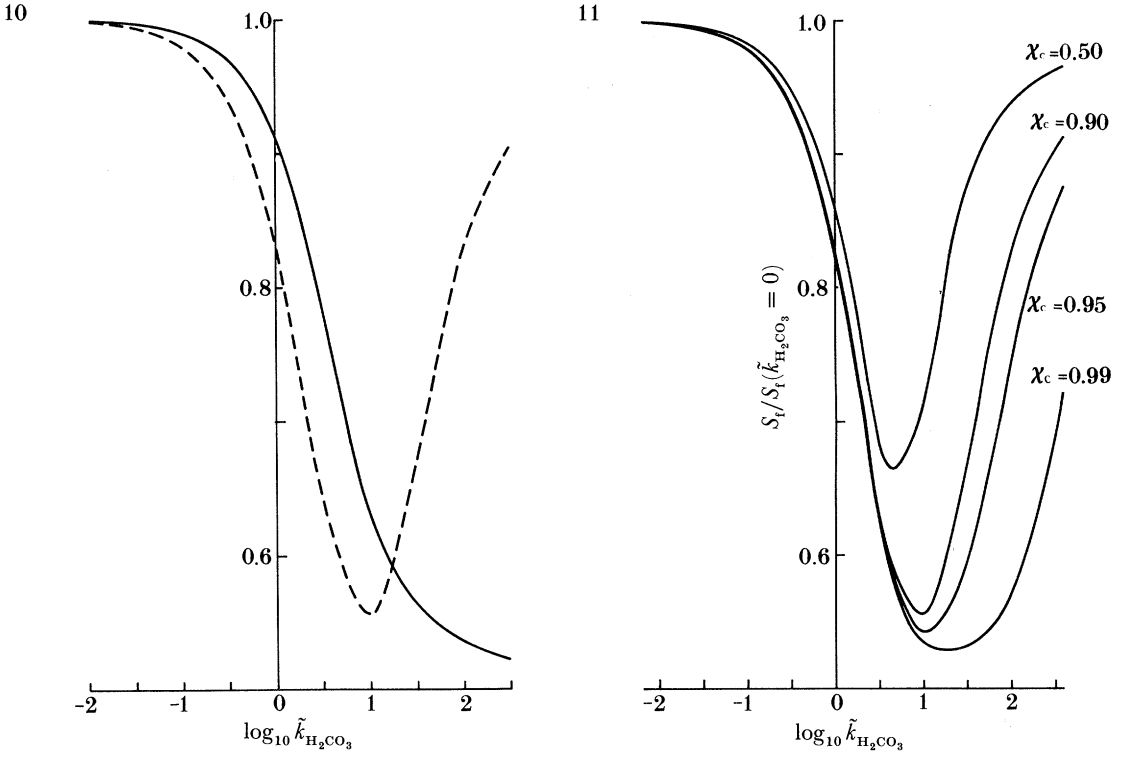

FIGURE 10. $S_f/S_f(\tilde{k}_{H_2CO_3} = 0)$ (dashed line) and $[J_{H^+}/J_{H^+}(\tilde{k}_{H_2CO_3} = 0)]$ (solid line) against $\tilde{k}_{H_2CO_3}$ for the transport-controlled reaction of H^+ at calcite for $\chi_c = 0.9$. The parameters used are as figure 9.

FIGURE 11. $S_f/S_f(\tilde{k}_{H_2CO_3} = 0)$ against $\tilde{k}_{H_2CO_3}$ for the transport-controlled reaction of H^+ at calcite with crystal–electrode geometries defined by $\chi_c = 0.99$, 0.95, 0.9 and 0.5.

profile closer to the crystal surface, as illustrated by figure 11, which shows $S_f/S_f(\tilde{k}_{H_2CO_3} = 0)$ as a function of $\tilde{k}_{H_2CO_3}$ for a transport-controlled reaction, with $\chi_c = 0.5$, 0.9, 0.95 and 0.99, i.e. $x_c = 0.05$, 0.09, 0.095 and 0.099 cm. The other parameters were as used to generate figure 10. The implications are that, at least in principle, one is able to tune the crystal–electrode geometry to minimize the effect of homogeneous kinetics on S_f–$\tilde{k}_n$ behaviour by working at high or low $\tilde{k}_{H_2CO_3}$. This would be of particular use when, for example, there was uncertainty in measured homogeneous rate constants, as is the case of the dehydration of carbonic acid (see above).

Returning to figure 8*a*, *b*, we can identify the regions over which the homogeneous reaction has little influence on the S_f–$\tilde{k}_1$ behaviour by generating contour diagrams with lines of equal $[S_f(\tilde{k}_{H_2CO_3} = 0) - S_f]/S_f(\tilde{k}_{H_2CO_3} = 0)$ as a function of $\tilde{k}_{H_2CO_3}$ and $\tilde{k}_1$. Figure 12*a*, *b* show the data of figure 8*a*, *b* presented in this way.

Through equation (29), using typical experimental values of $k_{H_2CO_3} = 20\ s^{-1}$, $h = 0.01$, $x_{c+e} = 0.4$ and $w = 0.6$ cm, with $10^{-3} \leqslant V_f \leqslant 5 \times 10^{-1}\ cm^3\ s^{-1}$, we deduce $0.65 \leqslant \tilde{k}_{H_2CO_3} \leqslant 40.7$. Unfortunately, within this range of $\tilde{k}_{H_2CO_3}$, $S_f \to S_f\ (\tilde{k}_{H_2CO_3} = 0)$, only for $S_f \approx 1$, (see figures 8 and 12). One thus concludes that it is not possible to 'outrun' the homogeneous kinetics with the present experimental set-up given the value of $k_{H_2CO_3}$. Therefore the homogeneous reaction needs to be included in the modelling of the experimental results.

Finally, we need to consider the effect of the parallel reaction between calcite and water,

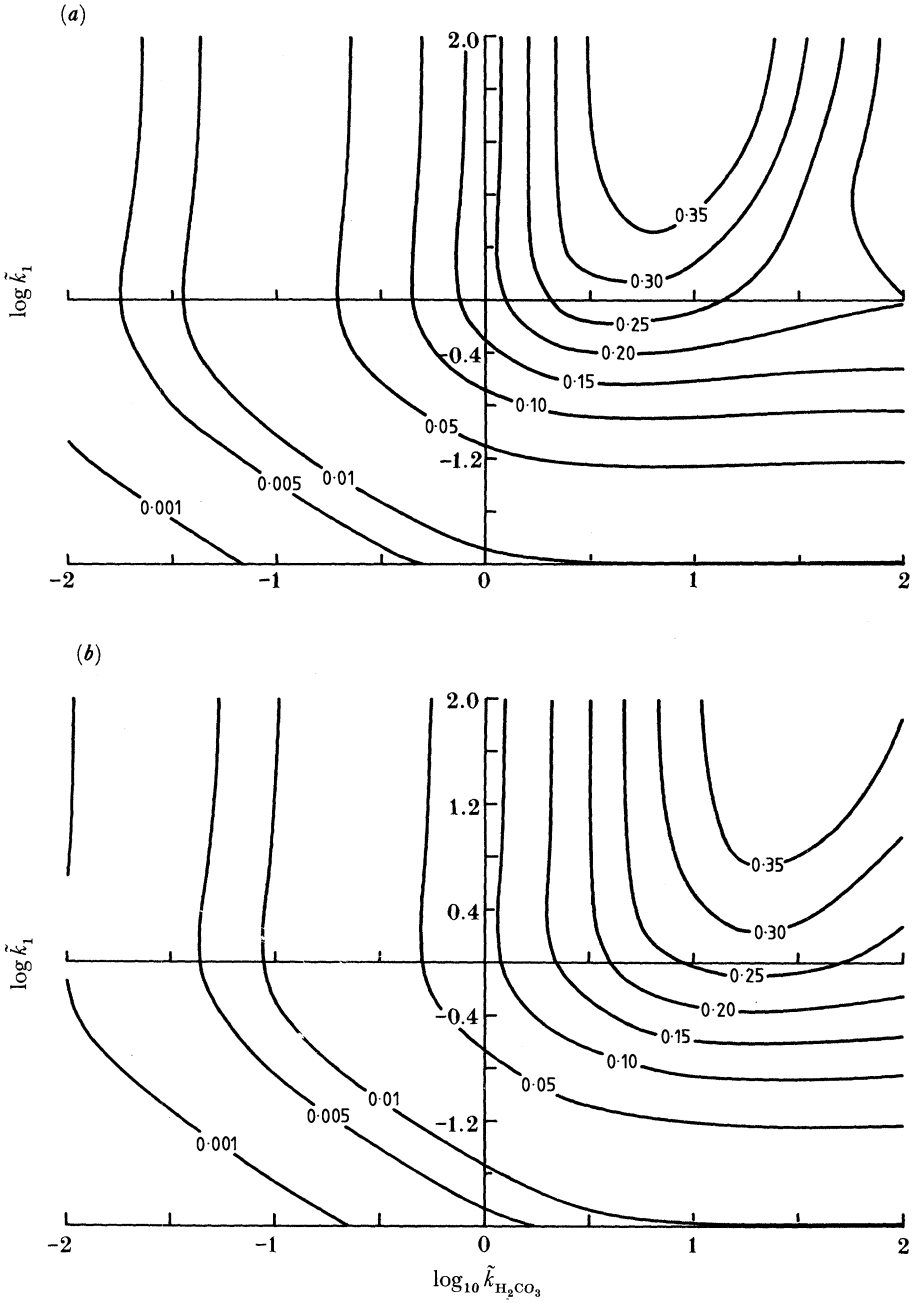

FIGURE 12. The data in figure 8*a*, *b* presented as $[S_f(\tilde{k}_{H_2CO_3} = 0) - S_f]/S_f(\tilde{k}_{H_2CO_3} = 0)$ against $\tilde{k}_{H_2CO_3}$ and $\tilde{k}_1$.

defined by reaction [3], on the S_f–$\tilde{k}_n$–$\tilde{k}_{H_2CO_3}$ behaviour for the reaction of H^+ with calcite. Compton & Daly (1986) have shown that the rate of this process in KCl solutions is particularly sensitive to the surface morphology of the crystal; rougher crystals are found to be more reactive. In the following paper, Compton & Pritchard have deduced that the reaction rate at high pH is given by the equation

$$R_{H_2O} = k_3'(1 - (K_{HCO_3^-} - [Ca^{2+}]_s\,[HCO_3^-]_s)/(K_{sp}^{CaCo_3}[H^+]_s)), \qquad (31)$$

where $K_{sp}^{CaCO_3}$ is the calcite solubility product and $K_{HCO_3^-}$ is the acid dissociation constant for HCO_3^-). The subscript s denotes that the concentrations of Ca^{2+}, HCO_3^- and H^+ are those at the surface of the crystal. One of the consequences of this equation is that the rate of the reaction between calcite and water will be flow rate dependent, i.e. at slower flow rates R_{H_2O} will decrease as a result of the back reaction being promoted through an increase in $[Ca^{2+}]_s$ and $[HCO_3^-]_s$ and decrease in $[H^+]_s$. Compton & Pritchard measured k_3' as 9.5×10^{-11} mol cm^{-2} s^{-1} for a crystal polished to 0.25 μm, and 2.8×10^{-10} mol cm^{-2} s^{-1} for a crystal treated with 10^{-3} M HCl solution for 30 min. Before extrapolating their results to the region pH 3–4, we need to assess the effect of (i) the higher concentration of H^+ that will be present at the crystal surface when dissolution in the acid régime is not transport controlled, and (ii) the differences (if any) in the crystal surface morphology for the two pH regions. To take account of the first point, we consider the fastest first-order process that may be studied with the flow cell technique, which is around 0.1 cm s^{-1} (see table 4), and calculate the concentration of H^+ on the crystal surface. This then corresponds to the minimum H^+ concentration we will encounter. The resulting profiles are shown in figure 13*a*, *b* for the two extremes of $[H^+]^\infty$ to be studied, i.e. 1×10^{-6} mol cm^{-3} and 2.5×10^{-7} mol cm^{-3}, and for typical experimental parameters of $x_c = 0.35$, $h = 0.01$, $d = 0.6$ cm, with $V_f = 5 \times 10^{-1}$, 5×10^{-2} and 10^{-3} cm^3 s^{-1}. It is clear that for $V_f \geqslant 5 \times 10^{-2}$ cm^3 s^{-1}, $[H^+]_s > 0.1\ [H^+]^\infty$ over the entire crystal. As an aside, the low surface concentration when $V_f = 10^{-3}$ cm^3 s^{-1} results, in part, from a trend

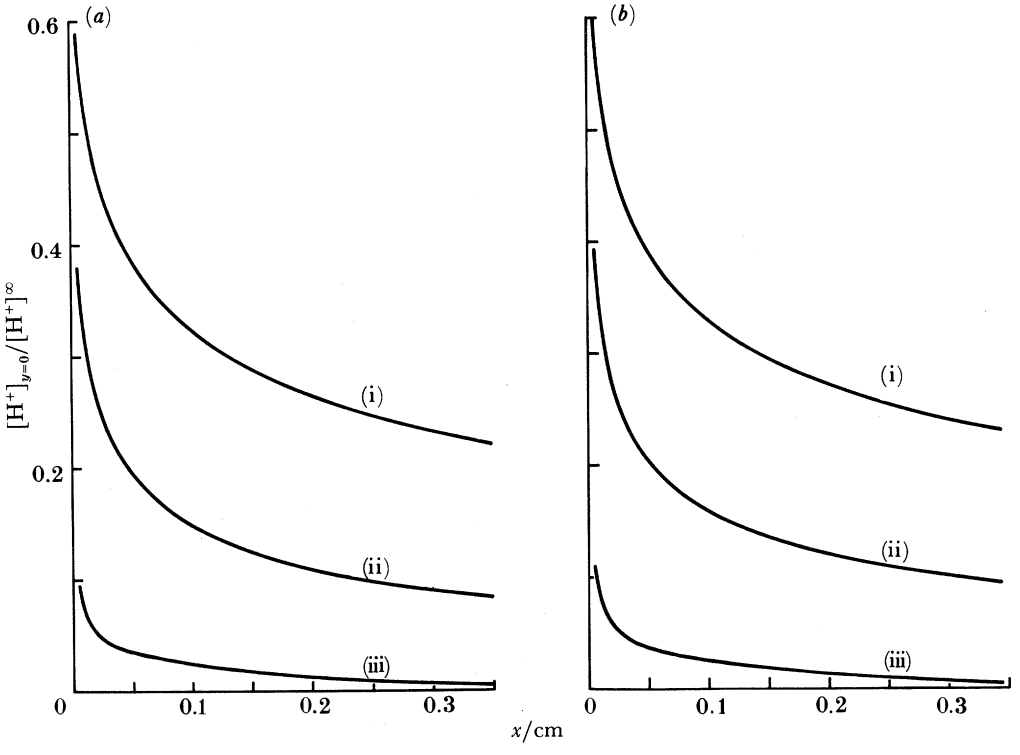

FIGURE 13. Surface concentration of H^+ along a crystal, 0.35 cm in length with channel parameters: $h = 0.01$, $d = 0.6$ cm, and $V_f = 5 \times 10^{-1}$ (i), 5×10^{-2} (ii) and 10^{-3} (iii) cm^3 s^{-1}. The data relate to $[H^+]^\infty$ of (*a*) 10^{-6} mol cm^{-3} and (*b*) 2.5×10^{-7} mol cm^{-3}.

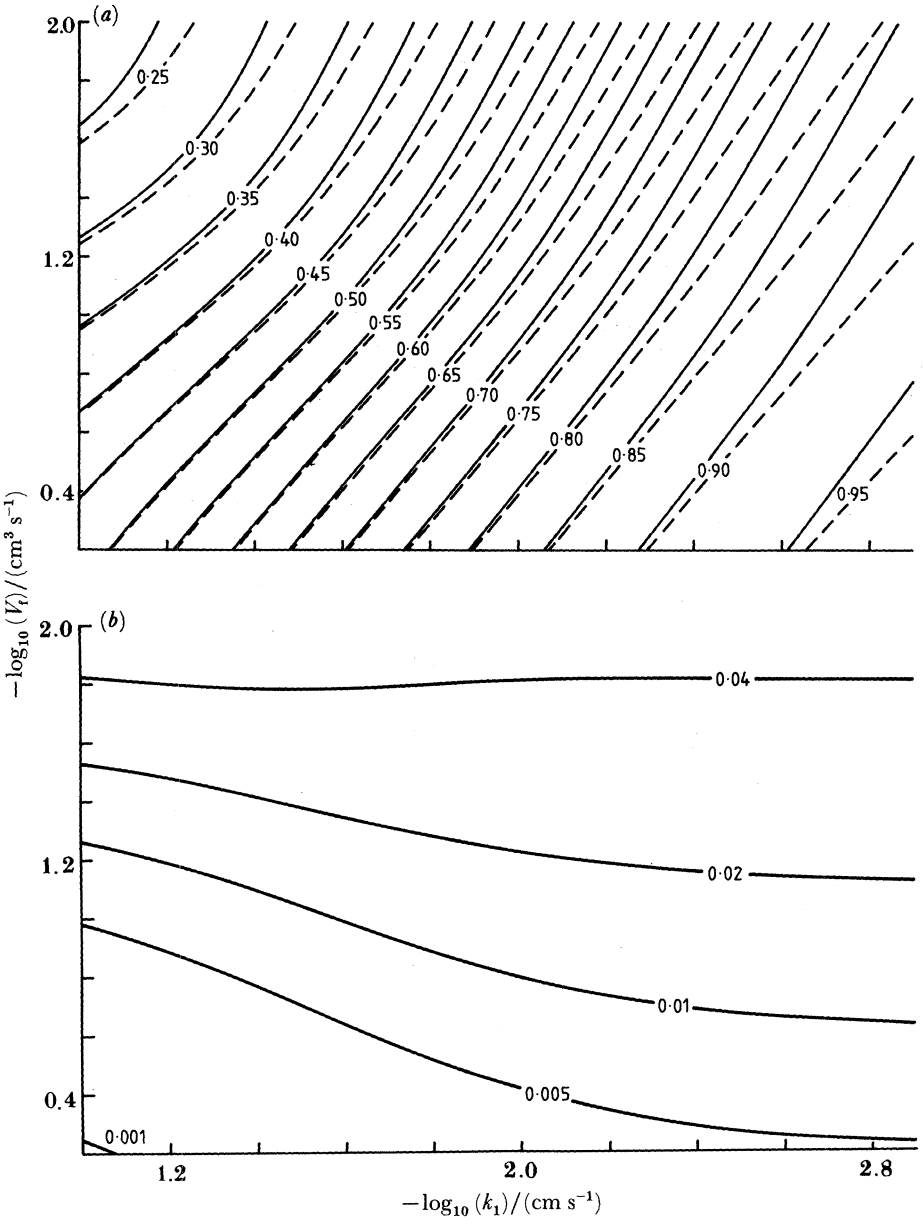

FIGURE 14. (*a*) Contour plot of S_f against $\log_{10} k_1$ and $\log_{10} V_f$ with the following parameters: $x_c = 0.35$, $x_{c+e} = 0.40$, $h = 0.01$, $d = 0.6$ cm, $[H^+]^\infty = 10^{-6}$ mol cm^{-3} and $k_0 = 0$ mol cm^{-2} s^{-1} (solid line); 7×10^{-10} mol cm^{-2} s^{-1} (dashed line). The constants describing the homogeneous reactions are as defined previously. (*b*) Contour plot of $\{S_f(k_0 = 0) - S_f(k_0 = 7 \times 10^{-10}\ \mathrm{mol\ cm^{-2}\ s^{-1}})\}/S_f(k_0 = 0)$ against $\log_{10} k_1$ and $\log_{10} V_f$. The parameters are as defined for (*a*).

towards thin-layer cell behaviour (giving rise to a value for S_f of 5.96×10^{-2}, which is essentially as predicted for a transport-controlled process, and thus of little use experimentally).

Now, equation (31) may be rewritten solely in terms of H^+, by considering the following mass-conservation equations, which apply with the approximation that $D_{H^+} = D_{HCO_3^-} = D_{H_2CO_3}$,

$$[H^+]^\infty \approx [H^+]_s + [HCO_3^-]_s\,(1 + (2[H^+]_s/K_{H_2CO_3})), \tag{32}$$

$$[Ca^{2+}]_s \approx [HCO_3^-]_s\,(1 + ([H^+]_s/K_{H_2CO_3})). \tag{33}$$

Thus

$$R_{H_2O} \approx k_3' \left(1 - \frac{K_{HCO_3^-}}{K_{sp}^{CaCO_3}[H^+]_s}\left[\frac{[H^+]^\infty - [H^+]_s}{1 + (2[H^+]_s/K_{H_2CO_3})}\right]^2\left[1 + \frac{[H^+]_s}{K_{H_2CO_3}}\right]\right). \quad (34)$$

Given the magnitudes of $K_{HCO_3^-}$ ($= 1.41 \times 10^{-10}$ mol dm^{-3}), $K_{sp}^{CaCO_3}$ ($= 1.33 \times 10^{-8}$ mol^2 dm^{-6}), $K_{H_2CO_3}$ and $[H^+]_s$ (shown in figure 13*a*, *b*), equation (34) reduces to

$$R_{H_2O} = k_3'. \quad (35)$$

That is to say that under the conditions used in this study the back reaction will be negligible, and thus the reaction rate will be expected to be flow rate independent, at least over the range of flow rates to be used. This brings us to the second point, which concerns the value of k_3' to be used. It follows from the work of Compton & Pritchard (1990) that a value of 2.8×10^{-10} mol cm^{-2} s^{-1} is appropriate.

Returning to figure 13*a*, *b*, and noting (*a*) the magnitude of $[H^+]_s$ and (*b*) the likely rate of the reaction of calcite with water (*ca.* 2.8×10^{-10} mol cm^{-2} s^{-1}), we may reasonably assume that the surface concentration of H^+ will not be affected by the levels of OH^- produced through this reaction. The reaction between calcite and water therefore merely serves to increase the concentration of HCO_3^- produced at the crystal surface. We may account for this theoretically by modifying boundary condition (26):

$$0 < x \leqslant x_c (y = 0), \quad D_{H^+}\partial[H^+]/\partial y = k_n[H^+]^n = -D_{HCO_3^-}(\partial[HCO_3^-]/\partial y) - k_0, \quad (36)$$

where k_0 is the rate of the reaction of H_2O with calcite (i.e. k_3' in the chemical scheme of §2). The changes to the BIFD calculation are described in Appendix B.

The effect of including the parallel reaction of calcite with water on S_f is seen in figure 14*a*, which shows a contour plot of S_f against $\log_{10} k_1$ and $\log_{10} V_f$ for $[H^+]^\infty = 10^{-3}$ M, with typical experimental parameters, as defined for the generation of figure 13*a*, *b*. The difference between the sets of data in figure 14*a* reflects the effect of the additional reaction between calcite and water (which has been assumed as 7×10^{-10} mol cm^{-2} s^{-1}, i.e. the mean of the results of Compton & Pritchard (1990) and Rickard & Sjöberg (1983)). It is clear from figure 14*b* that the parallel reaction has little influence on the S_f behaviour describing the reaction between calcite and H^+, particularly for fast flow rates or large k_1 or both.

4. Cell and flow system design

The flow cell used to carry out dissolution experiments is shown in figure 15. It comprises a cell unit and a crystal wall section. The channel unit itself is 40 mm long and 6 mm wide. The (minimum) depth is around 0.2 mm, but this can be adjusted by the addition of Teflon 'spacers' between the cell unit and cover plate. A precise value for the depth is obtained, each time the cell is assembled, from the slope of a Levich (I_{lim}–$V_f^{\frac{1}{3}}$) plot (equation (A 29)), using a species with known diffusion coefficient, which undergoes simple electron transfer, uncomplicated by homogeneous or heterogeneous kinetics.

For dissolution studies from the calcite cleavage plane, the crystal wall section simply consists of a single crystal, with an area of *ca.* 50 mm × 15 mm, which is freshly cleaved immediately before use. Work on crystals for which the cleavage plane is polished use smaller crystals (*ca.* 10 mm × 8 mm) cast in a block of araldite (*ca.* 50 mm × 15 mm).

The deeper duct sections at each end of the channel serve to equalize the pressure across the

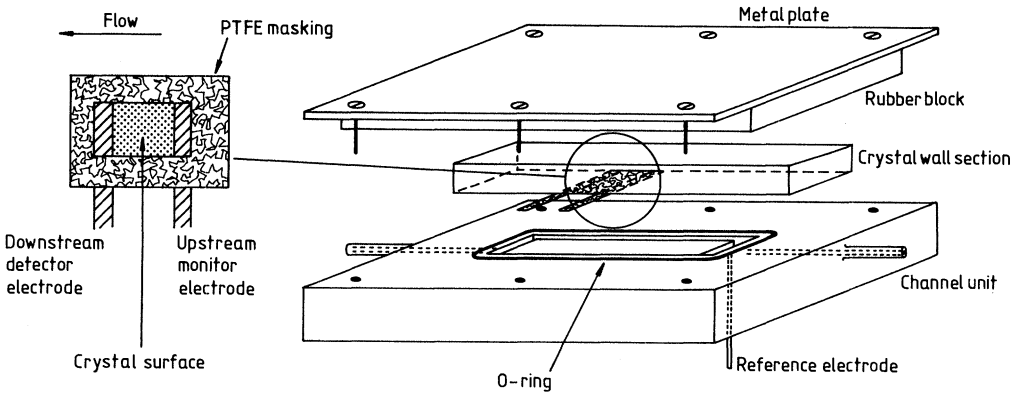

FIGURE 15. Flow cell for the study of calcite dissolution.

width of the channel. The upstream duct contains a silver wire coated with AgCl, which, in chloride solutions, acts as a silver–silver-chloride reference electrode (as part of the standard three-electrode system for the amperometric measurement of protons).

Two thin strips of platinum foil are deposited on the crystal, using a rubber based glue, around 3–4 mm apart, as shown in figure 15, and serve as working electrodes. The crystal surface upstream of the upstream electrode is masked from the solution with thin PTFE tape, and this electrode, which is approximately 2 mm long, thus serves to check the (bulk) concentration of protons before the solution passes over the calcite surface (equation (A 29)). The second electrode is around 0.5 mm long and acts as the detector electrode, measuring the concentration of protons after the solution has flowed over the crystal. Note that, with the above dimensions, the ratio of crystal-length : detector-electrode-length is around eight, thereby maximizing the sensitivity in the measurement of S_f, in accordance with the theoretical analysis presented above.

The edges of the crystal and electrodes are also insulated from the solution, so that the width of the exposed surface is *ca.* 4 mm. Thus once the cell is assembled, the interface is located within the region over which (14) is valid, deviations from this expression having been shown to occur over distances *ca.* h (Coles & Compton 1983) from the walls of the cell in the z direction.

The duct is produced by mating the channel and crystal wall units together through the application of mechanical pressure. The O-ring around the channel forms the necessary seal.

To meet the criterion regarding chemostatic control of the reaction, the flow system, into which the cell is plumbed, is designed so that solution flows to waste rather than recirculates. It consists of a glass reservoir (1 dm^3 capacity) and several metres of 1.5 mm bore PTFE tubing, jacketed with an argon purged tube to prevent the ingress of oxygen. A platinum gauze counter-electrode is located immediately downstream of the cell, ensuring that counter electrode products are flushed away and cannot interfere with the dissolution and electrode processes. Flow is achieved by gravity feed rather than pumping, the latter method being prone to produce pulsation problems (Brett & Oliviera Brett 1986). Deoxygenated electrolyte is fed from the reservoir via one of several calibrated capillaries capable of delivering a total flow rate range of 10^{-3}–5×10^{-1} $cm^3\ s^{-1}$. The adjustment of the rate of flow within each range is achieved by varying the height between the reservoir and the tip of the capillary, where the electrolyte runs to waste. With volume flow rates of this order, the cell dimensions defined above, and a

diffusion coefficient for H^+ of 7.6×10^{-5} cm^2 s^{-1} (Landsberg *et al.* 1961) lateral diffusion contributes by no more than 0.5% above the transport limited current predicted by the Levich equation (A 29) in the worst possible case, and so the approximation given by equation (15) is justified.

Electrical contact to the two working electrodes is facilitated by extending the foils beyond the edge of the crystal wall section as illustrated in figure 15. Thermostatting of the experiments is achieved by locating the cell and about one metre of the preceding tubing within an air thermostat, allowing temperature control to (25 ± 0.5) °C.

5. Experimental

(*a*) *Materials*

Solutions were made up by using water purified with an Elgastat (High Wycombe, Buckinghamshire, U.K.) UHQ apparatus, which provided water of resistivity greater than 10^7 Ω cm. BDH AnalaR grade reagents (potassium chloride, hydrochloric acid (1 M volumetric), potassium ferricyanide, sodium hydroxide) were used throughout. Semi-optical quality Iceland Spar crystals, which originated from Chihuahua, Mexico, were obtained from Richard Tayler Minerals (Cobham, Surrey, U.K.). Chemical analysis of this material is given in table 5, along with the corresponding analysis of similar material used by Sjöberg (1978). The superior quality of our calcite is apparent. Carbon dioxide and argon were supplied by the British Oxygen Company.

Table 5. Analysis of Iceland Spar crystals, and comparison with those used by Sjöberg (1978)

element	concentration/(p.p.m. by mass) this work	Sjöberg (1978)
Cd	< 5	< 30
Cu	< 5	< 5
Fe	< 10	< 50
Mn	< 5	500
Na	< 10	< 1000
P	< 50	< 100
Sb	< 20	< 30
Zn	< 5	< 300

(*b*) *Techniques*

(i) *Fabrication of Araldite–calcite crystal wall section*

These were produced by setting a single crystal of Iceland Spar in a block of Araldite epoxy resin (cast using Resin CY219 and hardener HY219). The dimensions are provided in §4. The resulting plate was polished firstly with 45 and 30 μm Bramet abrasive pads (Engis, Maidstone, Kent, U.K.) and then with a succession (down to 0.25 μm) of finer diamond-lapping compounds. The finished surface was rinsed with dilute hydrochloric acid (*ca.* 1 mM). Crystals of calcite were cast into cylinders of Araldite in a similar fashion, with the cleavage plane protruding from, but parallel to, the end of the cylinder. By freshly cleaving before use, rotating disc studies of dissolution from the cleavage plane could be effected.

PHILOSOPHICAL TRANSACTIONS OF THE ROYAL SOCIETY A MATHEMATICAL, PHYSICAL & ENGINEERING SCIENCES

(ii) *Amperometric measurements of* H^+

Simple experiments on the reduction of H^+ at a platinum channel electrode indicated that the response of the electrode to H^+ became progressively less reversible (and reproducible) unless the electrode was 'activated' (or 'potentiodynamically cleaned') by periodically taking the potential positive (to around +1300 mV against Ag/AgCl) for a few seconds (Hammett 1924; Yeager *et al.* 1953; Bockris *et al.* 1957; Shibata 1958; Will & Knorr 1960; Anson & King 1962; Breiter 1963; Dietz & Görr 1963; Gilman 1963; Shibata 1963; Frech & Kuwana 1964; Giner 1964; Hoare 1964; Brummer *et al.* 1965; Gilman 1965; Breiter 1966; Biegler 1967; Gilman 1967; James 1967; Heindrichs & Vielstich 1968; Adams 1969; Biegler 1969; Clark *et al.* 1972; Vielstich *et al.* 1972; MacDonald & Duke 1973; Stulik & Hora 1976; Woods 1976; Baruzzi *et al.* 1985; Johnson *et al.* 1986). After each anodic pulse, the electrode was stepped back to around −250 mV. The current–potential behaviour for the reduction of H^+ was then measured by scanning the potential cathodically at a rate such that the recorded behaviour was indistinguishable from that of the true steady-state (Compton & Unwin 1986*b*). In this way reproducible current–potential curves were obtained and, in particular, the transport-limited current-flow rate behaviour was found to be Levich in nature, giving a value for the diffusion coefficient of H^+ of 7.6×10^{-5} cm^2 s^{-1} in close agreement with a previous measurement (Landsberg *et al.* 1961).

The effect of CO_2 on the current–potential behaviour was studied by conducting the experiments described above under an atmosphere of CO_2, rather than argon. CO_2 is electroinactive at the potentials of interest, but reacts with an intermediate of the H^+ reduction, namely adsorbed H$^{\cdot}$, to give an adsorbed 'reduced' CO_2 species (Giner 1963; Brummer 1966; Breiter 1967; Biegler 1968; Breiter 1968; Brummer & Cahill 1968; Kamath & Hira Lal 1968; Brummer & Cahill 1969; Stonehart 1973; Sobkowski & Czerwinski 1974, 1975; Andreev *et al.* 1982; Beden *et al.* 1982; Baruzzi *et al.* 1983; Leiva *et al.* 1985; Mikhailova *et al.* 1985; Arvia & Giordano 1986; Rach & Heitbaum 1986). The effect of this was to accelerate the rate of 'deactivation' of the platinum electrode. However, provided the potential was pulsed positive (stripping the adsorbed species from the electrode) before the current–potential behaviour for the reduction of H^+ was recorded, reproducible curves could be obtained. One may readily conclude that amperometric detection of H^+ thus constitutes a valid means of following the calcite dissolution process, so long as the above points are noted.

(iii) *Microscopy*

Calcite crystal samples were gold-coated using an Edwards E4E12 Sputterer with diode sputter attachment. Film thicknesses so obtained were of the order of 20 nm. Micrographs of these samples were then taken with a Zeiss Universal R-Pol microscope in conjunction with either a Normarski DIC or Watson Interference Objective.

(iv) *Computations*

Computer programs were written in FORTRAN 77 and executed on the Oxford University VAX cluster (two dual-processor 8800s and two 8700s).

PHILOSOPHICAL TRANSACTIONS OF THE ROYAL SOCIETY A MATHEMATICAL, PHYSICAL & ENGINEERING SCIENCES

6. Verification of the experimental strategy

In this section we report the results of experiments designed to test the validity of the experimental approach. These fall into four areas:

(*a*) checking the hydrodynamics of the cell described in §4;

(*b*) determining the time required for a cleaved crystal to become fully reactive, i.e. for dissolution to reach the steady state;

(*c*) measuring the surface topography of a calcite surface subjected to dissolution, and considering the effect this will have on flow through the cell;

(*d*) estimating the effect of an indentation (resulting from prolonged dissolution) on channel flow, and thereby delineating the timescale over which experiments can be carried out.

(*a*) *Cell hydrodynamics*

The hydrodynamics of the cell described in §4 were verified by studying (i) the reduction of ferricyanide ions in aqueous solution (*ca.* pH 13) at a platinum channel electrode,

$$Fe(CN)_6^{3-} + e^- \rightleftarrows Fe(CN)_6^{4-},$$

and (ii) the reduction of H^+ at the same cell geometry.

Current–voltage curves were recorded over a wide range of flow rates and the resulting transport-limited currents measured. Analysis of the recorded behaviour in terms of the Levich equation (A 29) is provided in figure 16. The required cube-root dependence of I_{lim} on flow

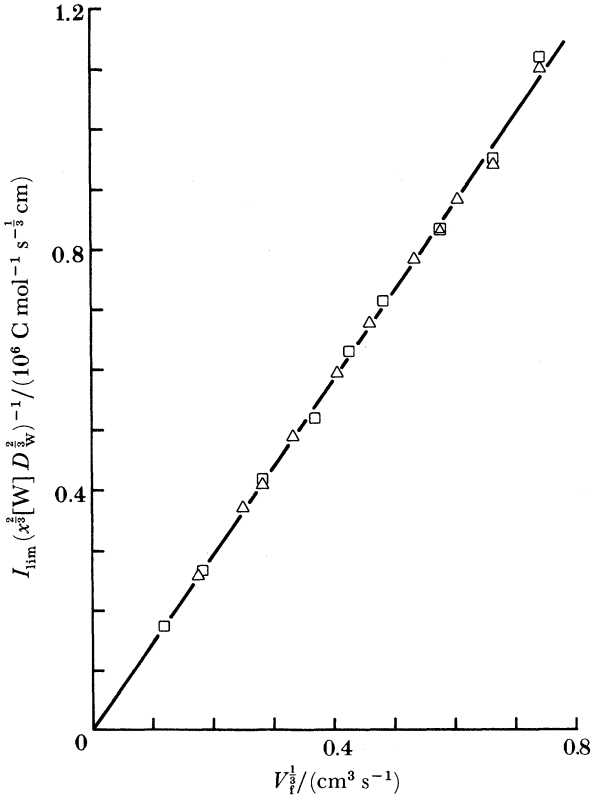

Figure 16. Transport-limited current-flow rate behaviour for the reduction of H^+ (□) and $Fe(CN)_6^{3-}$ (△) at a platinum channel electrode. W refers to H^+ or $Fe(CN)_6^{3-}$, and x to $(x_{c+e} - x_c)$.

rate is seen to be experimentally verified for both chemical systems. It is therefore reasonable to conclude that the hydrodynamics of the flow cell are as described theoretically in §3(*b*). Coupling the results in figure 16 to the known diffusion coefficients for ferricyanide and H^+, of 7.6×10^{-6} cm^2 s^{-1} (von Stackelberg *et al.* 1953) and 7.6×10^{-5} cm^2 s^{-1} (Landsberg *et al.* 1961) respectively, allowed a precise value of $h = 0.091$ mm to be calculated for this particular case.

(*b*) *Time for a calcite cleavage plane to become fully reactive*

Previous studies, using light microscopy to investigate the etching of calcite in acidic solutions, indicate that dissolution takes place (predominantly) at dislocations emerging at the crystal surface (Kieth & Gilman 1960; Thomas & Renshaw 1965) producing etch pits with a density of around 10^3 cm^{-2}. A high density (*ca.* 10^6 cm^{-2}) of smaller background pits is also observed (Thomas & Renshaw 1965), attributed to nucleation at ionic vacancies in the calcite lattice.

Given that dissolution results in the formation of etch pits, the question arises as to the time required for a cleaved calcite crystal to become fully reactive, i.e. for the pits to merge, so that steady-state dissolution is measured. This is readily answered by measuring the surface morphology of calcite crystals subjected to dissolution for various times. As these measurements were specifically confined to short times (a few minutes), the study was carried out using the rotating disc technique. Figure 17 shows a differential interference contrast (DIC) micrograph of a calcite surface, after rotation at 9 Hz in an aqueous 1 mM HCl solution for 60s. It is clear that even at this stage the surface is very nearly fully reactive.

The transformation of Unwin & Compton (1988), which relates the mass transport parameters of the channel and rotating disc electrodes,

$$x_d/\delta_d = 0.858(hD_{H^+}x_c/\bar{U})^{\frac{1}{3}}/0.643W^{-\frac{1}{2}}\nu^{\frac{1}{6}}D_{H^+}^{\frac{1}{3}} = 1, \tag{37}$$

where W is the disc rotation speed (hertz), allows the rate of mass-transport in the flow cell to be estimated for which the topography shown in figure 17, plate 1 would result. In equation (37), x_d and δ_d represent the average diffusion layer and diffusion layer thicknesses at the channel and rotating disc electrode, respectively (determined from the expressions for the transport-limited current at the two electrodes). We deduce that the conditions used to produce the surface shown in figure 17, corresponds to $x_d = 4.21 \times 10^{-3}$ cm, and thus to $V_f = 2.7 \times 10^{-2}$ cm^3 s^{-1} for a cell geometry with $h = 0.01$, $x_c = 0.35$ and $w = 0.6$ cm. We therefore conclude that provided the solution is passed over the crystal for the first few minutes of the experiment at a reasonable flow rate (10^{-2}–10^{-1} cm^3 s^{-1}), measurements made thereafter will pertain to steady-state dissolution.

(*c*) *Topography of a dissolving calcite surface*

Examining the extent to which the crystal surface is roughened as a consequence of dissolution is essential, to check that this will not disrupt the desired flow cell hydrodynamics, which were shown to operate in an assembled cell in §6*a*.

Interference light microscopy constitutes a powerful method of highlighting very shallow features (Tolansky 1973, p. 210). The interference effect resulting from the recombination of (monochromatic) light reflected from the sample, with that from a reference plane, leads to a contour map of interference fringes on the image; the height changing by $\frac{1}{2}\lambda$ in moving from fringe to fringe. Given that, in principle, it ought to be possible to determine the position of a

fringe down to $\frac{1}{10}$ of its width (Haynes 1984), this technique allows vertical surface changes of *ca.* 30 nm (for $\lambda = 590$ nm) to be measured. Although this degree of precision may be more difficult to attain with very irregular surfaces, it is clear that the method is ideal for the purpose described here.

Figure 18, plate 1, shows an interferogram of a calcite surface subjected to dissolution under identical conditions to that in figure 17. The surface is observed to be essentially flat: one fringe covers the entire plane. The surface morphology resulting from more prolonged dissolution is illustrated in figure 19*a–d*, plates 2 and 3. These are interferograms taken at selected areas down a crystal (total length 6.54 mm) subjected to dissolution in 2 mM HCl for 50 minutes in a channel flow cell characterized by $h = 0.02$ cm, and in which a solution flow rate of $V_f = 7.4 \times 10^{-2}$ cm^3 s^{-1} was used. The overall surface roughness is seen to be no greater than four fringes (i.e. less than 1.2 μm) in any area. This is around the level to which a hydrodynamic electrode is generally polished to ensure laminar flow conditions, and we thus conclude that the surface morphology resulting from dissolution will not perturb the cell hydrodynamics.

(*d*) *The effect of an indentation on channel flow*

Section 6(*c*) served to illustrate that the topography of the dissolving calcite surface would not influence the cell hydrodynamics. It also needs to be recognized, however, that the dissolution process will lead to the formation of an indentation in the channel wall (see, for example, the downstream edge of figure 19*d*). This will limit the timescale over which measurements can be made.

That indentation formation has a negligible effect on transport to (and thus the signal at) the detector electrode can readily be checked, at the end of a particular run, by measuring the transport-limited current for the reduction of ferricyanide ions, as described in §6*a*. It can also be shown that the size of the indentation, resulting from dissolution, is likely to be negligible, as follows. The geometry of the calcite cleavage rhomb (see, for example, Reeder 1983) allows

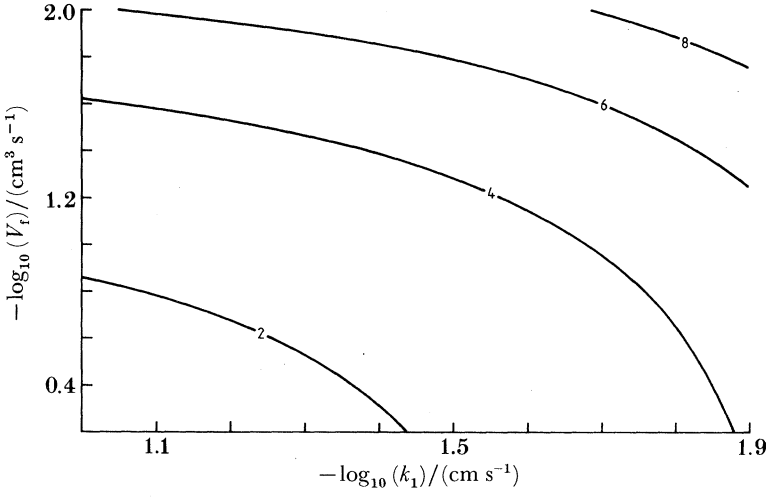

FIGURE 20. Time required (as a function of V_f and k_1) for an indentation with an average depth of 6×10^{-4} cm to be formed in a channel as a result of dissolution from the calcite crystal. The parameters are as for figure 14*a*. The figures on the contours refer to 10^4 s.

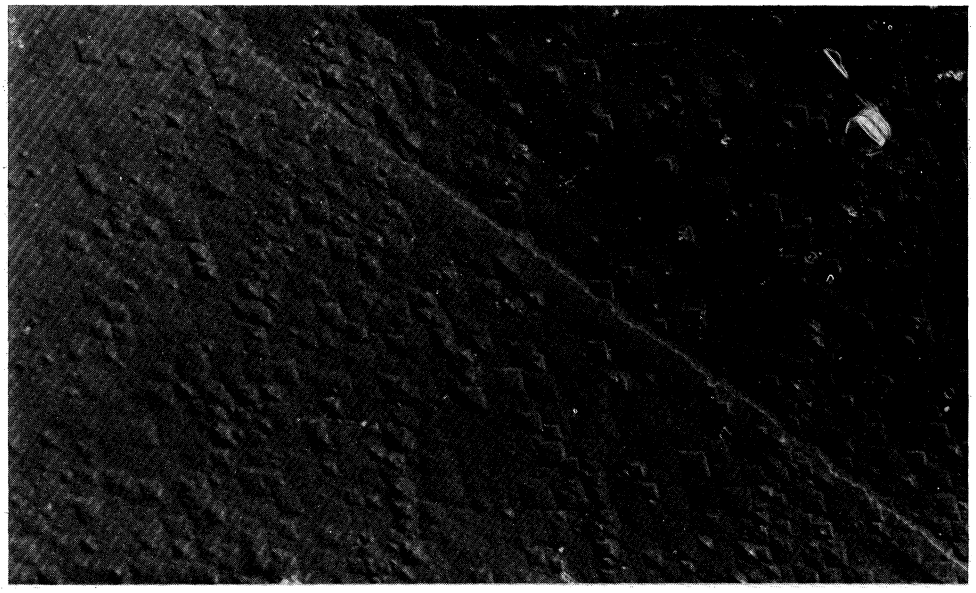

FIGURE 17. DIC micrograph (179×) of a cleaved calcite crystal, after rotation at 9 Hz in an aqueous 1 mM HCl solution for 60 s.

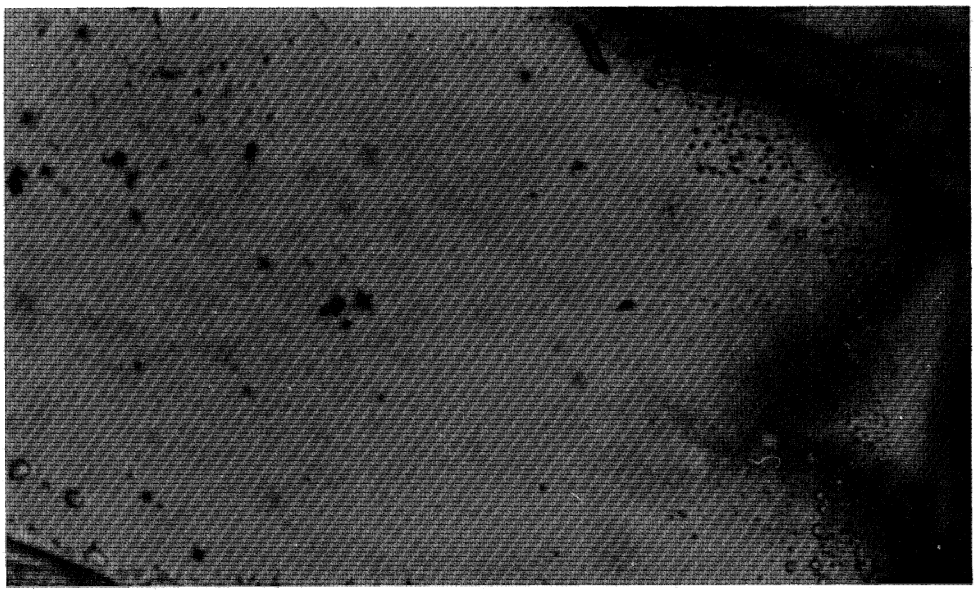

FIGURE 18. Interferogram (222×) of the surface shown in figure 17.

(*Facing p.* 30)

PHILOSOPHICAL TRANSACTIONS OF THE ROYAL SOCIETY A MATHEMATICAL, PHYSICAL & ENGINEERING SCIENCES

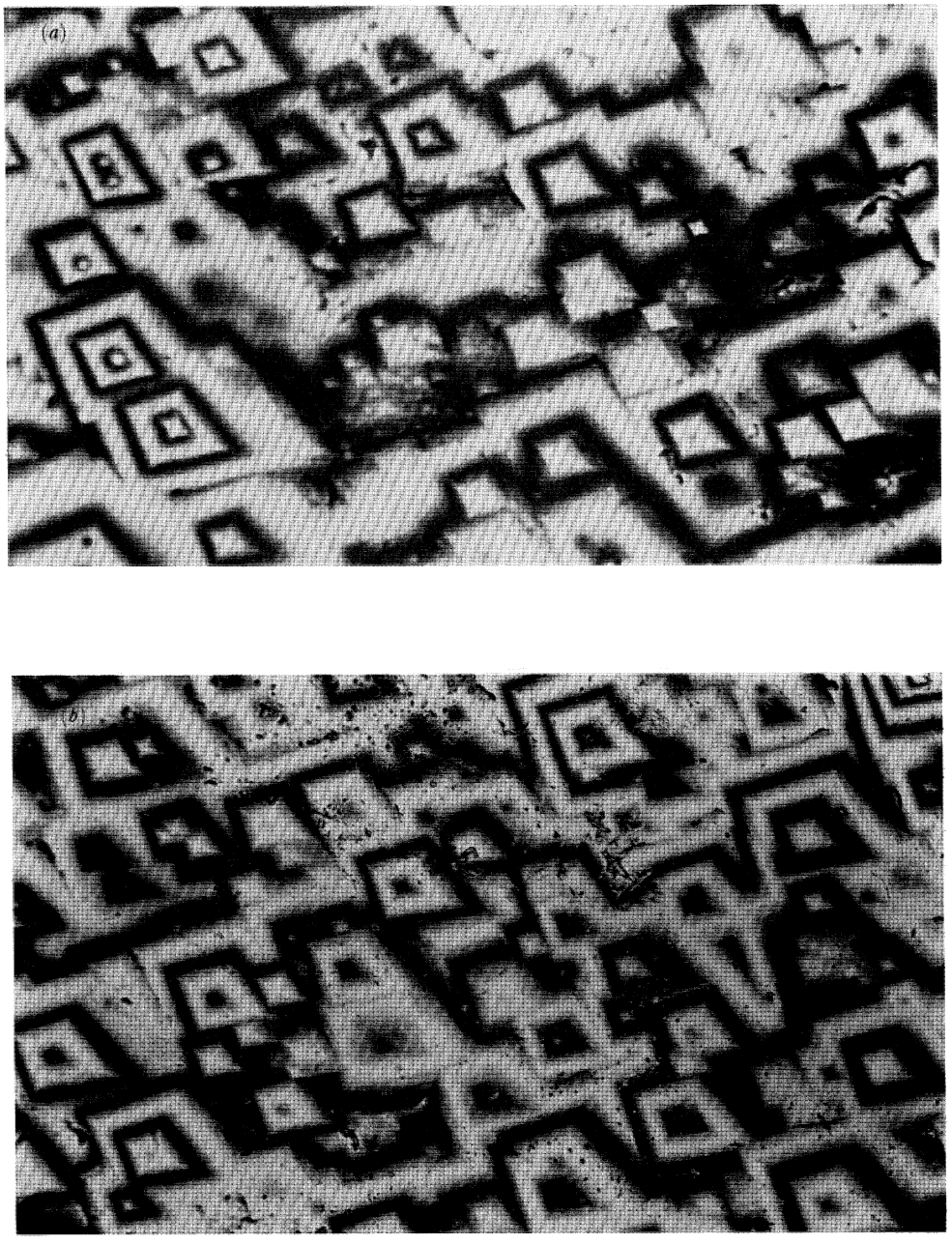

FIGURE 19*a*, *b*. For description see opposite.

PHILOSOPHICAL TRANSACTIONS OF THE ROYAL SOCIETY A MATHEMATICAL, PHYSICAL & ENGINEERING SCIENCES

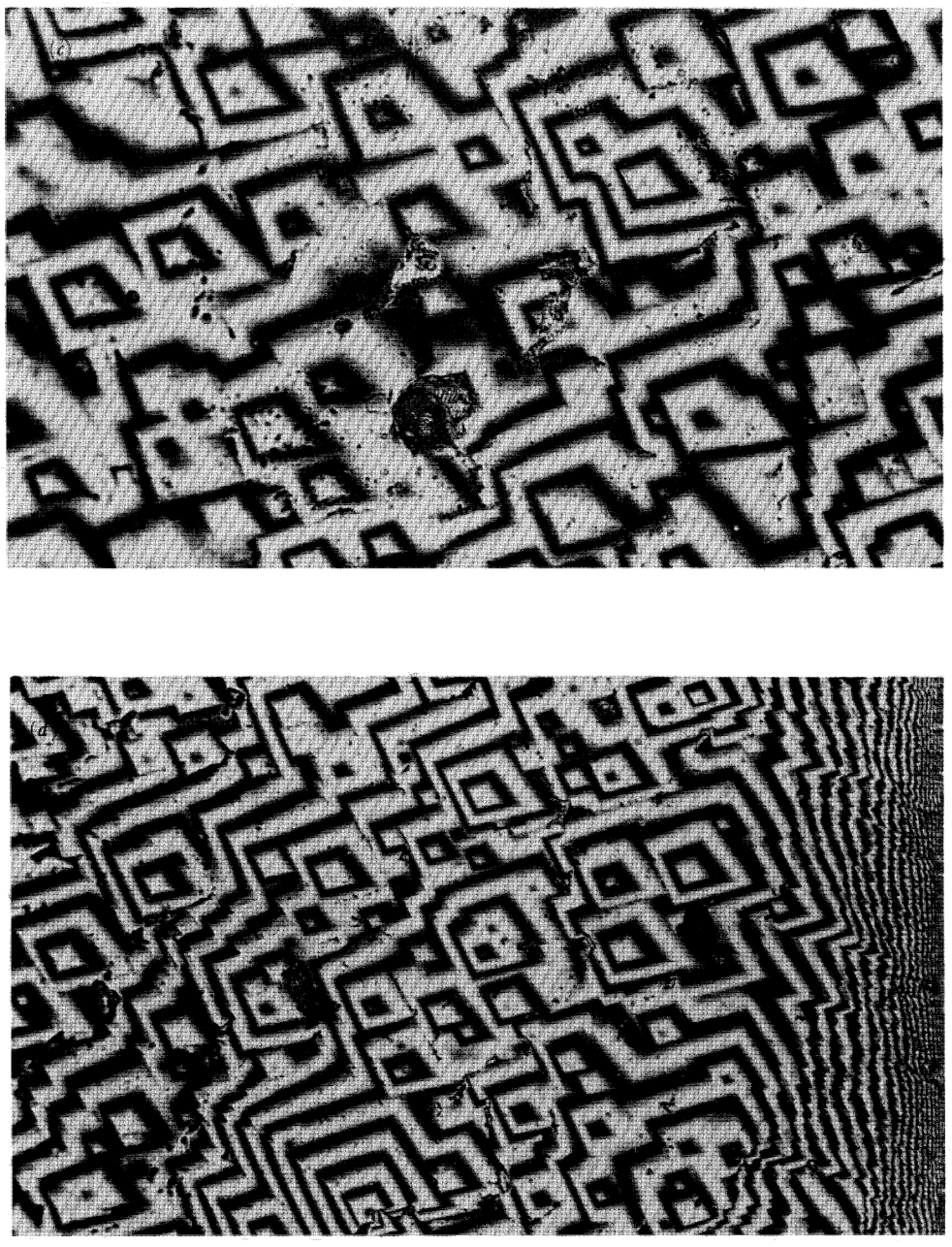

FIGURE 19. Interferograms (222 ×) at selected areas along a calcite cleavage plane subjected to dissolution in 2 mM HCl for 50 m in a channel flow cell characterized by $h = 0.02$ cm, $d = 0.6$ cm, and in which a solution flow rate of 7.4×10^{-2} cm^3 s^{-1} was used. The regions illustrated are: (*a*) 0.28–0.85 mm; (*b*) 2.56–3.13 mm; (*c*) 4.26–4.83 mm; (*d*) 5.97–6.54 mm from the upstream edge of the crystal. Flow is from left to right.

PHILOSOPHICAL TRANSACTIONS OF THE ROYAL SOCIETY A MATHEMATICAL, PHYSICAL & ENGINEERING SCIENCES

the computed dissolution flux (averaged over the crystal) to be expressed in terms of a vertical dissolution velocity and thus indentation depth as a function of time. Figure 20 is an illustrative example of the time required for an indentation with an average depth of 6×10^{-4} cm to be formed in a channel of $h = 0.01$ cm (i.e. for the overall height of the channel to increase by 3 %), as a consequence of calcite dissolution by 1 mM H^+. The range of k_1 and V_f have been chosen so that they relate to the worst possible cases to be encountered (with regard to shortening the time available for making measurements). It is clear from figure 20 that more than adequately long times should generally be available for data acquisition before problems due to indentation formation are encountered.

7. Results and discussion

The flow cell described above was used to study the dissolution of calcite in aqueous solutions of HCl. Three separate concentrations were used: 0.25×10^{-6}, 0.50×10^{-6} and 1.00×10^{-6} mol cm^{-3}. In each case inert supporting electrolyte in the form of KCl (1 M) was added. The monitor electrode–crystal–detector electrode geometries used for each run are shown in table 6. For each concentration of HCl, the transport limited current relating to the reduction of H^+ was measured as a function of flow rate, first for the upstream electrode and then for the detector electrode. After each dissolution experiment, a solution of potassium ferricyanide was passed through the flow system and the limiting current on the detector electrode, relating to one-electron reduction to ferrocyanide, was measured. Figure 21 *a–c* shows the results of the experiments with both H^+ and $Fe(CN)_6^{3-}$. In these figures data is presented in the form of plots of $I_{lim}/x^{\frac{2}{3}}[W]^{\infty} D_W^{\frac{2}{3}}$ ($W = H^+$ or $Fe(CN)_6^{3-}$; $x = x_m$ or $x_{c+e} - x_c$) against (flow rate)$^{\frac{1}{3}}$. The form of the ordinate/abscissa is suggested by the Levich equation and allows the comparison of data obtained on different species and with different flow geometries. In the case where the species participating in the electrode reaction is not involved in any heterogeneous or homogeneous kinetic processes within the flow cell, straight line behaviour is expected for the data shown in figure 21 *a–c*.

It is apparent from figure 21 *a–c* that the reduction of both H^+ at the upstream ('monitor') electrode and $Fe(CN)_6^{3-}$ at the detector electrode show 'Levich' behaviour, and this both confirms that the hydrodynamics within the flow cell are as suggested, and permits the calculation of an accurate value of h for the assembled flow cell. Moreover, the fact that 'Levich' behaviour persists even after the dissolution experiments have been completed shows that any roughening (formation of etch pits) of the crystal surface that might arise during dissolution is of such dimensions as have no influence over the cell hydrodynamics and hence no perceptible influence on the mathematical model detailed above.

We now consider the data shown for the reduction of H^+ at the detector electrode. It is clear that the flux of protons reaching this electrode is less than expected on the basis of the Levich equation and this may be attributable to the loss of H^+ through reaction at the calcite surface upstream of the detecting electrode. The theory given above permits the calculation of the $I_{lim}/V_f^{\frac{1}{3}}$ behaviour if it is assumed that the reaction of H^+ with $CaCO_3$ is transport controlled. The predicted behaviour, assuming $k_{H_2CO_3} = 20$ s^{-1} and $K_{H_2CO_3} = 3.06 \times 10^{-4}$ M is shown in figure 21 *a–c*. There are marked deviations of experiment from theory, particularly at fast flow rates, and this is indicative of a finite heterogeneous rate of the reaction concerned. The rates of mass transport in the flow cell are sufficiently high that the rate-limiting step is not mass

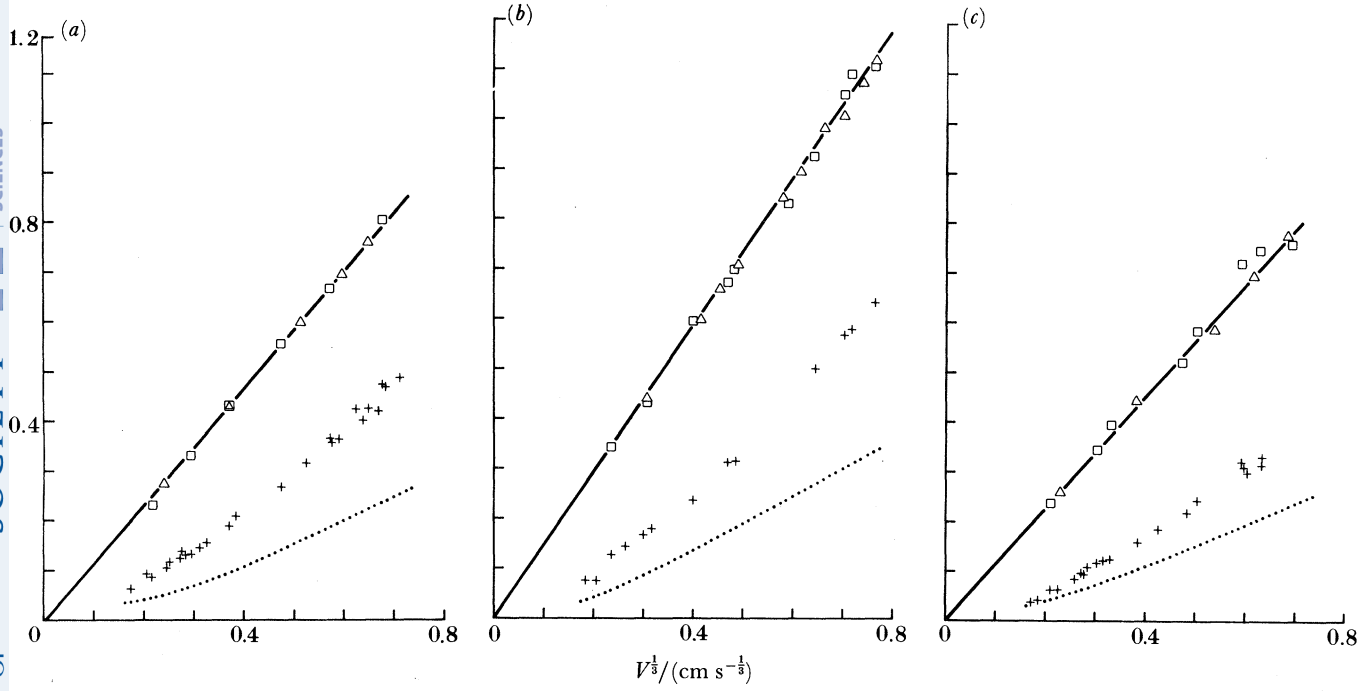

FIGURE 21. Transport-limited current-flow rate behaviour for the reduction of: H^+ at the monitor electrode (□); H^+ at the detector electrode (+); $Fe(CN)_6^{3-}$ at the detector electrode (△), for $[H^+]^\infty = 10^{-6}$ mol cm^{-3} (*a*), 5×10^{-7} mol cm^{-3} (*b*) and 2.5×10^{-7} mol cm^{-3} (*c*). The dotted lines show the behaviour expected for H^+ reduction at the detector electrode if the reaction between calcite and H^+ was transport-controlled.

TABLE 6. FLOW CELL PARAMETERS USED TO STUDY THE DISSOLUTION OF CALCITE IN 1, 0.5 AND 0.25 MM AQUEOUS HCl SOLUTIONS

$[H^+]$/mM	x_m/cm	x_c/cm	x_{c+e}/cm	h/cm
1.0	0.133	0.313	0.368	0.0129
0.5	0.114	0.398	0.451	0.0091
0.25	0.130	0.337	0.389	0.0134

transfer, as in all previous studies, but rather the rate of reaction of H^+ at the crystal. Accordingly the deviation from transport-controlled theory is greatest at faster flow rates.

For the purpose of analysis, we concentrate on the data obtained at fast flow rates, as this is likely to provide the most veracious heterogeneous rate law and rate constant for the following reasons:

(1) from the working curves presented in §3(*b*) we observed that $(dS_f/d\tilde{k}_n)$ was largest at small $\tilde{k}_n$ (i.e. large V_f);

(2) the effect of the parallel reaction with water is more likely to be negligible under such conditions (see figure 14*b*);

(3) the boundary condition, described by (36), used in the theory is more likely to hold (see above);

(4) the Lévêque approximation will be valid, and so measured values of S_f can be converted to a normalized rate constant $\tilde{k}_n$ (where n is $\frac{1}{2}$, 1 or 2). (The required dependence of $\tilde{k}_n$ on $V_f^{-\frac{1}{3}}$ then provides a means of discriminating between each of the possible mechanisms.)

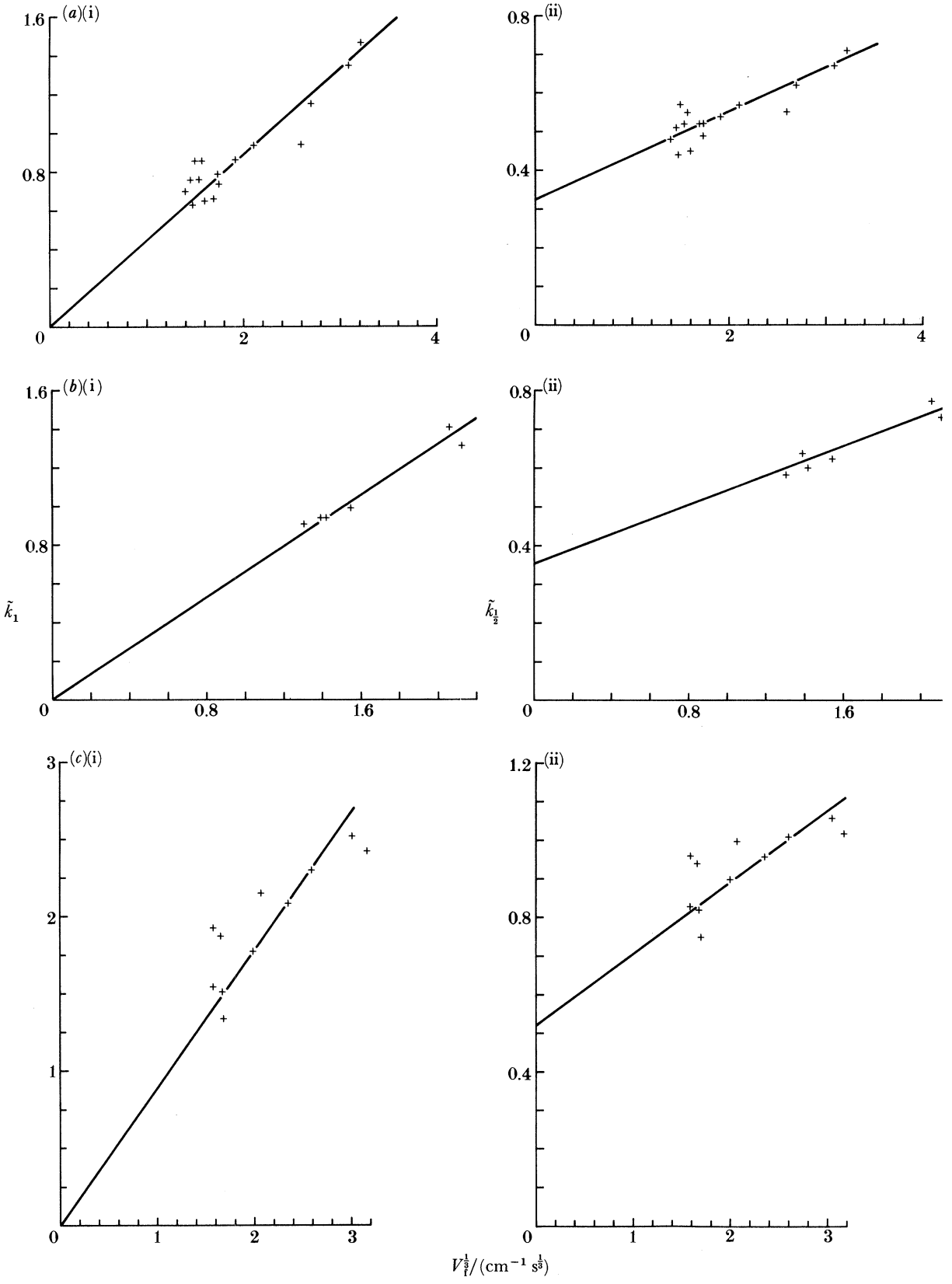

FIGURE 22. Analysis of the data for H^+ reduction at the detector electrode (of figure *a*, *b*, *c*) in terms of (on the left-hand side) a first-order process and (on the right-hand side) a half-order process, assuming $k_{H_2CO_3} = 20\ s^{-1}$ and $K_{H_2CO_3} = 3.06 \times 10^{-4}$ M.

PHILOSOPHICAL TRANSACTIONS OF THE ROYAL SOCIETY A MATHEMATICAL, PHYSICAL & ENGINEERING SCIENCES

$I_{\lim}$ values are readily converted to S_f values, by comparing the former to the simple electron-transfer behaviour displayed for the reduction of H^+ at the monitor electrode and ferricyanide at the detector electrode. Analysis proceeds as follows. 'Working contour plots' of S_f against $\tilde{k}_{H_2CO_3}$ and $\tilde{k}_n$ are readily generated for specified bulk concentrations of H^+ and crystal–electrode geometries, as described in §3(*b*), but now experimentally determined S_f values form the contours. For particular values of S_f and $\tilde{k}_{H_2CO_3}$ (deduced from the experimental parameters and an assumed value of $k_{H_2CO_3}$, see equation (29)), a corresponding $\tilde{k}_n$ value can therefore be obtained. It then follows from the expressions for $\tilde{k}_n$ (see above) that a plot of $\tilde{k}_n$ against $V_f^{-\frac{1}{3}}$ will be linear and intercept the origin, if the correct value of n has been chosen. On this basis, analysis of the data in terms of a second-order heterogeneous process proved to be completely unsatisfactory even with grossly extreme values of $k_{H_2CO_3}$ and k_3' and this mechanism was thus readily eliminated.

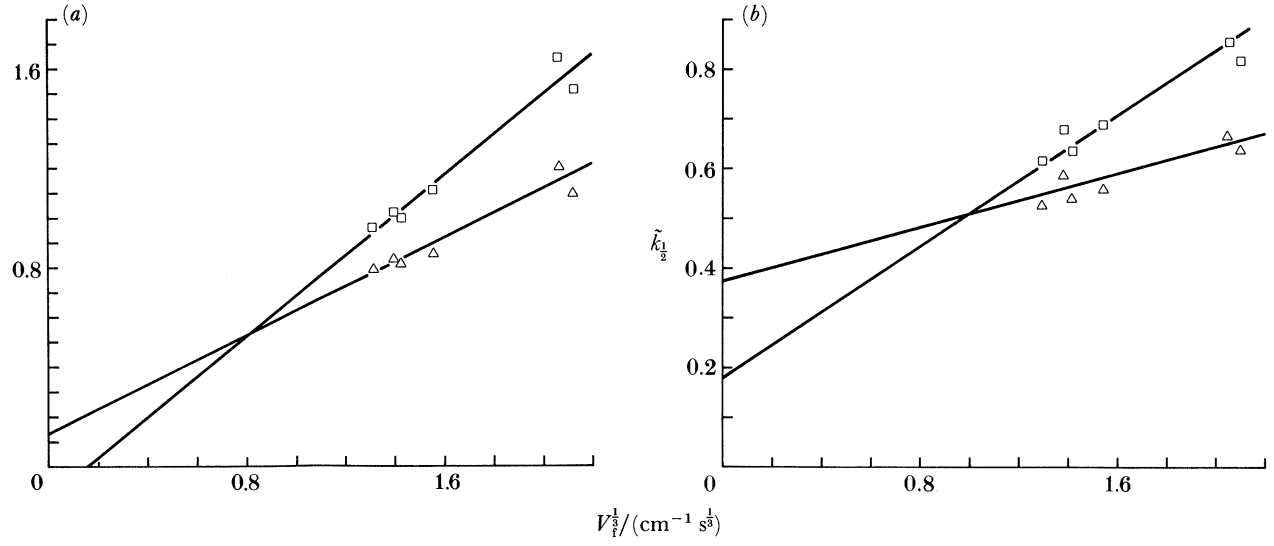

FIGURE 23. Analysis of the 0.5 mM HCl data (figure 20*b*) in terms of (*a*) a first-order process and (*b*) a half-order process but assuming a value for $k_{H_2CO_3}$ of 15 s^{-1} (□) or 29 s^{-1} (△), rather than 20 s^{-1} (as in figure 22*b*).

This therefore leaves the half- and first-order heterogeneous processes to be considered. Analysis of the data in figure 21*a–c* in terms of these two mechanisms is shown in figure 22*a–c*. In converting the experimental parameters to a value of $\tilde{k}_{H_2CO_3}$ we have assumed $k_{H_2CO_3} = 20\ s^{-1}$ to be reasonable, whereas the 'working plots' were specifically for $k_3' = 2.7 \times 10^{-10}$ mol cm^{-2} s^{-1}. For each concentration of H^+ considered, a rather better relation between $\tilde{k}_n$ and $V_f^{-\frac{1}{3}}$ is obtained for $n = 1$ rather than $\frac{1}{2}$. Even if the extremes in previously measured values of $k_{H_2CO_3}$ (15 and 29 s^{-1}) (see table 3) are used in the analysis, agreement with theory is conclusively better for $n = 1$. Figure 23*a*, *b* shows the 0.5 mM HCl data analysed in this way. The gradients of the straight line plots (i) of figure 22*a–c* together with the experimental parameters allow the first-order rate constants shown in table 7 to be deduced. Assuming $k_{H_2CO_3} = 20\ s^{-1}$, the rate constant is found to be (0.043 ± 0.015) cm s^{-1}, but notice that this value is extremely sensitive to the assumed value of $k_{H_2CO_3}$. We thus conclude that although the process is first order, the precise value of the rate constant may require revision were the currently accepted values for $k_{H_2CO_3}$ and $K_{H_2CO_3}$ found to be different upon any future remeasurements.

Table 7. Measured first-order heterogeneous rate constants for the reaction between H^+ and calcite

$[H^+]^\infty$/mM	k_1/(cm s^{-1})		
	$k_{H_2CO_3} = 15$ s^{-1}	$k_{H_2CO_3} = 20$ s^{-1}	$k_{H_2CO_3} = 29$ s^{-1}
1.0	0.031	0.028	0.027
0.5	0.055	0.048	0.042
0.25	0.063	0.052	0.047

It should be pointed out that the rate constant for the dissolution process may be sensitive to surface charge. For the concentration range of HCl used in this work (0.25–1.0×10^{-3} M), the BIFD calculation predicts an average surface concentration of Ca^{2+} in the narrow range 0.8–1.8×10^{-3} M for $k_1 = 0.043$ cm s^{-1} with the full range of flow rates and channel–crystal geometries defined above. It has been shown (Foxall *et al.* 1979) that under the conditions of our experiments the surface potential depends in a nernstian way on the Ca^{2+} ion concentration. However, the range of $[Ca^{2+}]_s$ identified above corresponds to a variation of only *ca.* 5 mV, about a mean of +50 mV, in the surface charge, assuming our crystals to behave analogously to the material used by Foxall *et al.* (1979). Thus our experiments are conducted under conditions of essentially constant surface charge. Future experiments will be conducted to quantify any effects of this on the dissolution reaction.

8. Conclusions

A new strategy for studying heterogeneous reactions at the solid–liquid interface has been proposed, designed, tested and applied to the study of calcite dissolution at pH < 4. The reaction between H^+ and calcite is shown, for the first time, to be a first-order heterogeneous reaction of H^+, with a rate constant of (0.043 ± 0.015) cm s^{-1}, under the assumption that $k_{H_2CO_3} = 20$ s^{-1} and $K_{H_2CO_3} = 3.06 \times 10^{-4}$M.

We thank the SERC and Ciba-Geigy Industrial Chemicals for a CASE studentship for P.R.U., Keith Pritchard, Michael Lees and Alan Gerrard for useful discussions, and Garry Grigg and Philip Sylvester for their help and expertise with the microscopy. We are grateful to Margot Long for typing the manuscript and to the late David Kozlow for drawing the figures.

Appendix A. Analytical solution to equation (16) using the Lévêque approximation (21)

(*a*) *Heterogeneous consumption of* R *upstream of the detector electrode is zero order in* R

Adopting the Lévêque approximation (21), along with the following normalized variables:

$$\xi = (3V_f/2h^2 \, \mathrm{d}Dx_{c+e})^{\frac{1}{3}} y, \tag{A 1}$$

$$\chi = x/x_{c+e}, \tag{A 2}$$

reduces (16) to the following form:

$$0 = \partial^2[R]/\partial\xi^2 - \xi \, \partial[R]/\partial\chi. \tag{A 3}$$

PHILOSOPHICAL TRANSACTIONS OF THE ROYAL SOCIETY A MATHEMATICAL, PHYSICAL & ENGINEERING SCIENCES

Likewise, the boundary conditions (17)–(20) become

$$\chi = 0 \text{ (all } \xi), \quad [\mathrm{R}] = [\mathrm{R}]^{\infty}, \tag{A 4}$$

$$0 < \chi \leqslant \chi_{\mathrm{c}} \ (\xi = 0), \quad \left.\frac{\partial [\mathrm{R}]}{\partial \xi}\right|_{\xi=0} = \tilde{k}_0', \tag{A 5}$$

$$\chi_{\mathrm{c}} < \chi \leqslant 1 \ (\xi = 0), \quad [\mathrm{R}] = 0, \tag{A 6}$$

$$0 < \chi \leqslant 1 \ (\xi \to \infty), \quad [\mathrm{R}] \to [\mathrm{R}]^{\infty}, \tag{A 7}$$

where
$$\tilde{k}_0' = (2h^2 \, \mathrm{d}x_{\mathrm{c+e}}/3V_{\mathrm{f}} D_{\mathrm{R}}^2)^{\frac{1}{3}} k_0/[\mathrm{R}]^{\infty} = \tilde{k}_0 [\mathrm{R}]^{\infty}, \tag{A 8}$$

and
$$\chi_{\mathrm{c}} = x_{\mathrm{c}}/x_{\mathrm{c+e}}. \tag{A 9}$$

To solve (A 3), [R] is split into two parts (Compton 1980) such that

$$[\mathrm{R}] = [\mathrm{R}]_1 + [\mathrm{R}]_2, \tag{A 10}$$

and in the region of the crystal, $0 < \chi \leqslant \chi_{\mathrm{c}}$,

$$[\mathrm{R}] = [\mathrm{R}]_1, \quad [\mathrm{R}]_2 = 0. \tag{A 11}$$

Laplace transformation of (A 3) with respect to χ (transform variable p) as applied to this region gives

$$\partial^2 \bar{r}_1^{\chi}/\partial \xi^2 = p \xi \bar{r}_1^{\chi}, \tag{A 12}$$

where
$$r_1 = [\mathrm{R}]^{\infty} - [\mathrm{R}]_1, \tag{A 13}$$

and $\bar{f}^{\chi}$ denotes the Laplace transform of f with respect to x. The solution to (A 12) is

$$\bar{r}_1^{\chi} = A \times \mathrm{Ai}\,(p^{\frac{1}{3}} \xi), \tag{A 14}$$

where the constant A is fixed by the boundary conditions and $\mathrm{Ai}\,(x)$ is the Airy function (Abramowitz & Stegun 1966, p. 446). By definition $\bar{r}_1^{\chi}$ must satisfy

$$\bar{r}_1^{\chi} = ([\mathrm{R}]^{\infty}/p) - \overline{[\mathrm{R}]}_1^{\chi}, \tag{A 15}$$

thus
$$([\mathrm{R}]^{\infty}/p) - \overline{[\mathrm{R}]}_1^{\chi} = A \times \mathrm{Ai}\,(p^{\frac{1}{3}} \xi). \tag{A 16}$$

At the crystal surface:

$$-\left.\frac{\partial \overline{[\mathrm{R}]}_1^{\chi}}{\partial \xi}\right|_{\xi=0} = A \times p^{\frac{1}{3}} \mathrm{Ai}'\,(0) \tag{A 17}$$

$$= -\tilde{k}_0'/p, \tag{A 18}$$

which gives an expression for A:

$$A = -\tilde{k}_0'/p^{\frac{4}{3}} \mathrm{Ai}'\,(0) \tag{A 19}$$

and so
$$\overline{[\mathrm{R}]}_1^{\chi} = \frac{\tilde{k}_0' \, \mathrm{Ai}\,(p^{\frac{1}{3}} \xi)}{p^{\frac{4}{3}} \mathrm{Ai}'\,(0)} + \frac{[\mathrm{R}]^{\infty}}{p}. \tag{A 20}$$

In the region of the detector electrode, $\chi_{\mathrm{c}} < \chi \leqslant 1$, equation (A 3) may be written as:

$$0 = \partial^2 [\mathrm{R}]_2/\partial \xi^2 - \xi \, \partial [\mathrm{R}]_2/\partial \chi_{\mathrm{e}}, \tag{A 21}$$

where
$$\chi_{\mathrm{e}} = \chi - \chi_{\mathrm{c}}. \tag{A 22}$$

Laplace transformation of (A 21) with respect to χ_e (transform variable q) gives the ordinary differential equation in Laplace space:

$$\partial^2\overline{[R]}_2^{\chi_e}/\partial\xi^2 = q\xi\overline{[R]}_2^{\chi_e}, \tag{A 23}$$

which has the solution

$$\overline{[R]}_2^{\chi_e} = B \times \mathrm{Ai}\,(q^{\frac{1}{3}}\xi) \tag{A 24}$$

B is a constant. Now, from (A 6) and (A 10):

$$(\overline{[R]}_2^{\chi_e})_{\xi=0} = (\overline{[R]}_1^{\chi_e})_{\xi=0} \tag{A 25}$$

$$= \mathscr{L}_{\chi_e}\mathscr{L}_{\chi}^{-1}(\overline{[R]}_1^{\chi})_{\xi=0}, \tag{A 26}$$

where $\mathscr{L}_{\chi}f$ and $\mathscr{L}_{\chi}^{-1}\bar{f}^{x}$ denote the Laplace transform of f and inversion of $\bar{f}^{x}$. Equation (A 24) along with (A 26) and (A 20) gives the following for $\overline{[R]}_2^{\chi_e}$:

$$\overline{[R]}_2^{\chi_e} = \frac{\mathrm{Ai}\,(q^{\frac{1}{3}}\xi)\,[R]^{\infty}}{\mathrm{Ai}\,(0)}\mathscr{L}_{\chi_e}\left\{1+\frac{\tilde{k}_0'\,\mathrm{Ai}\,(0)\,\chi^{\frac{1}{3}}}{\Gamma(\frac{4}{3})\,\mathrm{Ai}'\,(0)\,[R]^{\infty}}\right\}, \tag{A 27}$$

where Γ is the Gamma function.

Now, the shielding factor, S_f – the ratio of the current at the detector electrode due to the transport-limited electrolysis of the reactant to the transport-limited current when there is no heterogeneous consumption of the reactant upstream of the electrode – is defined, for this case specifically, by

$$S_f = \frac{I_{\lim}}{I_{\lim}(k_0=0)} = \frac{1.238(x_{c+e})^{\frac{2}{3}}}{[R]^{\infty}(x_{c+e}-x_c)^{\frac{2}{3}}}\int_{\chi_c}^{1}\frac{\partial[R]}{\partial\xi}\bigg|_{\xi=0}, \tag{A 28}$$

where $I_{\lim}(k_0=0)$ was derived by Levich (1962):

$$I_{\lim}(k_0=0) = 0.925nF[R]^{\infty}(V_f D_R^2(x_{c+e}-x_c)^2/h^2d)^{\frac{1}{3}}w. \tag{A 29}$$

Equation (A 28) may be written as:

$$S_f = \frac{1.238(x_{c+e})^{\frac{2}{3}}}{[R]^{\infty}(x_{c+e}-x_c)^{\frac{2}{3}}}\int_{\chi_c}^{1}\left\{\frac{\partial[R]_1}{\partial\xi}\bigg|_{\xi=0}-\frac{\partial[R]_2}{\partial\xi}\bigg|_{\xi=0}\right\}d\chi, \tag{A 30}$$

which indicates that appropriate functions to invert from Laplace space are

$$\mathscr{L}_{\chi_e}^{-1}\frac{1}{q}\frac{\partial\overline{[R]}_2^{\chi_e}}{\partial\xi}\bigg|_{\xi=0} = \int_0^{\chi_e}\frac{\partial[R]_2}{\partial\xi}\bigg|_{\xi=0}d\chi_e \tag{A 31}$$

and

$$\mathscr{L}_{\chi}^{-1}\frac{1}{p}\frac{\partial\overline{[R]}_1^{\chi_e}}{\partial\xi}\bigg|_{\xi=0} = \int_0^{\chi_e}\frac{\partial[R]_1}{\partial\xi}\bigg|_{\xi=0}d\chi. \tag{A 32}$$

First considering equation (A 31):

$$\mathscr{L}_{\chi_e}^{-1}\frac{1}{q}\frac{\partial\overline{[R]}_2^{\chi_e}}{\partial\xi}\bigg|_{\xi=0} = \frac{\mathrm{Ai}'\,(0)\,[R]^{\infty}}{\mathrm{Ai}\,(0)}\mathscr{L}_{\chi_e}^{-1}\frac{1}{q^{\frac{2}{3}}}\left[\mathscr{L}_{\chi_e}\left\{1+\frac{\mathrm{Ai}\,(0)}{\mathrm{Ai}'\,(0)}\frac{\tilde{k}_0'}{[R]^{\infty}}\frac{(\chi_c+\chi_e)^{\frac{1}{3}}}{\Gamma(\frac{4}{3})}\right\}\right]. \tag{A 33}$$

PHILOSOPHICAL TRANSACTIONS OF THE ROYAL SOCIETY A MATHEMATICAL, PHYSICAL & ENGINEERING SCIENCES

Applying the convolution theorem (Miles 1971, p. 17) and integrating by parts gives

$$\mathscr{L}^{-1}_{\chi_e}\frac{1}{q}\frac{\partial[\bar{R}]_2^{\chi_e}}{\partial\xi}\bigg|_{\xi=0} = \frac{1}{2\Gamma(\frac{2}{3})}\left[\frac{3\mathrm{Ai}'(0)}{\mathrm{Ai}(0)}[R]^{\infty}(1-\chi_c)^{\frac{2}{3}} + \frac{\tilde{k}'_0}{\Gamma(\frac{4}{3})}\left\{3(1-\chi_c)^{\frac{2}{3}}(\chi_c)^{\frac{1}{3}} + \int_{\chi_c}^{1}(1-\chi)^{\frac{2}{3}}\chi^{-\frac{2}{3}}\mathrm{d}\chi\right\}\right]. \quad (A\ 34)$$

Equation (A 32) is readily inverted:

$$\mathscr{L}^{-1}_{\chi}\frac{1}{p}\frac{\partial[\bar{R}]_1^{\chi}}{\partial\xi}\bigg|_{\xi=0} = \tilde{k}'_0(1-\chi_c). \quad (A\ 35)$$

Thus

$$S_f = \frac{1.238(x_{c+e})^{\frac{2}{3}}}{[R]^{\infty}(x_{c+e}-x_c)^{\frac{2}{3}}}\left(\tilde{k}'_0(1-\chi_c) - \frac{1}{2\Gamma(\frac{2}{3})}\left[\frac{3\mathrm{Ai}'(0)}{\mathrm{Ai}(0)}[R]^{\infty}(1-\chi_c)^{\frac{2}{3}} + \frac{\tilde{k}'_0}{\Gamma(\frac{4}{3})}\left\{3(1-\chi_c)^{\frac{2}{3}}(\chi_c)^{\frac{1}{3}} + \int_{\chi_c}^{1}(1-\chi)^{\frac{2}{3}}\chi^{-\frac{2}{3}}\mathrm{d}\chi\right\}\right]\right). \quad (A\ 36)$$

(*b*) *Heterogeneous consumption of* R *upstream of the detector electrode is first order in* R

We have presented a derivation of this case elsewhere (Unwin *et al.* 1988), and thus simply quote the result:

$$\begin{aligned}
S_f = \frac{0.9025x_{c+e}^{\frac{2}{3}}}{(x_{c+e}-x_c)^{\frac{2}{3}}}\Bigg\{&\frac{3}{2\Gamma(\frac{2}{3})}\Bigg((1-\chi_c)^{\frac{2}{3}}\Bigg[\mathrm{e}^{-\chi_c/\beta^3} + \frac{(\chi_c/\beta^3)^{\frac{2}{3}}}{\Gamma(\frac{5}{3})} - \frac{\mathrm{e}^{-\chi_c/\beta^3}}{\Gamma(\frac{5}{3})}\int_0^{\chi_c/\beta^3}\lambda^{\frac{2}{3}}\mathrm{e}^{\lambda}\,\mathrm{d}\lambda - \frac{(\chi_c/\beta^3)^{\frac{1}{3}}}{\Gamma(\frac{4}{3})} \\
&+ \frac{\mathrm{e}^{-\chi_c/\beta^3}}{\Gamma(\frac{4}{3})}\int_0^{\chi_c/\beta^3}\lambda^{\frac{1}{3}}\mathrm{e}^{\lambda}\,\mathrm{d}\lambda\Bigg] + \int_{\chi_c}^{1}\frac{(1-\chi)}{\beta^3}\Bigg[\frac{2(\chi/\beta^3)^{-\frac{1}{3}}}{3\Gamma(\frac{5}{3})} - \mathrm{e}^{-\chi/\beta^3} \\
&+ \frac{\mathrm{e}^{-\chi_c/\beta^3}}{\Gamma(\frac{5}{3})}\int_0^{\chi_c/\beta^3}\lambda^{\frac{2}{3}}\mathrm{e}^{\lambda}\,\mathrm{d}\lambda - \frac{(\chi/\beta^3)^{\frac{2}{3}}}{\Gamma(\frac{5}{3})} - \frac{(\chi/\beta^3)^{-\frac{2}{3}}}{3\Gamma(\frac{4}{3})} \\
&- \frac{\mathrm{e}^{-\chi_c/\beta^3}}{\Gamma(\frac{4}{3})}\int_0^{\chi_c/\beta^3}\lambda^{\frac{1}{3}}\mathrm{e}^{\lambda}\,\mathrm{d}\lambda + \frac{(\chi/\beta^3)^{\frac{1}{3}}}{\Gamma(\frac{4}{3})}\Bigg]\mathrm{d}\chi\Bigg) + \frac{(1-\chi_c^{\frac{2}{3}})}{\Gamma(\frac{5}{3})} \\
&- \frac{\beta(1-\chi_c^{\frac{1}{3}})}{\Gamma(\frac{4}{3})} - \beta^2\,\mathrm{e}^{-\beta^{-3}}\Bigg(1 - \frac{3}{\Gamma(\frac{1}{3})}\Bigg[\frac{\mathrm{e}^{1/\beta^3}}{\beta} \\
&- \int_0^{1/\beta^3}\lambda^{\frac{1}{3}}\mathrm{e}^{\lambda}\,\mathrm{d}\lambda\Bigg] + \frac{3}{2\Gamma(\frac{2}{3})}\Bigg[\frac{\mathrm{e}^{1/\beta^3}}{\beta^2} - \int_0^{1/\beta^3}\lambda^{\frac{2}{3}}\mathrm{e}^{\lambda}\,\mathrm{d}\lambda\Bigg]\Bigg) \\
&- \beta^2\,\mathrm{e}^{-\chi_c/\beta^3}\Bigg(1 - \frac{3}{\Gamma(\frac{1}{3})}\Bigg[\left(\frac{\chi_c}{\beta}\right)^{\frac{1}{3}}\mathrm{e}^{\chi_c/\beta^3} - \int_0^{\chi_c/\beta^3}\lambda^{\frac{1}{3}}\mathrm{e}^{\lambda}\,\mathrm{d}\lambda\Bigg] \\
&+ \frac{3}{2\Gamma(\frac{2}{3})}\Bigg[\left(\frac{\chi_c}{\beta^3}\right)^{\frac{2}{3}}\mathrm{e}^{\chi_c/\beta^3} - \int_0^{\chi_c/\beta^3}\lambda^{\frac{2}{3}}\mathrm{e}^{\lambda}\,\mathrm{d}\lambda\Bigg]\Bigg)\Bigg\}, \quad (A\ 37)
\end{aligned}$$

where $$\beta = -\mathrm{Ai}'(0)/\mathrm{Ai}(0)\,\tilde{k}_1, \tag{A 38}$$

and $$\tilde{k}_1 = k_1\left(\frac{2h^2 x_{c+e} d}{3V_f D^2}\right)^{\frac{1}{3}}. \tag{A 39}$$

In the limit of small $\tilde{k}_1$, equation (A 38) may be simplified:

$$S_f = \frac{-0.9025 x_{c+e}^{\frac{2}{3}}}{(x_{c+e}-x_c)^{\frac{2}{3}}}\left\{\left(\sum_{m=1}^{\infty}\frac{(-1)^{m-1}\beta^{-m}(1-\chi_c^{\frac{1}{3}(2+m)})}{\Gamma[\frac{1}{3}(5+m)]}\right)\right.$$
$$+\frac{3}{2\Gamma(\frac{2}{3})}\left[(1-\chi_c)^{\frac{2}{3}}\left(1-\sum_{m=1}^{\infty}\frac{(-1)^{m-1}\beta^{-m}\chi_c^{\frac{1}{3}m}}{\Gamma[\frac{1}{3}(3+m)]}\right)\right.$$
$$\left.\left.-\int_{\chi_c}^{1}(1-\chi)^{\frac{2}{3}}\sum_{m=1}^{\infty}\frac{(-1)^{m-1}\beta^{-m}\chi^{\frac{1}{3}(m-3)}}{\Gamma[\frac{1}{3}(3+m)]}\times\tfrac{1}{3}m\,\mathrm{d}\chi\right]\right\}. \tag{A 40}$$

Whereas for large $\tilde{k}_1$, S_f takes the form:

$$S_f = \frac{-0.9025 x_{c+e}^{\frac{2}{3}}}{(x_{c+e}-x_c)^{\frac{2}{3}}}\left\{\left(\sum_{m=1}^{5}\frac{(-1)^{m-1}\beta^{m-1}(1-\chi_c^{\frac{1}{3}(3-m)})}{\Gamma[\frac{1}{3}(6-m)]}\right)\right.$$
$$+\frac{3}{2\Gamma(\frac{2}{3})}\left[(1-\chi_c)^{\frac{2}{3}}\left(1-\sum_{m=1}^{3}\frac{(-1)^{m-1}\beta^{m-1}\chi_c^{\frac{1}{3}(1-m)}}{\Gamma[\frac{1}{3}(4-m)]}\right)\right.$$
$$\left.\left.-\int_{\chi_c}^{1}(1-\chi)^{\frac{2}{3}}\sum_{m=1}^{3}\frac{(-1)^{m-1}\beta^{m-1}\chi^{-\frac{1}{3}(m+2)}}{\Gamma[\frac{1}{3}(4-m)]}\times\tfrac{1}{3}(1-m)\,\mathrm{d}\chi\right]\right\}, \tag{A 41}$$

which is a good description provided sufficient convergence results with three terms.

The integrals in equations (A 36), (A 37), (A 40) and (A 41) are readily evaluated numerically using standard routines, e.g. the NAG subroutines D01 BAF, D01 BAZ and D01 GAF are suitable.

Appendix B. BIFD calculation of shielding factors

The two-dimensional finite-difference grid for the calculation of shielding factors at the channel electrode via the BIFD method is defined in figure 24. It has been shown elsewhere

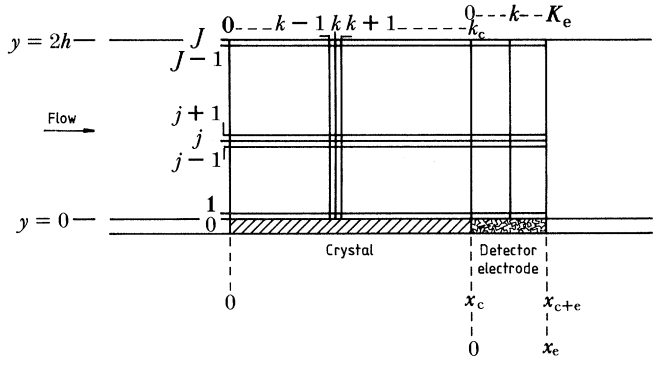

Figure 24. Two-dimensional finite difference grid for the BIFD calculation of shielding factors.

(Compton *et al.* 1988*a*, *d*; Compton & Pritchard 1990) that the application of this numerical method condenses the convective–diffusion equations relating to channel electrode problems to the solution of the following matrix equation:

$$\begin{bmatrix} d_1 \\ d_2 \\ \vdots \\ d_j \\ \vdots \\ d_{J-2} \\ d_{J-1} \end{bmatrix} = \begin{bmatrix} b_1 & c_1 & 0 & & & & \\ a_2 & b_2 & c_2 & 0 & & & \\ & \ddots & \ddots & \ddots & & & \\ 0 & & a_j & b_j & c_j & 0 & \\ & & & \ddots & \ddots & \ddots & \\ & & & & a_{J-2} & b_{J-2} & c_{J-2} \\ & & & & 0 & a_{J-1} & b_{J-1} \end{bmatrix} \begin{bmatrix} u_1 \\ u_2 \\ \vdots \\ u_j \\ \vdots \\ u_{J-2} \\ u_{J-1} \end{bmatrix}. \tag{B 1}$$

The mechanics of the method of solution can be found in Compton *et al.* (1988*a*, *d*) and Compton & Pritchard (1990). In this Appendix we simply provide expressions for the matrix elements in (B 1) for the various problems considered in this paper.

TABLE 8. VALUES FOR THE MATRIX ELEMENTS a_j, b_j, c_j, d_j AND u_j IN THE REGION OF THE CRYSTAL ($1 \leqslant k \leqslant K_c$) AND ELECTRODE ($1 \leqslant k \leqslant K_e$) WHEN R REACTS ON THE CRYSTAL VIA AN nth ORDER HETEROGENEOUS PROCESS

	n	k	j
$a_j = -\lambda_j^*$	n	$1, 2 \ldots K_c; 1, 2 \ldots K_e$	$2, 3 \ldots J-1$
$b_j = \lambda_j^c + 1$	0	$1, 2 \ldots K_c$	1
$b_j = 2\lambda_j^c + 1 - \lambda_j^c \{1 + (\Delta y k_n / D_R)\,[g^R_{0,k+1}[R]^\infty]^{n-1}\}^{-1}$	$\neq 0$	$1, 2 \ldots K_c$	1
$b_j = 2\lambda_j^e + 1$	n	$1, 2 \ldots K_e$	1
$b_i = 2\lambda_j^* + 1$	n	$1, 2 \ldots K_c; 1, 2 \ldots K_e$	$2, 3 \ldots J-1$
$c_j = -\lambda_j^*$	n	$1, 2 \ldots K_c; 1, 2 \ldots K_e$	$2, 3 \ldots J-2$
$d_j = g^R_{j,k} - (\lambda_j^c \Delta y k_n / D_R [R]^\infty)$	0	$1, 2 \ldots K_c$	1
$d_j = g^R_{j,k}$	$\neq 0$	$1, 2 \ldots K_c$	1
$d_j = g^R_{j,k}$	n	$1, 2 \ldots K_e$	1
$d_j = g^R_{j,k}$	n	$1, 2 \ldots K_c; 1, 2 \ldots K_e$	$2, 3 \ldots J-1$
$u_j = g^R_{j,k}$	n	$1, 2 \ldots K_c; 1, 2 \ldots K_e$	$1, 2 \ldots J-1$

Table 8 gives values for the matrix elements for the case when R reacts on the crystal via an nth order heterogeneous process. In this table:

$$g^R = [R]/[R]^\infty, \tag{B 2}$$

$$\lambda_j^* = D_R \Delta x_* h^3 d / V_f j (\Delta y)^3 (2h - j\Delta y), \tag{B 3}$$

where

$$\Delta y = 2h/J, \tag{B 4}$$

$$\Delta x_* = x_*/K_*, \tag{B 5}$$

and $*$ is c or e, where c and e denote the zones of the crystal or electrode respectively.

S_f is calculated from

$$S_f = \sum_{k=1}^{k=K_e} g^R_{1,k} \Big/ \sum_{k=1}^{k=K_e} g^R_{1,k}(k_n = 0). \tag{B 6}$$

Table 9 provides the new expressions for b_1 and d_1 when the reaction of R at the crystal is parallel zeroth and nth order. Table 10 defines d_j and b_1 for H^+ and HCO_3^- for the calcite dissolution problem. In this latter table the additional superscript, HCO_3^- or H^+, on λ^* is required to account for the difference in the diffusion coefficients of these two species, and

$$g^{H^+} = [H^+]/[H^+]^\infty, \quad g^{HCO_3^-} = [HCO_3^-]/[H^+]^\infty. \tag{B 7}$$

Note that the remaining matrix elements for this problem for both H^+ and HCO_3^- are as defined in table 8.

TABLE 9. MODIFICATION TO b_1 AND d_1 FROM THOSE GIVEN IN TABLE 8 WHEN THE HETEROGENEOUS REACTION AT THE CRYSTAL IS PARALLEL ZEROTH AND nth ORDER IN THE REACTANT, R

matrix/vector element	value	k
b_1	$1+2\lambda_1^c-\lambda_1^c\left[1+\dfrac{\Delta y k_n}{D_R}\{g^R_{0,k+1}[R]^\infty\}^{n-1}\right]^{-1}$	$1,2\ldots K_c$
d_1	$g^R_{1,k}-\dfrac{\lambda_1^c\,\Delta y k_0}{D_R[R]^\infty}\left[1+\dfrac{\Delta y k_n}{D_R}\{g^R_{0,k+1}[R]^\infty\}^{n-1}\right]^{-1}$	$1,2\ldots K_c$

TABLE 10. MATRIX/VECTOR ELEMENT MODIFICATIONS, FROM THOSE GIVEN IN TABLE 8, FOR THE DESCRIPTION OF THE CALCITE DISSOLUTION PROBLEM

matrix/vector element	H^+	k	j
d_j	$g^{H^+}_{j,k}-\left(\dfrac{k_{H_2CO_3}g^{H^+}_{j,k}g^{HCO_3^-}_{j,k}}{(K_{H_2CO_3}/[H^+]^\infty)+g^{H^+}_{j,k}+g^{HCO_3^-}_{j,k}}\right)\dfrac{\lambda_j^{*H^+}(\Delta y)^2}{D_{H^+}}$	$1,2,\ldots,K_c;$ $1,2,\ldots,K_e$	$1,2,\ldots,J-1$
	HCO_3^-	k	j
	$g^{HCO_3^-}_{j,k}-\left(\dfrac{k_{H_2CO_3}g^{HCO_3^-}_{j,k}g^{H^+}_{j,k}}{(K_{H_2CO_3}/[H^+]^\infty)+g^{HCO_3^-}_{j,k}+g^{H^+}_{j,k}}\right)\dfrac{\lambda_j^{*HCO_3^-}(\Delta y)^2}{D_{HCO_3^-}}$	$1,2,\ldots,K_c$ $1,2,\ldots,K_e$	$2,3,\ldots,J-1$ $1,2,\ldots,J-1$
	$g^{HCO_3^-}_{j,k}-\left(\dfrac{k_{H_2CO_3}g^{HCO_3^-}_{j,k}g^{H^+}_{j,k}}{(K_{H_2CO_3}/[H^+]^\infty)+g^{HCO_3^-}_{j,k}+g^{H^+}_{j,k}}\right)\dfrac{\lambda_j^{cHCO_3^-}(\Delta y)^2}{D_{HCO_3^-}}$ $+\lambda_j^{cHCO_3^-}(D_{H^+}/D_{HCO_3^-})\,(g^{H^+}_{1,k+1}-g^{H^+}_{0,k+1})$	$1,2,\ldots,K_c$	1
matrix/vector element	H^+	k	j
b_1	$(2\lambda_1^{cH^+}+1)-\lambda_1^{cH^+}\left[1+\dfrac{\Delta y k_n}{D_{H^+}}\{g^{H^+}_{0,k+1}[H^+]^\infty\}^{n-1}\right]^{-1}$	$1,2,\ldots,K_c$	1
	$2\lambda_1^{eH^+}+1$	$1,2,\ldots,K_e$	1
	HCO_3^-	k	j
	$\lambda_1^{*HCO_3^-}+1$	$1,2,\ldots,K_c$ $1,2,\ldots,K_e$	1

The implementation of boundary condition (36) changes the expression for d_1 (for HCO_3^-) in the zone of the crystal to:

$$d_1 = g^{HCO_3^-}_{1,k}-\left(\frac{k_{H_2CO_3}g^{HCO_3^-}_{1,k}g^{H^+}_{1,k}}{(K_{H_2CO_3}/[H^+]^\infty)+g^{HCO_3^-}_{1,k}+g^{H^+}_{1,k}}\right)\frac{\lambda_1^{cHCO_3^-}(\Delta y)^2}{D_{HCO_3^-}} + (\lambda_1^{cHCO_3^-}/D_{HCO_3^-})\,(D_{H^+}(g^{H^+}_{1,k+1}+g^{H^+}_{0,k+1})+k_0\Delta y). \tag{B 8}$$

References

Abramowitz, M. & Stegun, I. A. 1966 *Handbook of mathematical functions*. New York: Dover.
Adams, R. N. 1969 *Electrochemistry at solid electrodes*. New York: Marcel Dekker.
Anderson, J. L. & Moldoveanu, S. 1984 *J. electroanal. Chem.* **179**, 107–117.
Andreev, V. N., Vasiliev, Yu. B., Osetrova, N. V. & Yastrebova, T. N. 1982 *Soviet Electrochem.* **19**, 338–340.
Anson, F. C. & King, O. M. 1962 *Analyt. Chem.* **34**, 362–365.
Aoki, K., Tokuda, K. & Matsuda, H. 1987 *J. electroanal. Chem.* **217**, 33–47.
Arvia, A. J. & Giordano, M. C. 1986 *An. Asoc. quím. argent.* **74**, 1–9.
Barton, A. F. M. & Wilde, N. M. 1971*a* *Trans. Faraday Soc.* **67**, 3590–3597.
Barton, A. F. M. & Wilde, N. M. 1971*b* *N.Z. Jl Sci.* **14**, 608–620.
Barton, A. F. M. & McConnel, S. R. 1974 *J. chem. Soc. Faraday Trans.* I **70**, 2355–2361.
Barton, A. F. M. & McConnel, S. R. 1975 *N.Z. Jl Sci.* **18**, 85–92.
Barton, A. F. M. & McConnel, S. R. 1979*a* *J. chem. Soc. Faraday Trans.* I **75**, 971–983.
Barton, A. F. M. & McConnel, S. R. 1979*b* *Chem. Austral.* **46**, 427–433.
Barton, P. & Vatanathan, T. 1976 *Environ. Sci. Technol.* **10**, 262–266.
Baruzzi, A. M., Leiva, E. P. M. & Giordano, M. C. 1983 *J. electroanal. Chem.* **158**, 103–114.
Baruzzi, A. M., Leiva, E. P. M. & Giordano, M. C. 1985 *J. electroanal. Chem.* **189**, 257–269.
Baumann, J., Buhmann, D., Dreybrodt, W. & Schulz, H. D. 1985 *Chem. Geol.* **53**, 219–228.
Beden, B., Bewick, A., Razaq, M. & Weber, J. 1982 *J. electroanal. Chem.* **139**, 203–206.
Berger, R. L. & Stoddart, L. C. 1965 *Rev. scient. Instrum.* **36**, 78–84.
Berner, R. A. 1971 *Principles of chemical sedimentology*. New York: McGraw-Hill.
Berner, R. A. & Morse, J. W. 1974 *Am. J. Sci.* **274**, 108–134.
Bickley, W. 1937 *Phil. Mag.* **7**, 727–731.
Biegler, T. 1967 *J. electrochem. Soc.* **114**, 1261–1262.
Biegler, T. 1968 *J. phys. Chem.* **72**, 1571–1577.
Biegler, T. 1969 *J. electrochem. Soc.* **116**, 1131–1137.
Bird, R. B., Stewart, W. E. & Lightfoot, E. N. 1960 *Transport phenomena*. New York: John Wiley.
Bockris, J. O'M., Immar, I. A. & Aug, A. K. M. S. 1957 *J. phys. Chem.* **61**, 879–886.
Boguski, A. 1876 *Chem. Ber.* **9**, 1442, 1599, 1646.
Boguski, A. & Kajander, T. 1877 *Chem. Ber.* **10**, 34.
Boomer, D. R., McCune, C. C. & Fogler, H. S. 1972 *Rev. Scient. Instrum.* **43**, 225–229.
Brett, C. M. A. & Oliveira Brett, A. M. C. F. 1986 In *Comprehensive chemical kinetics* (ed. C. H. Bamford & R. G. Compton), vol. 26. Amsterdam: Elsevier.
Breiter, M. W. 1963 *Electrochim. Acta* **8**, 973–983.
Breiter, M. W. 1966 *Electrochim. Acta* **11**, 905–909.
Breiter, M. W. 1967 *Electrochim. Acta* **12**, 1213–1218.
Breiter, M. W. 1968 *J. electroanal. Chem.* **19**, 131–136.
Brian, P. L. T., Hales, H. B. & Sherwood, T. K. 1969 *A.I.Ch.E.Jl* **15**, 727–733.
Brinkman, R., Margaria, R. & Roughton, F. J. W. 1933 *Phil. Trans. R. Soc. Lond.* A **232**, 65–97.
Brummer, S. B. 1966 *J. electrochem. Soc.* **113**, 1043.
Brummer, S. B., Ford, J. I. & Turner, M. J. 1965 *J. phys. Chem.* **69**, 3424–3433.
Brummer, S. B. & Turner, M. J. 1967 *J. phys. Chem.* **71**, 3902–3906.
Brummer, S. B. & Cahill, K. 1968 *Discuss. Faraday Soc.* **45**, 67–78.
Brummer, S. B. & Cahill, K. 1969 *J. electroanal. Chem.* **21**, 463–482.
Brunner, E. 1904 *Z. phys. chem.* **47**, 79–86.
Buhmann, D. & Dreybrodt, W. 1985*a* *Chem. Geol.* **48**, 189–211.
Buhmann, D. & Dreybrodt, W. 1985*b* *Chem. Geol.* **53**, 109–124.
Cheng, V. K., Coller, B. A. W. & Powell, J. L. 1984 *Faraday Discuss. chem. Soc.* **77**, 243–256.
Clark, D., Fleischmann, M. & Pletcher, D. 1972 *J. electroanal. Chem.* **36**, 137–146.
Cochran, W. G. 1934 *Proc. Camb. phil. Soc.* **30**, 365–375.
Coles, B. A. & Compton, R. G. 1983 *J. electroanal. Chem.* **144**, 87–98.
Compton, R. G. 1980 D.Phil. thesis, Oxford University, U.K.
Compton, R. G. & Daly, P. J. 1984 *J. Colloid Interface Sci.* **101**, 159–166.
Compton, R. G. & Daly, P. J. 1987 *J. Colloid Interface Sci.* **115**, 493–498.
Compton, R. G. & Pritchard, K. L. 1990 *Phil. Trans. R. Soc. Lond.* A. **330**, 47–70. (Following paper.)
Compton, R. G. & Unwin, P. R. 1986*a* *J. electroanal. Chem.* **205**, 1–20.
Compton, R. G. & Unwin, P. R. 1986*b* *J. electroanal. Chem.* **206**, 57–67.
Compton, R. G., Daly, P. J. & House, W. A. 1986 *J. Colloid Interface Sci.* **113**, 12–20.
Compton, R. G., Coles, B. A. & Pilkington, M. B. G. 1988*a* *J. chem. Soc. Faraday Trans.* I **84**, 4347–4353.
Compton, R. G., Coles, B. A., Stearn, G. M. & Waller, A. M. 1988*b* *J. chem. Soc. Faraday Trans.* I **84**, 2357–2367.
Compton, R. G., Pilkington, M. B. G. & Stearn, G. M. 1988*c* *J. chem. Soc. Faraday Trans.* I **84**, 2155–2171.

PHILOSOPHICAL TRANSACTIONS OF THE ROYAL SOCIETY A MATHEMATICAL, PHYSICAL & ENGINEERING SCIENCES

Compton, R. G., Stearn, G. M., Unwin, P. R. & Barwise, A. J. 1988*d* *J. appl. Electrochem.* **18**, 657–665.
Czerwinski, A. & Sobkowski, J. 1975 *J. electroanal. Chem.* **59**, 41–46.
Daly, P. J. 1985 Ph.D. thesis, Liverpool University, U.K.
Davison, W. & House, W. A. 1988 *Wat. Res.* **22**, 577–583.
Dietz, H. & Göhr, H. 1963 *Electrochim. Acta* **8**, 343–359.
Dreybrodt, W. 1981 *Chem. Geol.* **31**, 245–269.
Eigen, M., Kustin, K. & Maas, G. 1961 *Z. phys. chem.* **30**, 130–136.
Eigen, M. & Hammes, G. 1963 In *Advances in enzymology* (ed. F. F. Nord). New York: John Wiley.
Eisenberg, M., Tobias, C. W. & Wilke, C. R. 1954*a* *J. electrochem. Soc.* **101**, 306–319.
Eisenberg, M., Tobias, C. W. & Wilke, C. R. 1954*b* *Am. Inst. chem. Engng Symp. Ser.* 16, **51**, 1–16.
Erga, O. & Terjesen, S. G. 1956 *Acta chem. scand.* **10**, 872–874.
Ferret, J., Gout, R., Kihn, Y. & Sevely, J. 1987 *Physics Chem. Minerals* **15**, 163–170.
Filinovskii, V. Yu. & Pleskov, Yu. V. 1984 In *Comprehensive treatise of electrochemistry* (ed. E. Yeager, J. O'M. Bockris, B.E. Conway & S. Sarangapani), vol. 9. New York: Plenum Press.
Flanagan, J. B. & Marcoux, L. 1974 *J. phys. Chem.* **78**, 718–723.
Fosdick, L. E. & Anderson, J. L. 1986 *Analyt. Chem.* **58**, 2481–2485.
Fosdick, L. E., Anderson, J. L., Baginski, T. A. & Jaeger, R. C. 1986 *Analyt. Chem.* **58**, 2750–2756.
Fosdick, L. E. & Anderson, J. L. 1988 *Analyt. Chem.* **60**, 156–168.
Foxall, T., Peters, G. C., Rendall, H. M. & Smith, A. L. 1979 *J. chem. Soc. Faraday Trans.* I **75**, 1034–1039.
Fraser, J. E. & Britt, D. L. 1982 *Liming of acidified waters.* Mclean, Virginia: General Research Corp.
Frech, W. G. & Kuwana, T. 1964 *J. phys. Chem.* **68**, 1279–1284.
Gabe, D. R. 1974 *J. appl. Electrochem.* **4**, 91–108.
Gabe, D. R. & Walsh, F. C. 1983 *J. appl. Electrochem.* **13**, 3–21.
Gibbons, B. H. & Edsall, J. T. 1963 *J. biol. Chem.* **238**, 3502–3507.
Gibson, Q. H. & Roughton, F. J. W. 1955 *Proc. R. Soc. Lond.* B **143**, 310–334.
Gilman, S. 1963 *J. phys. Chem.* **67**, 78–84.
Gilman, S. 1965 *J. electroanal. Chem.* **9**, 276–281.
Gilman, S. 1967 In *Electroanalytical chemistry* (ed. A. J. Bard), vol. 2. New York: Marcel Dekker.
Giner, J. 1963 *Electrochim. Acta* **8**, 857–865.
Giner, J. 1964 *Electrochim. Acta* **9**, 63–77.
Glauert, M. B. 1956 *J. Fluid Mech.* **1**, 625–643.
Gortikov, V. M. & Panteleva, L. I. 1937 *J. gen. Chem. U.S.S.R.* **7**, 56–64.
Hammett, L. P. 1924 *J. Am. chem. Soc.* **46**, 7–19.
Harned, H. S. & Owen, B. B. 1943 *The physical chemistry of electrolyte solutions.* New York: Reinhold Publishing.
Haynes, R. 1984 *Optical microscopy of materials.* Glasgow: International Textbook Co.
Heindrichs, A. & Vielstich, W. 1968 *Messtechnik* **9**, 234–238.
Ho, C. & Sturtevant, J. M. *J. biol. Chem.* **235**, 3499–3501.
Hoare, J. P. 1964 *Electrochim. Acta* **9**, 599–605.
Hultberg, H. & Anderson, I. B. 1982 *Wat. Air Soil Pollut.* **28**, 311–331.
Jacobson, R. L. & Langmuir, D. 1974 *Geochim. cosmochim. Acta* **38**, 301–318.
James, S. D. 1967 *J. electrochem. Soc.* **114**, 1113–1119.
Johnson, D. C., Polta, J. A., Polta, T. Z., Glen, G. N., Johnson, J., Tang, A. P.-C., Yeo, I.-H. & Baur, J. 1986 *J. chem. Soc. Faraday Trans.* I **82**, 1081–1098.
Kamath, V. N. & Hira Lal, J. 1968 *J. electroanal. Chem.* **19**, 137–145.
Karshin, V. P. & Grigoryan, V. A. 1970 *Russ. J. phys. Chem.* **44**, 762–763.
Kaye, C. A. 1957 *J. Geol.* **65**, 35–46.
Kier, R. S. 1980 *Geochim. cosmochim. Acta* **44**, 241–252.
Kieth, R. E. & Gilman, J. J. 1960 *Acta metall.* **8**, 1–10.
King, C. V. & Liu, C. L. 1933 *J. Am. chem. Soc.* **55**, 1928–1940.
Knoche, W. 1980 In *Biophysics and physiology of carbon dioxide* (ed. C. Bauer, G. Gros & H. Bartels), pp. 3–11. Berlin: Springer-Verlag.
Landsberg, R., Greissler, W. & Müller, S. 1961 *Z. Chem.* **1**, 169–174.
Leiva, E. P., Santos, E., Cerviño, R. M., Giordano, M. C. & Arvia, A. J. 1985 *Electrochim. Acta* **30**, 1111–1114.
Lessmark, O. & Thörnelöf, E. 1986 *Wat. Air Soil Pollut.* **31**, 809–815.
Lévêque, M. A. 1928 *Annls Mines. Mem.*, ser 12, **13**, 201–257.
Levich, V. G. 1942 *Acta phys.-chim. URSS* **17**, 257–260.
Levich, V. G. 1962 *Physicochemical hydrodynamics.* Englewood Cliffs, New Jersey: Prentice-Hall.
Linge, H. G. & Nancollas, G. H. 1973 *Calc. Tiss. Res.* **12**, 193–208.
Litt, M. & Serad, G. 1964 *Chem. Engng Sci.* **19**, 867–884.
Lund, K., Fogler, H. S., McCune, C. C. & Ault, J. W. 1973 *Chem. Engng Sci.* **28**, 691–700.
Lund, K., Fogler, H. S., McCune, C. C. & Ault, J. W. 1975 *Chem. Engng Sci.* **30**, 825–835.
MacDonald, A. & Duke, P. D. 1973 *J. Chromatogr.* **83**, 331–342.

PHILOSOPHICAL TRANSACTIONS OF THE ROYAL SOCIETY A MATHEMATICAL, PHYSICAL & ENGINEERING SCIENCES

McDonald, D. D. & Wright, G. A. 1970 *Can. J. Chem.* **48**, 2847–2852.
Magid, E. & Turbeck, B. O. 1968 *Biochim. biophys. Acta* **165**, 515–523.
Meares, P. 1984 *Faraday Discuss. Chem. Soc.* **77**, 7–16.
Mikhailova, A. A., Osetrova, N. V. & Vasiliev, Y. B. 1985 *Soviet Electrochem.* **21**, 985–988.
Miles, J. 1971 *Integral transforms in applied mathematics*. Cambridge University Press.
Moelwyn-Hughes, E. A. 1933 *The kinetics of reactions in solution*. Oxford University Press.
Moldoveanu, S., Handler, G. S. & Anderson, J. L. 1984 *J. electroanal. Chem.* **179**, 119–130.
Morse, J. W. 1974 *Am. J. Sci.* **274**, 97–107.
Morse, J. W. & Berner, R. A. 1979 In *Chemical modeling in aqueous systems* (ed. E. A. Jenne). *Am. chem. Soc. Symp. Ser.* **93**, 499–535.
Morse, J. W. 1983 *Rev. Mineral.* **11**, 227–267.
Nestaas, I. & Terjesen, S. G. 1969 *Acta chem. scand.* A **23**, 2519–2531.
Patel, R. C., Boe, R. J. & Atkinson, G. 1973 *J. sol. Chem.* **2**, 357–372.
Pearson, R. G., Meeker, R. E. & Basala, F. 1956 *J. Am. chem. Soc.* **78**, 709–713.
Peterson, M. N. A. 1966 *Science, Wash.* **154**, 1542–1544.
Plummer, L. N. & Wigley, T. M. L. 1976 *Geochim. cosmochim. Acta* **40**, 191–202.
Plummer, L. N., Wigley, T. M. L. & Parkhurst, D. L. 1978 *Am. J. Sci.* **278**, 179–216.
Plummer, L. N., Parkhurst, D. L. & Wigley, T. M. L. 1979 In *Chemical modeling in aqueous systems* (ed. E. A. Jenne) (*Am. chem. Soc. Symp. Ser.* **93**), pp. 537–573.
Rach, E. & Heitbaum, J. 1986 *Electrochim. Acta* **31**, 477–479.
Reddy, M. M. 1983 *Sci. Géol. Mém.* **71**, 109–121.
Reeder, R. J. 1983 *Rev. Mineral.* **11**, 1–47.
Rickard, D. T. & Sjöberg, E. L. 1983 *Am. J. Sci.* **283**, 815–830.
Rossi-Bernardi, L. & Berger, R. L. 1968 *J. biol. Chem.* **243**, 1297–1302.
Roughton, F. J. W. 1941 *J. Am. chem. Soc.* **63**, 2930–2934.
Scheuer, P., Brownell, R. & Lu Valle, J. 1958 *J. phys. Chem.* **62**, 809–811.
Schlichting, H. 1933 *Z. angew. Math. Mech.* **13**, 260–270.
Shibata, S. 1958 *J. chem. Soc. Japan* **79**, 239–243.
Shibata, S. 1963 *Bull. chem. Soc. Japan* **36**, 525–527.
Sillen, L. G. & Martell, A. E. 1964 *Chem. Soc. Lond. spec. Publ.* **17**, 754 pp.
Sippel, R. F. & Glover, E. D. 1964 *Geochim. cosmochim. Acta* **28**, 140–144.
Sirs, J. 1958 *Trans. Faraday Soc.* **54**, 207–212.
Sjöberg, E. L. 1976 *Geochim. cosmochim. Acta* **40**, 441–447.
Sjöberg, E. L. 1978 *Stockholm Contrib. Geol.* **32**, 1–96.
Sjöberg, E. L. 1983 *Sci. Géol.Mém.* **71**, 119–128.
Sjöberg, E. L. & Rickard, D. T. 1983 *Geochim. cosmochim. Acta* **47**, 2281–2285.
Sjöberg, E. L. & Rickard, D. T. 1984 *Chem. Geol.* **42**, 119–136.
Sjöberg, E. L. & Rickard, D. T. 1985 *Chem. Geol.* **49**, 405–413.
Smith, G. D. 1985 *Numerical solution of partial differential equations: finite difference methods*. Oxford: Clarendon Press.
Sobkowski, J. & Czerwinski, A. 1974 *J. electroanal. Chem.* **55**, 391–397.
Sobkowski, J. & Czerwinski, A. 1975 *J. electroanal. Chem.* **65**, 327–333.
Soustelle, M., Guilhot, B. & Cournil, M. 1985 *Material Science Monographs* **28**A, 533–539.
Spiro, M. & Jago, D. S. 1982 *J. chem. Soc. Faraday Trans.* I **78**, 295–305.
Spiro, M. 1984 *Faraday Discuss. chem. Soc.* **77**, 309–312.
Spring, W. 1887 *Z. phys. chem.* **1**, 209–226.
Spring, W. 1888 *Z. phys. chem.* **2**, 13–22.
Stonehart, B. 1973 *Electrochim. Acta* **18**, 63–68.
Stulik, K. & Hora, V. 1976 *J. electroanal. Chem.* **70**, 253–263.
Stumm, W. & Morgan, J. J. 1981 *Aquatic chemistry*. New York: Wiley.
Sverdrup, H. & Bjerle, I. 1982 *Vatten.* **38**, 59–66.
Sverdrup, H. 1983 *Chem. Scripta* **22**, 12–16.
Sverdrup, H. 1984 In *Lake and reservoir management*. Washington, D.C.: U.S. EPA.
Sverdrup, H. & Bjerle, I. 1984 *Vatten.* **39**, 41–49.
Sverdrup, H. 1986 *Wat. Air Soil Pollut.* **31**, 828–832.
Terjesen, S. G., Erga, O., Thorsen, G. & Ve, A. 1961 *Chem. Engng Sci.* **14**, 277–288.
Thomas, J. M. & Renshaw, G. D. 1965 *Trans. Faraday Soc.* **61**, 791–796.
Tolansky, S. 1973 *An introduction to interferometry*. London: Longman.
Tominaga, H., Adzum, H. & Isobe, T. 1939 *Bull. chem. Soc. Japan* **14**, 348–352.
Tomson, M. B. & Nancollas, G. H. 1978 *Science, Wash.* **200**, 1059–1060.
Unwin, P. R. & Compton, R. G. 1988 *J. electroanal. Chem.* **245**, 287–298.
Unwin, P. R. & Compton, R. G. 1989 In *Comprehensive chemical kinetics* (ed. R. G. Compton & A. Hamnett), vol. 29, pp. 173–296. Amsterdam: Elsevier.

PHILOSOPHICAL TRANSACTIONS OF THE ROYAL SOCIETY A MATHEMATICAL, PHYSICAL & ENGINEERING SCIENCES

Unwin, P. R., Barwise, A. J. & Compton, R. G. 1989 *J. Colloid Interface Sci.* **128**, 208–215.
van Eldick, R. & Palmer, D. A. 1982 *J. sol. Chem.* **11**, 339–346.
Vielstich, W., Heindrichs, A. & von Gostiša-Michelčić, B. 1972 *Ber. BunsenGes phys. Chem.* **76**, 19–23.
von Karman, T. 1921 *Z. angew. Math. Mech.* **1**, 233–258.
von Stackelberg, M., Pilgram, M. & Toome, V. 1953 *Z. Elektrochem.* **57**, 342–344.
von Tress, M., Loeppert, R. H. & Matis, J. H. 1985 *Soil. Sci.* **49**, 302–306.
Walker, A. C., Bray, U. B. & Johnston, J. 1927 *J. Am. chem. Soc.* **49**, 1235–1256.
Warfringe, P., Sverdrup, H. & Bjerle, I. 1984 *Chem. Scripta* **24**, 67–72.
Wentzler, T. H. & Aplan, F. F. 1972 *Proc. Symp. AIME*, 513–523.
Weyl, P. K. 1958 *J. Geol.* **66**, 163–177.
Will, F. G. & Knorr, C. A. 1960 *Z. Elektrochem.* **64**, 258–261.
Wissbrun, K. F., French, D. M. & Patterson, A. J. 1954 *J. phys. Chem.* **58**, 693–695.
Woods, R. 1976 In *Electroanalytical chemistry* (ed. A. J. Bard), vol. 9. New York: Marcel Dekker.
Wright, R. F. 1985 *Can. J. Fish. Aquat. Sci.* **42**, 1103–1107.
Yamada, J. & Matsuda, H. 1973 *J. electroanal. Chem.* **44**, 189–198.
Yeager, E., Oey, T. S. & Hovorka, E. 1953 *J. Phys. Chem.* **57**, 268–275.

PHILOSOPHICAL TRANSACTIONS OF THE ROYAL SOCIETY A MATHEMATICAL, PHYSICAL & ENGINEERING SCIENCES

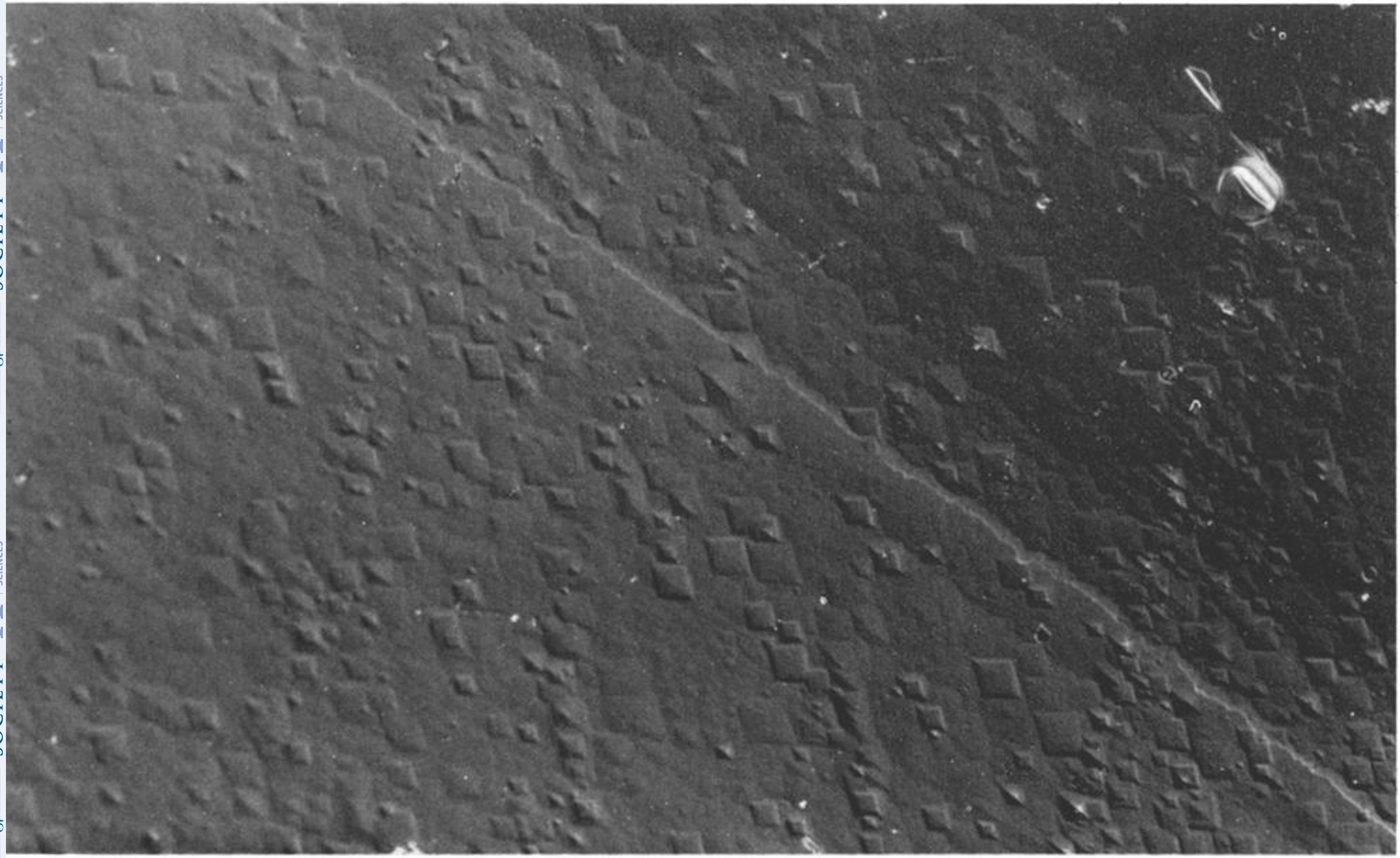

FIGURE 17. DIC micrograph (179×) of a cleaved calcite crystal, after rotation at 9 Hz in an aqueous 1 mM HCl solution for 60 s.

PHILOSOPHICAL TRANSACTIONS OF THE ROYAL SOCIETY A MATHEMATICAL, PHYSICAL & ENGINEERING SCIENCES

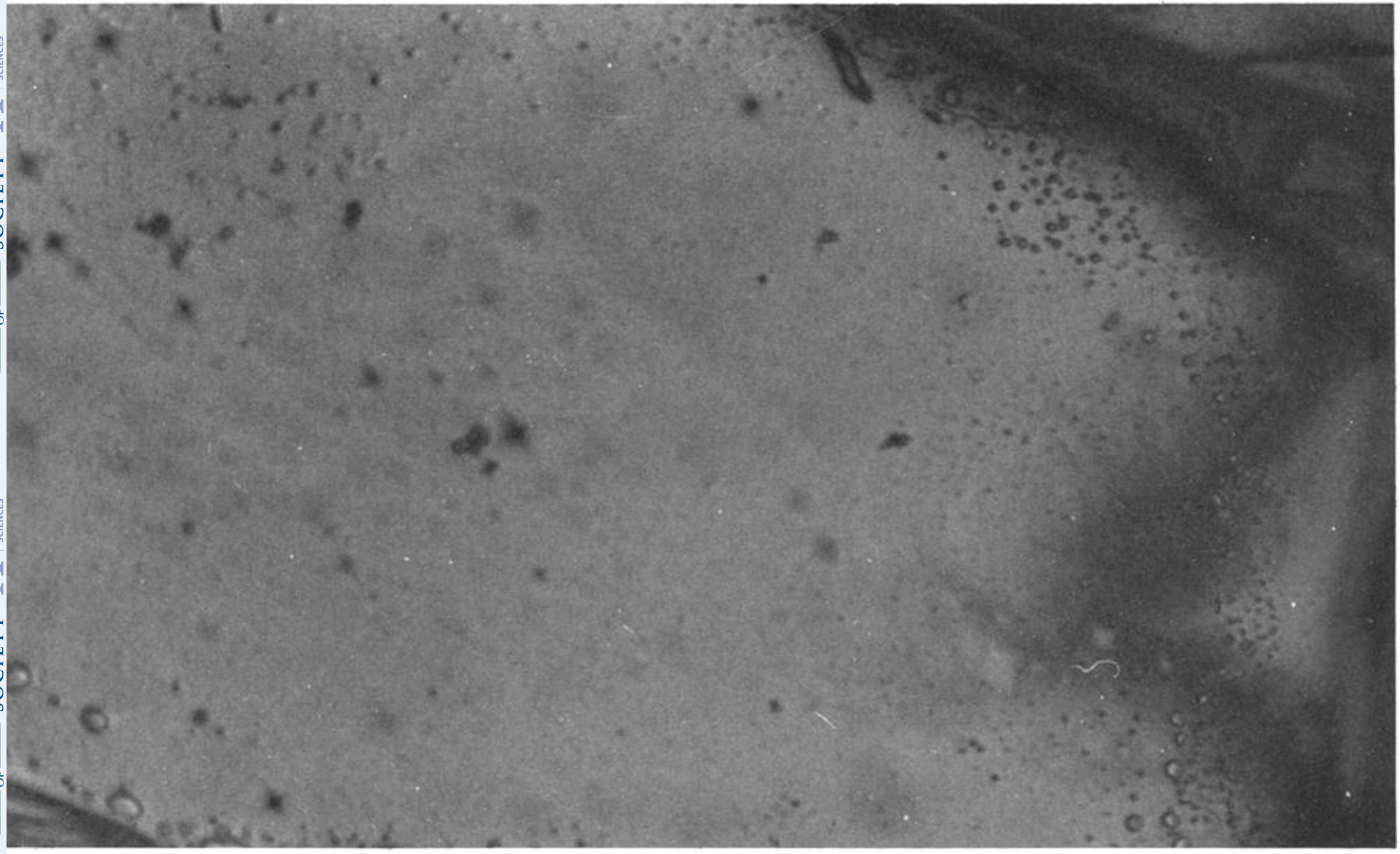

FIGURE 18. Interferogram (222×) of the surface shown in figure 17.

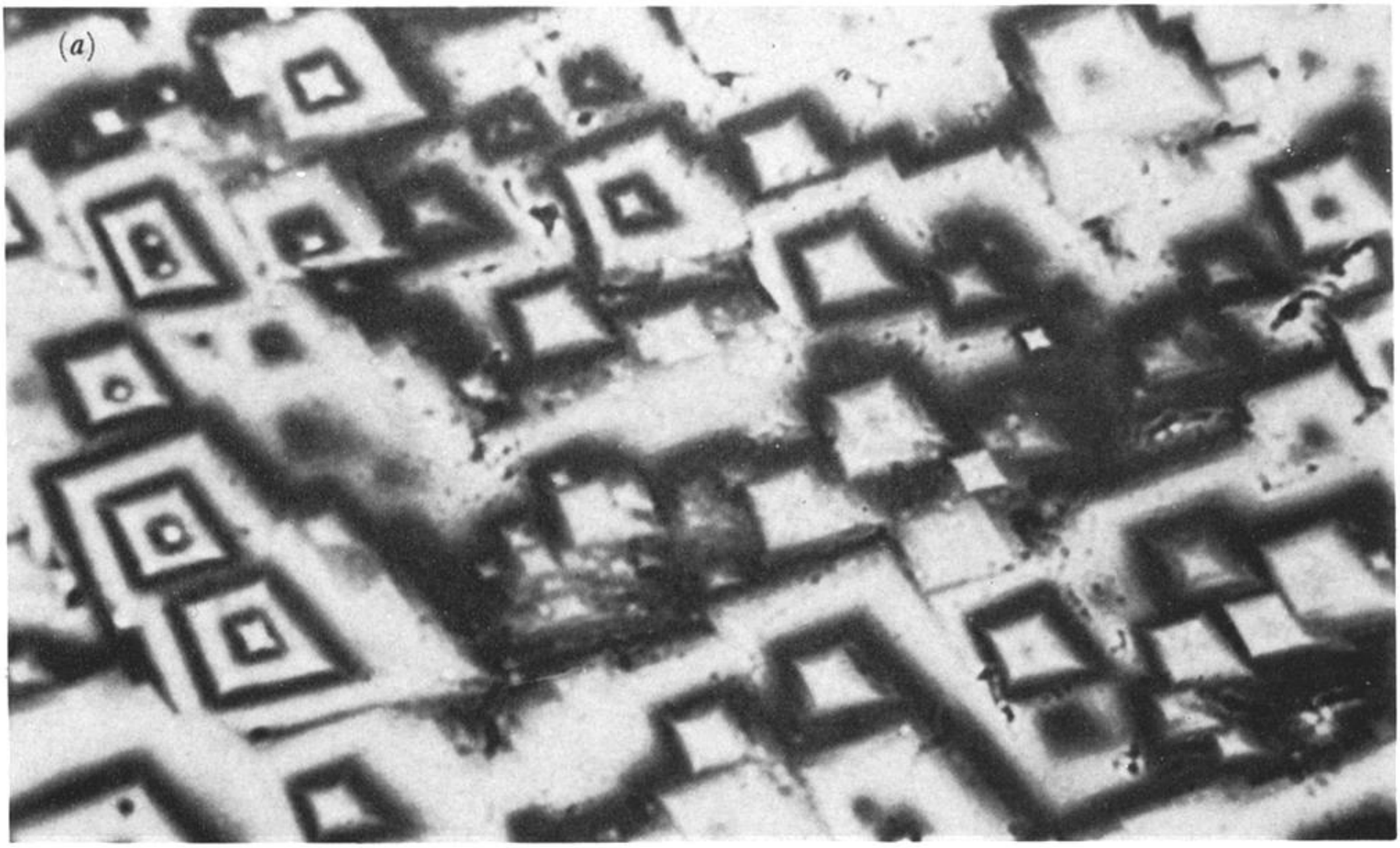

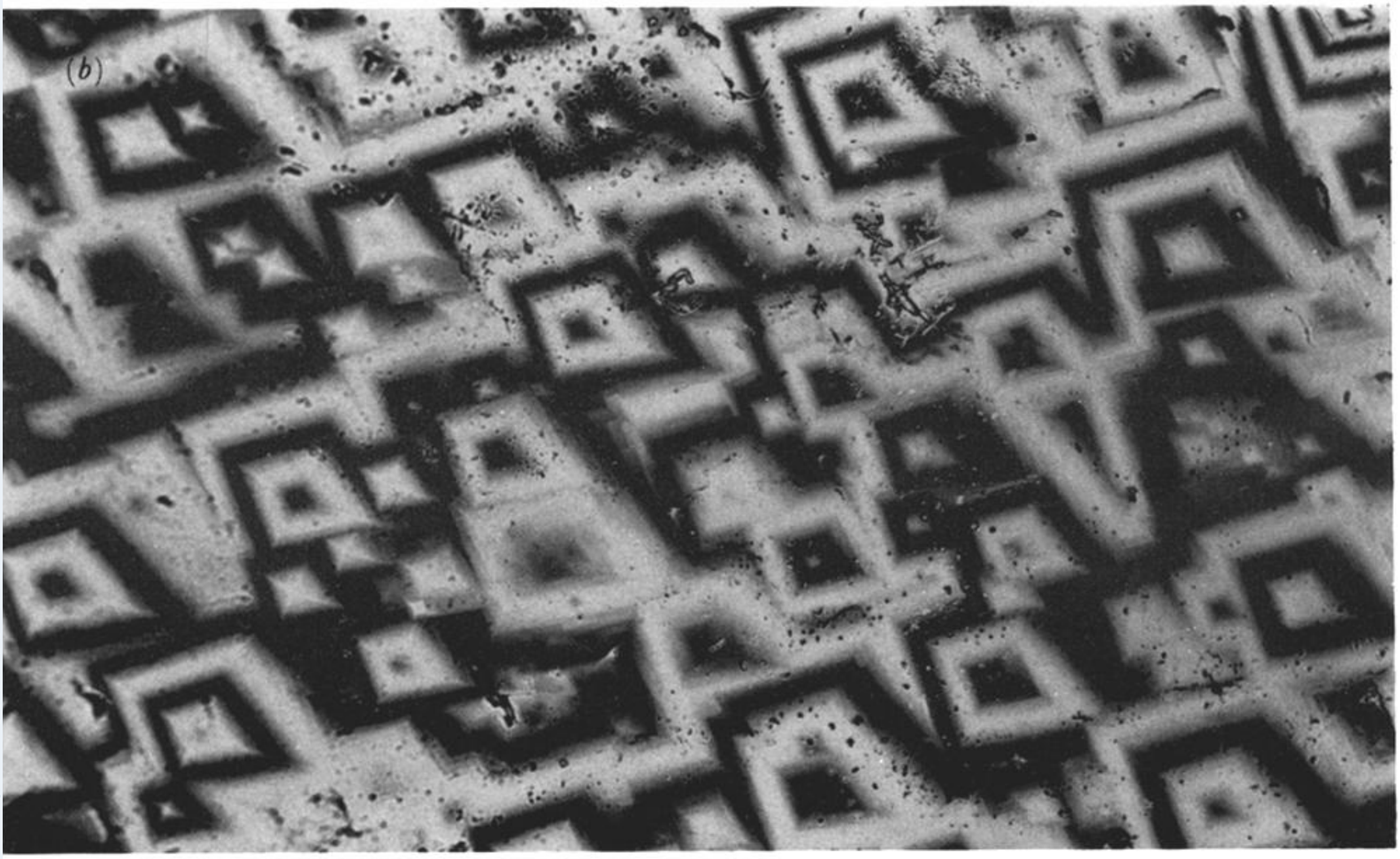

FIGURE 19*a*, *b*. For description see opposite.

FIGURE 19. Interferograms (222 ×) at selected areas along a calcite cleavage plane subjected to dissolution in 2 mM HCl for 50 m in a channel flow cell characterized by $h = 0.02$ cm, $d = 0.6$ cm, and in which a solution flow rate of 7.4×10^{-2} cm^3 s^{-1} was used. The regions illustrated are: (*a*) 0.28–0.85 mm; (*b*) 2.56–3.13 mm; (*c*) 4.26–4.83 mm; (*d*) 5.97–6.54 mm from the upstream edge of the crystal. Flow is from left to right.